OTS: $2.75

N64-17889 N64-17894

CODE-1

SOLAR PROTON MANUAL

edited by *Frank B. McDonald*, ed. Washington, NASA, Dec. 1963

122p refs

contributed by

C. E. Fichtel, D. E. Guss, H. H. Malitson,

K. G. McCracken, K. W. Ogilvie,

and W. R. Webber

Goddard Space Flight Center,

Greenbelt, Maryland

typist: contents

6

(Some support code all thru)

Avail thru N64-17894

SOLAR PROTON MANUAL

Edited by Frank B. McDonald

Contributed by C. E. Fichtel, D. E. Guss,
H. H. Malitson, K. G. McCracken, K. W. Ogilvie,
and W. R. Webber

Goddard Space Flight Center
Greenbelt, Maryland

NATIONAL AERONAUTICS AND SPACE ADMINISTRATION

SOLAR PROTON MANUAL

edited by
Frank B. McDonald

contributed by
C. E. Fichtel, D. E. Guss, H. H. Malitson,
K. G. McCracken, K. W. Ogilvie,
and W. R. Webber

Goddard Space Flight Center

SUMMARY

Solar particle outbursts are studied in an attempt to summarize the experimental knowledge in this field for the benefit of the spacecraft design engineer. A phenomenological description of solar particle events is presented and time histories and tabulated data are given for the major events. The anisotropy of high energy solar cosmic rays observed in several events is also treated.

CONTENTS

iii

PREFACE

The acceleration of nuclei by the sun is of fundamental scientific importance. A complete understanding of the acceleration and propagation of these nuclei through interplanetary space should add greatly to our knowledge of solar processes and assist in arriving at an understanding of the galactic cosmic radiation. From an engineering standpoint, these solar particle outbursts also pose important considerations for manned space travel. This volume is an attempt to summarize the experimental knowledge in this field for the benefit of the spacecraft design engineer. A complete revision is planned for the near future which will emphasize the scientific aspects.

The first chapter provides a complete phenomenological description of the solar particle events. The second chapter provides a time history of major events based on all available data. The agreement between the two independent estimates of intensity (Chapters 1 and 2) is excellent for all cases except the February 23, 1956 event; and this event will be treated separately in a supplement that will be available soon. The third chapter treats the observations of anisotropy of the high energy solar cosmic rays. The Appendixes present a tabulation of all known particle events, from which can be constructed an intensity versus frequency-of-occurrence listing.

It is planned that further supplements to this volume will be issued as new material becomes available. In particular, the Explorer XII data of Bryant, Cline, Desai, and McDonald have yielded valuable new information on the propagation of low and medium energy solar cosmic rays; this should be available by late 1962.

Frank B. McDonald

v

CHAPTER 1

A SUMMARY OF SOLAR COSMIC RAY EVENTS

by

Harriet H. Malitson and William R. Webber *(Minn. U.)*

GENERAL CHARACTERISTICS OF SOLAR COSMIC RAY EVENTS

Introduction

Although galactic cosmic radiation has been recognized and investigated for many years, the ability of the sun to produce large bursts of energetic particles was discovered only in 1946 (Reference 1) and the arrival of this solar cosmic radiation at the earth has been studied in detail only since 1956. In the twenty years preceding the solar cosmic ray event of February 23, 1956, there were only four cases of an increase of cosmic ray intensity at the earth (as measured at ground level by ionization-type detectors) that could be related to solar activity. Therefore the idea became widespread that these events were quite rare.

The introduction of the neutron monitor in 1949 (Reference 2) somewhat improved the sensitivity of the ground-level measurements, but the real breakthrough came recently with the use of particle counters and emulsions flown in balloons, satellites, and space probes. In addition, it has been found that the solar particle bursts may be detected indirectly through their effects on the absorption of VHF cosmic noise in the ionospheric D-layer over the polar caps — called a polar cap absorption event (PCA). A detailed discussion of the different methods for detecting solar cosmic rays and their relative sensitivities is presented in Chapter 2.

From the studies of solar particle bursts over the last few years by this wide variety of techniques, a reasonably complete picture of these events is beginning to emerge. The cosmic ray particles ejected from the sun are known to be primarily protons with a typically steep spectrum of energies ranging from less than 10 Mev to a few Bev. Such cosmic ray particles may be present near the earth in detectable numbers a significant fraction

---

*University of Minnesota.

of the time (10-20 percent), exceeding the normal galactic cosmic ray intensity for a much smaller period of time (1-2 percent) and occasionally for intervals of one or two days, reaching intensities many thousands of times greater than the galactic cosmic ray intensity.

The intensity-time, directional, spectral, and charge characteristics differ considerably from event to event. For example, some events may contain a relatively large fraction of high-energy particles, thus producing a rare effect in a sea-level detector; but, on the other hand contain few low energy particles, thus giving a small integrated particle intensity. The latter characteristic causes the event to be classified as a relatively small one. Other important dissimilarities exist from event to event, and for this reason we shall catalog some of the more important ones individually. However, we may define certain general characteristics — common to all events — which may aid in understanding these events.

The Intensity-Time Profile

A typical event will have a set of intensity-time profiles, one for each energy, such as those shown in Figure 1-1. Certain times characterize each profile:

1. The *onset-delay time* is defined as the time from the maximum of the visual flare intensity to the arrival of the first particles at the earth. This time is variable from event to event and is strongly energy-dependent, the higher energies arriving first. Onset-delay times may vary from a few minutes for high energy particles in some events to many hours for low energy particles in other events.
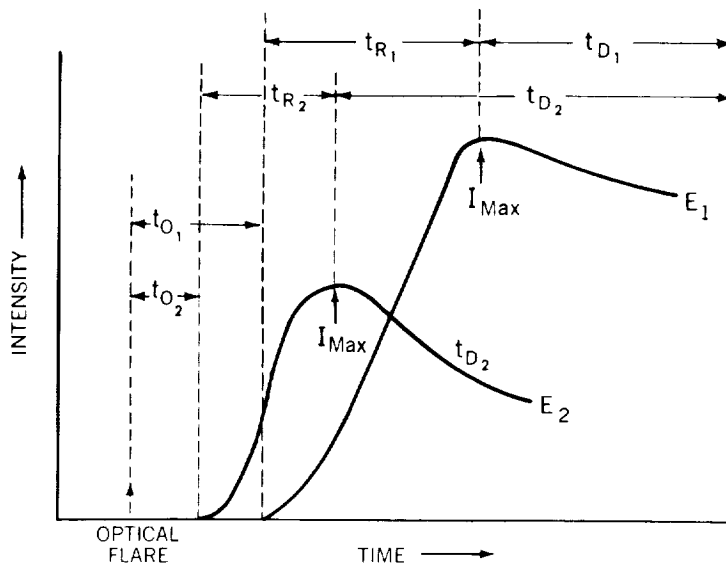

Figure 1-1—Intensity-time profiles for a typical event. Curve E_2 represents the arrival of particles of energies that are high in comparison with the energies of the particles represented by curve E_1. t_{O_1} and t_{O_2} are onset-delay times; t_{R_1} and t_{R_2}, rise times; and t_{D_1} and t_{D_2}, decay times.

2. The rise time is defined as the time interval from the first arrival at the earth of particles of a particular energy to the time at which maximum intensity of these particles is attained. This time also varies from event to event and is strongly energy-dependent, the higher energies reaching maximum intensity first. These times are usually related to the onset times in a particular event, and may range from a few minutes for high energy particles in some events to many hours for low energy particles in other events.

3. A growing body of evidence indicates that the decay of the intensity of the particles is an exponential at most times and for most energies (Reference 3). Thus we may define a characteristic *decay time* t_D and write the following equation for the intensity of flare particles with energies greater than some energy E at some time t after the maximum intensity $I_{Max}(E)$ has been attained:

$$I = I_{Max}(E) e^{-t/t_D} .$$

The time t_D is a function of energy and is variable from event to event. It may be changed during the course of an event by the arrival at the earth of a changed interplanetary field configuration, such as might be evidenced by a magnetic storm or other magnetic activity. The decay time may range from 3-4 hours for high energy particles in some events to 2-3 days for low energy particles in other events.

Anisotropies in the Flare Particles

For the most part the solar flare particles arrive at the earth very nearly isotropically (to within ± 5-10 percent) and the aforementioned intensity-time characteristics refer to this isotropic radiation. Frequently, however, significant anisotropies exist in the direction of arrival of solar flare particles in the earth's vicinity. In particular, the particles appear to arrive from a highly preferred and fairly narrow direction in space (for a detailed description, see Chapter 3). Such directional radiation is usually of short duration compared to the isotropic part; however, unusually high intensities may occur in the preferred direction for periods of a few minutes. It is also possible to define onset-delay, rise, and decay times for this directional radiation.

The Energy Spectrum of the Flare Particles

It is obvious from the foregoing discussion on the intensity-time characteristics of the flare particles and from the energy-dependence of each of the parameters involved that there is no unique energy spectrum for any one event. The spectrum measured in a single event will depend upon both the specific time in the event at which the measurements are made and the energy range of the measurements. Typical spectral shapes at different times in a single event may develop somewhat like those in Figure 1-2.
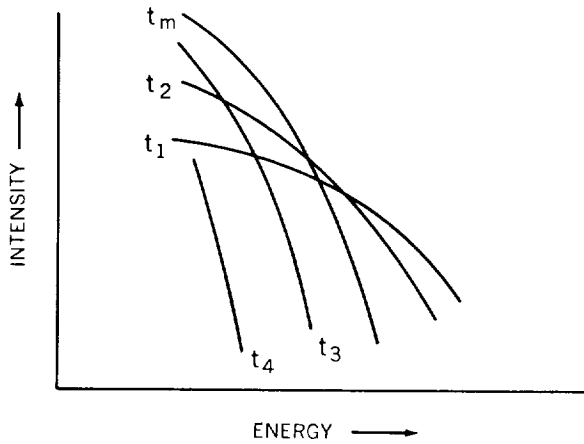
4

Figure 1-2—Typical energy spectra obtained at different times $(t_1 < t_2 < t_m < t_3 < t_4)$ during a single event.

It is useful, however, to define a typical flare particle energy spectrum for each event. Such a spectrum will be defined as the *differential energy spectrum* existing in the energy region above 30 Mev when the integral intensity of these particles is a maximum, i.e., when $I(> 30$ Mev) is a maximum. This spectrum will vary from event to event. If we define the characteristic differential spectrum as

$$\left(\frac{dI}{dE}\right)_0 = \frac{K}{E^{n_0}} \, ,$$

then n_0 varies in extreme cases from about 3.5 to 5.0. The time in the event when the above condition holds will vary with the event. Before this time the value of the n_0 may be much less than 3.5 to 5.0, particularly at low energies. Afterwards, n_0 may be greater than 3.5 to 5.0, particularly at high energies. The exponent n_0 merely characterizes the energy spectrum of the flare particles at a common time in different events. More complete details on the energy spectra and total intensities for selected events will be found in Chapter 2.

Charge Composition of the Flare Particles

The particles emitted in a solar flare burst are predominantly protons but in each event, to a greater or lesser degree, particles heavier than protons appear to be present — predominantly alpha particles but including nuclei in the CNO group at least (References 4, 5 and 6). To date these heavier particles have actually been observed during six solar cosmic ray events, by only one or two spot measurements during each event. In addition these measurements may represent intensity integrals of solar particles over several hours. For these reasons it is difficult to make definitive statements about the heavier particles. It is useful, however, to define the characteristic percentage of the heavier nuclei as that percentage present at the time when $I = I_{Max}(> 30$ Mev). This characteristic percentage apparently varies from event to event. The P/α ratio above a fixed energy (or energy per nucleon) may vary from 10 to 100, and the P/CNO ratio above a fixed energy (or energy per nucleon), may vary from 10^3 to 10^4. As far as *total* particle numbers are concerned, the heavier nuclei in solar flares are probably relatively less abundant than such

nuclei in the galactic radiation. However, the ratio may vary with time during the event. In addition, the ratio may depend on energy. In fact, it is important when studying these particles to determine whether their intensity-time and spectral characteristics may be explained more simply as a function of energy or of rigidity.

GENERAL CHARACTERISTICS OF SOLAR FLARES AND THEIR RELATION TO COSMIC RAY PRODUCTION

In the general sequence of events the solar cosmic rays arrive near the earth shortly after a flare occurs on the sun. As far as is known at present, particles with energies greater than a few Mev are not produced on the sun except in conjunction with solar flares. The relationships between the characteristics of the solar cosmic ray increase at the earth and the characteristics of the solar flare are obviously quite complex; but a number of very useful generalizations can be made about these phenomena. First, however, we should mention some features of the solar flares themselves.

A flare is observed optically as a sudden large increase in radiation intensity in a portion of the sun's atmosphere. A large flare usually has a filamentary structure, and may consist of one or several continuous strands of bright material. The flare may spread to nearby portions of the solar atmosphere during its lifetime, which can be several minutes or a few hours. However, maximum brightness (the flash phase) is attained rapidly, usually lasting for less than 5 minutes, and is followed by a slow decay. The light from a flare consists of monochromatic radiations characteristic of such elements as hydrogen; neutral and ionized helium; and ionized calcium, iron, and silicon. Flares are observed most often in the H-alpha line (the first line in the Balmer series of hydrogen). In a few exceptional cases, a large flare has been observed in integrated, or white light. The parameter used by solar observers to describe the size of a flare is *importance*, a measure of the area and brightness. The range of importance is from 1- flares (called subflares), with an average area of 100 millionths of the visible solar hemisphere, to 3 + flares, with areas approaching 5000 millionths.

A flare should not be considered as a separate and distinct event, but as only a *symptom* of something much more basic that is occurring within the sun. Unfortunately, our understanding of the total phenomenon is very incomplete at present. We do know that, with very few exceptions, flares originate in so-called *active regions* on the sun. Therefore, the study of flares begins with observations relating to the life histories of active regions. It is no easy task to interrelate such measurements because they are made in various ways depending on the height in the solar atmosphere of the phenomenon being observed, and its position on the solar disk.

6

GENERAL CHARACTERISTICS OF ACTIVE REGIONS AT DIFFERENT LEVELS IN THE SOLAR ATMOSPHERE

Photosphere

The photosphere is the "surface" of the sun observed in integrated light. On a white light photograph of the sun, the undisturbed parts of the disk appear to have a granular structure. Each "grain" is believed to be a convection cell. The active regions appear as groups of sunspots. Sunspots are cooler than the general photosphere (6000°K) with a temperature of about 4500°K. In a photograph of a sunspot, the central darker portion is called the umbra, and the surrounding grayish region, the penumbra. These spots or groups of spots cover about the same areas as flares — from a few millionths of the solar hemisphere to about 5000 millionths. The lower limit in both cases is set by observing conditions. Sunspots are associated with strong magnetic fields, often of the order of several thousand gauss.

Flares almost always occur within 10^5 km of a visible sunspot. They occur more frequently and with greater importance as the associated spot group becomes more complex magnetically. The position of a large flare relative to the umbrae of its associated spots may be significant in cosmic ray production.

Chromosphere

The chromosphere is the transition layer of the solar atmosphere, in which the temperature changes from the 6000°K of the photosphere to the million-degree temperature of the corona, or outer atmosphere. Density and pressure also undergo rather abrupt changes. Chromospheric photographs are usually taken in H-alpha, or in part of the K line of ionized calcium. Active regions show up on a K line spectroheliogram as bright patches called plages, which stand out from the "orange-peel" appearance of the undisturbed background. Flares develop from plages, often following the outline of a plage, and occur in the chromosphere (although the height varies somewhat from one flare to another).

The long, thin, dark features easily seen on spectroheliograms are called filaments when seen in projection against the solar disk, and prominences when seen as bright features at the limb, or edge. Some types of filaments are associated with active regions and exhibit various kinds of motions and disappearances, some of which seem to be related to flare and cosmic ray production.

When a cosmic ray flare is observed on the limb, material is often seen to be ejected from the flare vicinity in the form of surge-type prominences. Material ejected from flare regions can also be seen on the disk by moving the effective wavelength of the observing apparatus toward the violet so that doppler-shifted absorption by this material can be

observed. Shifting the wavelength toward the red shows that at least some of the material falls back again toward the chromosphere. Active loop prominences also appear frequently in regions that produce cosmic rays, especially in the post-maximum phase of large flares (Reference 7).

Corona

The outer part of the corona, or upper solar atmosphere, can be observed only during a total solar eclipse. However, at other times, with the birefringent filter, phenomena can be observed at the limb in the inner part of the corona, near the outer chromosphere. Active regions appear as bright spots in any one of several selected wavelengths corresponding to emission by highly ionized atoms in the corona. Coronal emission in the green or red line of highly ionized Fe is measured daily by several observatories. Emission in the yellow line of Ca XV (Ca with 14 of its electrons removed) indicates unusually high activity. Active regions also appear in the corona as bright spots in isophotal maps of radio emission from the sun.

GROWTH OF AN ACTIVE REGION

An active region begins as a small plage located in one of the two sunspot belts, either north or south, at a latitude of about 5 to 40 degrees, depending somewhat on the 11-year cycle of solar activity. A few days later, sunspots appear in the region, and proceed to grow in number and size as the size and brightness of the plage increase. Small flares occur and active filaments (or prominences) begin to appear. The spot group reaches maximum size, with large penumbrae, while the plage continues to spread. Flares become larger and more numerous, and it is at this stage of development, or somewhat later, that cosmic ray events tend to occur.

EVENTS AT THE EARTH FOLLOWING A FLARE

A solar flare* may be accompanied by any of the following occurrences at the earth; although very few flares produce all of them.

Sudden Ionospheric Disturbance

Minutes after the start of a flare, there is often a Sudden Ionospheric Disturbance (SID), which is an abrupt large increase in absorption in the D-region or lower E-region of the earth's ionosphere. SID's are caused by electromagnetic radiation from the sun (probably

---

*Optical and radio properties of certain selected flares are described in Appendix A.

chiefly in the X-ray part of the spectrum) and occur only on the sunlit hemisphere of the earth. SID's may be detected in the following ways: short wave fadeouts (SWF); sudden increase in cosmic noise absorption (SCNA); sudden enhancement of low-frequency atmospherics (SEA), sudden phase anomalies at VLF (SPA); and sudden signal enhancements at VLF (SES).

Radio Emission

During the first few minutes of the flare there may be a solar radio noise storm, consisting of bursts and outbursts (strong bursts of long duration), often over a wide range of frequencies. From the cosmic-ray point of view, this wide spectrum of RF emission may be even more important than the optical emission. This radiation extends over a range from about 10 to 10,000 Mc and the highest frequencies may be of particular importance (Reference 8 and 9). The relative increase in optical spectral emission is only a factor of 1 to 3 during such events, but the radio emission may increase by a factor of 10 to 100. This radio emission amounts, energetically, to only a few percent of the optical emission; but this fraction is comparable to that believed emitted in the form of cosmic rays in such an event. In a typical cosmic-ray-producing event, a strong burst of RF emission at frequencies greater than 1000 to 10,000 Mc occurs more or less simultaneously with the maximum intensity of the optical emission. The intensity-time characteristics of this initial burst of RF radiation are very similar to those of the optical emission. Later in the event the emission of frequencies less than 500 Mc builds up. This emission may become very intense and last for a number of hours; it is characterized by slow gradual decay in intensity, along with a movement of the center of emission outward from the solar disk. Such radiation is called Type-IV radio radiation and its presence during a flare is strongly correlated with the production of cosmic rays in the flare and their subsequent arrival at the earth (References 10 and 11). Present theories ascribe this Type-IV radiation — and, perhaps also the earlier burst of higher-frequency radiation coincident with the optical maximum — to synchrotron radiation. The latter probably is due to electrons accelerated along with the cosmic ray nuclei in the flare, but trapped for many hours in the expanded flare region by the local magnetic fields (Reference 12).

Ground-Level Cosmic-Ray Increase

In the rare ground-level cosmic ray increase, the arrival of high-energy particles at the earth is recorded within minutes of the time of maximum brightness of the solar flare.

Polar Cap Absorption Event

In polar cap absorption (PCA) events, the arrival of lower energy flare particles is recorded within a few hours after the maximum phase of the flare. Geometrical

considerations of the flare's position on the solar disk seem to play a major role in determining the characteristics of the cosmic ray increase observed in the vicinity of the earth. These considerations may include the depth on the solar atmosphere at which the flare occurs (Reference 13) and the flare's location on the solar disk relative to the sun-earth line (Reference 14). At present, a clear relationship with the intensity-time characteristics of the cosmic rays at the earth exists only for the latter consideration. It has definitely been established that solar flare particles display shorter onset-delay and rise times at the earth when the responsible flare is near the west limb of the sun. These times may be from 3 to 5 times shorter than the corresponding times for flares near the east limb. The above applies to both low and high energy particles. The more direct propagation of particles from flares near the west limb of the sun suggests that for two flares producing approximately equal numbers of particles, a greater peak intensity and perhaps a larger integrated intensity will be observed at the earth from the flare located nearer the west limb of the sun.

Geomagnetic Storm

One or two days after the solar flare, a geomagnetic storm may occur, indicating the arrival at the earth of large numbers of very low-energy (kev) particles; such clouds of particles, called plasmas, are electrically neutral as a whole. During a geomagnetic storm, small changes occur in the measured components of the earth's magnetic field. These small changes result in many spectacular effects, such as aurorae, ionospheric changes which disrupt radio communication, and apparent decreases in galactic cosmic ray intensity measured at ground level (Forbush decreases).

SPECIFIC FEATURES OF IMPORTANT SOLAR COSMIC RAY EVENTS AND RELATED SOLAR FLARES

During the period 1956-1961 nearly 50 solar cosmic ray outbursts have been recorded at the earth by a wide variety of techniques*. These events display an enormous range $(10^4 - 10^5)$ of integrated particle intensities over the duration of the outbursts. Of these events, approximately 30 of the largest — those with a minimum integrated intensity of 10^6 particles/cm^2 with energies greater than 30 Mev observed at the earth — have been selected for discussion here. These events are comparable to the integrated intensity of galactic radiation for one week; the smaller events obviously do not contribute appreciably to the enhancement of the cosmic ray intensity near the earth. Prior to 1956 it was not possible to make a size estimate on any of the solar cosmic ray events; therefore these events are not included, although undoubtedly many important ones occurred. The identification of a solar cosmic ray event by ionospheric absorption (riometer) data alone is not regarded as sufficient to make a specific size estimate. In fact, size estimates based on the relative

*All known events from 1949 to the present are tabulated in Appendix B.

ionospheric absorption may be grossly misleading, since the absorption may in many instances be produced by solar cosmic rays of much lower energy than the 30 Mev lower limit selected here, or by auroral electron effects. (The chosen lower energy limit represents a penetration of about 1 gm/cm^2.)

In order to obtain a relation between size and frequency of occurrence, rough size estimates have been made when direct measurements of solar cosmic ray intensities at the top of the atmosphere or in space near the earth at one time during the event were available. Detailed estimates of intensity-time characteristics, spectral distribution, and size have been made only when a number of direct measurements of solar cosmic ray intensities and/or spectra exist at the top of the atmosphere or in space near the earth for a particular event*.

These data, along with the integrated intensity of all solar particles with energies above 30 and above 100 Mev and the corresponding integrated skin or free-space dose in rads, are listed in Table 1-1 for the 30 events. By referring to this table, we may elaborate more critically on some features of specific solar flares and related cosmic ray events. First we note that although 30 separate events are cataloged over the six-year period, they occur in only 16 different active centers. During the last three years (1959-1961) this tendency is even more pronounced, for 18 separate events have been associated with only 5 different active centers. The active centers associated with these flares were usually already well developed when they appeared at the east limb of the sun. Only once did the same active center continue to produce large cosmic ray events during its subsequent appearance on the visible hemisphere of the sun. From four of these active centers (McMath Plage Numbers 3400, 5269, 5925 and 6171) have come over 90 percent of all of the solar cosmic rays observed at the earth in the last six years.

From Table 1-1, we note that, of the 30 events listed, 22 have been from flares in the sun's western hemisphere and 8 from the eastern. Of the 10 largest events, 6 have come from flares in the western hemisphere and 4 from flares in the eastern. Finally, from the 5 active regions that have produced 18 of the cosmic ray flares in the last three years, 11 of the flares have occurred while the active center was in the western hemisphere; and 7 in the eastern. Of these five active regions, the four major ones have been in the northern hemisphere and the remaining one in the southern.

From the above statistics we can say that for cosmic-ray-producing flares as a whole, there is a greater likelihood of observing cosmic rays at the earth when the flare is in the sun's western hemisphere. This situation suggests that on the average a greater fraction of the particles produced are received at the earth when the flare is nearest the west limb of

---

*The total integral intensities and characteristic spectra presented here were arrived at by an evaluation of the available data independent of the evaluation given in Chapter 2. The agreement is excellent except in the case of the February 23, 1956 event, which will be discussed separately. In Chapter 2 the detailed time histories of selected events are given when sufficient data have been available to make this practical. In the present chapter, an evaluation is made of all major events, from which a size versus frequency-of-occurrence table can be constructed by the reader.

the sun. A *large, important* cosmic-ray event is almost equally likely to arise from a flare in the western or eastern hemisphere. However, a distinct northern hemisphere preference is noted.

The correlation between the peak RF emission in the frequency range between 3,000 and 10,000 Mc during the flares, and the size of the cosmic ray event at the earth is sufficiently good that we can use the values of this peak RF emission to make fairly useful statements regarding the integrated size of the cosmic ray event. If the peak RF emission in this range exceeds $10,000 \times 10^{-22}$ w/m^2-cps, about 50 times normal, the integrated intensity of solar cosmic rays with energies above 30 Mev at the earth will generally exceed 10^8 particles/cm^2 (i.e., exceed the average yearly integrated intensity of galactic cosmic rays). If the peak RF emission in this range exceeds $3,000 \times 10^{-22}$ w/m^2-cps, the cosmic ray event will still be important and the integrated intensity of particles at energies greater than 30 Mev at the earth may still exceed 10^8 and will usually exceed 10^7 particles/cm^2. If the peak emission in this range is less than $1,000$ to $2,000 \times 10^{-22}$ w/m^2-cps, the cosmic ray event is usually not a major one.

Turning now to the characteristic intensity-time profiles of the solar cosmic rays as observed in the earth's vicinity, we see that the average initial delay from the time of the peak optical (and radio) emission until the first arrival of the isotropic component of solar particles at the earth (for particle energies above 100 Mev) is about 1/2 hour for flares in the western hemisphere and about 1-1/2 hours in the eastern. The average rise times for the particles with energies above 100 Mev are 2-3 hours and 6-8 hours for the western and eastern hemispheres respectively. The onset and rise times for the isotropic component of particles with energies above 30 Mev are longer by a factor of 2 in each event, but otherwise show the same characteristics.

A detailed examination of the rise-time characteristics for particles with energies above 100 Mev during a number of events reveals that this increase in solar particle intensity may be closely approximated by

$$I = I_{Max}(E)\, e^{-t/t_R} ,$$

where t_R is the characteristic rise time and t is measured from the time of peak intensity $I_{Max}(E)$ back to the time of the flare. In view of our previous statements t_R will be a function of the energy of the particles and also of the position of the flare on the sun.

The decay of intensity of the solar flare particles near the earth, like the onset characteristics, appears to be related in some lesser degree to the position of the flare on the sun. Thus, the time scales of the decays will be related to the time scales of the onsets just discussed, although there is not a strict one-to-one correspondence between these features. A detailed examination of the decay characteristics of a number of events reveals that the

Table 1-1

Solar Flare and Cosmic Ray Data Relating to
the Major Solar Cosmic Ray Outbursts Occurring
During the Years 1956-1961

Year	Date		Solar Flare Data			Cosmic Ray Data										
		Importance	Heliographic Position (degrees)	Time of Optical Maximum	Maximum 3-10 kMc Emission $\left(\frac{w}{m^2\text{-cps}}\times10^{-22}\right)$	Onset and Rise Time (hours)		Decay Time (hours)		Peak Intensity**		Characteristic Spectrum	Integrated Intensity $\left(\frac{particles}{cm^2\text{-sec}}\right)$		Integrated Skin Dose (rad)*	
						>30 Mev	>100 Mev	>30 Mev	>100 Mev	>30 Mev	>100 Mev		>30 Mev	>100 Mev	>30 Mev	>100 Mev
1956	Feb 23	3+	N22 W74	0340	20,000 at 0341	6-8	3-4	30	16	6,200	5,000	325	6.5×10^8	3.2×10^8	120	28
	Aug 31	3	N16 E16	1241		No detailed estimate possible							3×10^7		10	
	Jan 20	3+	S25 W30	1120						2,000-3,000	100-200		3×10^8	10^7	60	1.2
	Jul 03	3+	N14 W40	0740									1×10^7		3	
1957	Aug 29 to 31	(uncertain flare, possibly two events)				No detailed estimate possible							5×10^7		15	
	Oct 20	3+	S26 W45	1642		No detailed estimate possible				200-300	~10		1×10^7		3	
	Feb 09	2+	S12 W14	2142		No detailed estimate possible							5×10^6		1.5	
1958	Mar 23	3+	S14 E78	1005	10,000 at 1004			(40)	(20)	1,200-1,500	~50		2×10^8	5×10^6	50	0.7
	Jul 07	3+	N25 W08	0115	2,000 at 0112	10		32	16-20	1,500-2,000	~80		3×10^8	7×10^6	80	1.0
	Aug 16	3+	S14 W50	0440	6,200 at 0442			18		200			2×10^7		4	
	Aug 22	3	N18 W10	1448		10-12	3-4	20	8-12	500	20		5×10^7	1×10^6	20	0.15
	Aug 26	3	N20 W54	0027	6,700 at 0025	~9		(12)		1,100			5.3×10^7		17	

Year	Date															
	May 10	3+	N23 E47	2118	10,000	18-22	12-18	22	10-14	6,000-8,000	1,000	60	7×10⁸	7.5×10⁷	440	10
1959	Jul 10	3+	N22 E70	0222	15,000 at 0224	30-40	18-20	40	20	4,000	1,200	90	8.8×10⁸	1.0×10⁸	148	11
	Jul 14	3+	N16 E07	0349	6,300 at 0352	16-20	12-18	18	9-12	10,000-12,000	1,200	70	1.1×10⁹	6.3×10⁷	177	7.4
	Jul 16	3+	N08 W26	2145	6,500 at 2200	12-14	4-5	30	18	16,000-18,000	1,500	110	8.1×10⁸	1.3×10⁸	125	19
	Apr 01	3	N12 W10	0859		2-3	<1	12	4-6	50	6		2.7×10⁶	1.5×10⁵	0.6	0.001
	Apr 05	2+	N10 W61	0245	~8,000 at 0203			12		40			2×10⁶		0.7	
	Apr 28	3	S05 E34	0130		8-10	3-4	18 / 24	8	300	20		2.5×10⁷	7×10⁵	6	0.08
	May 04	3+	N14 W90	1020		2-3	<1	8	4	200	40		7×10⁶	7×10⁵	16	0.07
1960	May 06		uncertain flare							50-100			5×10⁶		1.5	
	Sep 03	3	N18 E88	0110	12,000 at 0108	12-16	7-9	32	26	240	60		4×10⁷	7×10⁶	4	0.6
	Nov 12	3+	N27 W02	1329	10,000 at 1329	12-16	8-10	18-24	14-18	12,000	2,500	145	1.4×10⁹	3.5×10⁸	205	33
	Nov 15	3+	N30 W32	0221	14,000 at 0227	10-16	3-5	16-20	8-12	6,000	2,400	135	5.2×10⁸	1.2×10⁸	100	12
	Nov 20	3	N28 W113	2020		3-4	~1	10-16	4-6	1,000	4,000		6×10⁷	6×10⁶	15	0.7
	Jul 11	3	S06 E32	1700	2,500	8-10	4	22-26	18	20	3		2×10⁶	3×10⁵	0.5	0.03
	Jul 12	3+	S07 E22	1030	7,500	8-12	6	16-20	12	120	15	50	1.0×10⁸	1.6×10⁶	10.5	.29
1961	Jul 18	3+	S06 W60	1010	5,000	6-10	2-3	24	12	2,500	600	135	2.1×10⁸	4.8×10⁷	27	3
	Jul 20	3+	S07 W90	(1600)	2,500	4-6	1.5	6-8	3	300	70		9×10⁶	1.2×10⁶	2.5	0.2
	Sep 28	3	N14 E30	2223								250	2.2×10⁵	9.7×10⁴	0.5	0.15

*In units of rads; 1 rad = 3.2×10^7 (particles/cm²) × average specific ionization in units of minimum ionization.

decay may be closely approximated by

$$I = I_{Max}(E) e^{-t/t_D} ,$$

where t_D is the characteristic decay time which depends on the energy and probably to some extent also on the flare's location; and t is measured from the time of the peak intensity $I_{Max}(E)$ to later times in the event. For particle energies greater than 100 Mev, t_D ranges from 10 to 20 hours in 15 of the 18 events in which it was possible to determine a characteristic decay time. There is some tendency for the longest characteristic decays to be associated with flares near the sun's east limb; and the three shortest decays, with characteristic times less than 10 hours, are all associated with flares occurring near the west limb (and in active centers which had previously produced cosmic rays). Consequently, there is the aforementioned relation between t_R and t_D. The average for the 18 events, considering particle energies greater than 100 Mev, is $t_D/t_R \approx 4$ with extremes from 1.5 to 6. The characteristic decay times for particles with energies exceeding 30 Mev are about twice as long as for particles with energies exceeding 100 Mev. A similar ratio for t_D/t_R also exists for the lower energy particles, since t_R for the latter is also twice t_R for particles with energies greater than 100 Mev.

The utilization of the characteristically similar intensity-time behavior for events having widely differing peak intensities and occurring at different locations on the sun permits a fairly simple estimate of the total integrated intensities of particles with energies greater than 30 Mev and those with energies greater than 100 Mev in space near the earth. Thus for J, the total integrated intensity in an event, we have

$$J(>E) = \int_{-\infty}^{0} I_{Max}(>E) e^{-t/t_R} dt + \int_{0}^{\infty} I_{Max}(>E) e^{-t/t_D} dt$$

$$= \left(t_R + t_D\right) I_{Max}(>E) ,$$

where zero time is the time of the peak intensity $I_{Max}(>E)$ of the particles whose total integrated intensity is to be determined. We recall that the characteristic spectra for each event, defined by the average differential spectral index n_0 existing at energies greater than 30 Mev when the intensity of these particles is a maximum $\left[\text{i.e.,} \; (dI/dE) = K/E^{n_0}\right]$, does not vary greatly from event to event and generally lies between 3.5 and 5.0. There is some tendency for the larger events to have the smaller values of n_0 (e.g., 3.5 to 4.0).

The total skin or free-space doses evaluated for each event depend only on the total integrated particle intensity/cm^2 and the average specific ionization (relative to the minimum ionization) of each particle. Meanwhile, the average specific ionization per particle depends on the spectral index of the radiation. As we have noted, this exponent varies over

the course of a single event, being smallest at earlier times and greatest at later times, and is also a function of the energy range considered. However, an average value over the course of an event is probably close to n_0; thus we use this value to obtain the average specific ionization per particle of the radiation. This ionization ranges from about 6 times minimum for an index of 3.5 to about 10 times minimum for an index of 5.0, assuming the incident radiation to be composed of protons only. (The minimum ionization is 1.6 Mev/gm-cm^2 in air or 2.6×10^{-6}erg/gm-cm^2. Since one roentgen equals 83.7 ergs/gm of air, an integrated intensity of 3.2×10^7 particles/cm^2 of minimum ionization produces a dose of one roentgen.)

Problems relating to the anisotropies of the flare particles and the charge composition are of major importance in the overall scientific interpretation of these events. These problems will be discussed in Chapters 2 and 3.

SUMMARY OF SOLAR COSMIC RAY EVENTS IN RELATION TO
DOSE RATES OBTAINED IN SPACE

The main objective of this summary of solar cosmic ray events is, of course, to attempt an evaluation in general terms of the radiation hazard in space presented by these events. It seems reasonable to evaluate the hazard in terms of the integrated dose of galactic radiation, for this radiation forms an almost constant background in space — and one so penetrating that reasonable shielding considerations have little effect on the intensity of the radiation. The free-space galactic particle intensity varies from 1.5 particles/cm^2-sec near sunspot maximum to about 4 particles/cm^2-sec near sunspot minimum. The integrated weekly rates are thus roughly 1×10^6 and 2.5×10^6 particles/cm^2 respectively; the yearly rates range from 5×10^7 to 1.2×10^8 particles/cm^2. (Assuming an average specific ionization about 4 times minimum for these galactic particles, the integrated weekly doses range from 0.1 to 0.3 rad and yearly doses from 6 to 20 rads.)

In Table 1-2 the yearly integrated intensities of solar particles above 30 and 100 Mev are compared with the total integrated intensity of galactic particles for the years 1956-1961. Over this six-year period the integrated intensity of solar cosmic rays with energies greater than 100 Mev and greater than 30 Mev are respectively, about 4 and about 50 times the total integrated galactic intensity. Most of the solar cosmic ray intensity occurs during the three particular years 1956, 1959, and 1960. In fact, most of the solar cosmic ray intensity comes from the solar events associated with only three active centers: McMath Plage 3400 for the February, 1956 event; 5269 for July, 1959; and 5925 for November, 1960. The remaining events during the six-year period contribute only 0.3 and 6 times the integrated galactic intensity above 100 Mev and 30 Mev, respectively. In addition a study of the smaller events not individually listed here reveals that, even if the frequency of these events is 20 to 30 a year, the integrated yearly intensity of solar cosmic

Table 1-2

Yearly integrated Intensities of Solar Cosmic Rays
with Energies Above 30 and 100 Mev and of
Galactic Cosmic Rays.

Year	Number of Events	Solar Cosmic Rays Integrated Intensity (particles/cm^2)		Galactic Cosmic Rays Integrated Intensity (particles/cm^2)
		> 30 Mev	> 100 Mev	
1956	2	8×10^9	8×10^8	1×10^8
1957	4 or 5	4×10^8	1.5×10^7	7×10^7
1958	6	1×10^9	1.4×10^7	6×10^7
1959	4	7×10^9	5.2×10^8	6×10^7
1960	8	5×10^9	4.1×10^8	8×10^7
1961	5	2.7×10^8	3.3×10^7	1×10^8
TOTAL	30	2.1×10^{10}	1.8×10^9	4.7×10^8

rays with energies greater than 30 Mev from these events is not likely to exceed that from galactic cosmic rays. Thus we can state that during a time scale of one year — neglecting the three largest events — the integrated intensities of solar cosmic rays with energies above 30 Mev and of galactic cosmic rays are comparable; and with a reasonable minimum shielding of only 3 to 4 gm/cm^2 the yearly average dose from solar cosmic rays is less than that from galactic cosmic rays (i.e., less than 20 rads).

Thus, the problem of radiation exposure from solar cosmic ray outbursts would reduce to the problem of such exposure from the few largest events. The total integrated dose from these events may present a problem, the seriousness of which depends on the amount of shielding — as can be seen from the doses due to particles with energies above 30 and 100 Mev (Table 1-1).

The statistics relating to the frequency of occurrence of the largest events are, of course, very limited — three events in six years, or an average of one event every two years. Only one of these three events would have been observable by the techniques used prior to 1950, when four events were recorded in about five years of observation. If we assume that the techniques in operation during this period could detect one out of three events of truly major importance, about 12 such events may have occurred during the

15-year period. These considerations are undoubtedly crude but they are the best available at present. Combined with the recent, more definitive data, they suggest that on the order of once every eighteen months an active region appears that will ultimately emit one or more major cosmic ray bursts. Although dozens of smaller events may occur during such a period, they are relatively unimportant in consideration of the overall integrated solar cosmic ray intensity.

It is quite certain that the appearance of active regions producing major cosmic ray bursts is *not* strongly correlated with the maximum in the eleven-year cycle of solar activity. During the recent maximum, 1957-58, no such major cosmic ray bursts were recorded, and the yearly integrated solar cosmic ray intensities at energies greater than 30 and 100 Mev were lower than for adjacent years of lower solar activity. From the limited number of large events available for study it appears that they are most frequent during periods of increasing and, particularly, decreasing solar activity, with the periods near maximum and minimum relatively free from such events. In other words, in periods of increasing or decreasing solar activity the frequency of potentially dangerous cosmic ray outbursts may be greater than one per eighteen months and, in periods near maximum or minimum, less than one per eighteen months.

CHAPTER 2

DETAILS OF INDIVIDUAL SOLAR PARTICLE EVENTS

by

Carl E. Fichtel, Donald E. Guss, and K. W. Ogilvie

[handwritten: for the Solar Proton Manual]

[handwritten: Dec. 1963   p 19-55   refs   (See N64-17889   10-28)   OTS: $2.75]

INTRODUCTION

[handwritten: A55]

This paper attempts to present a time history of the intensities and energies of solar cosmic ray particles detected at or near the earth. Ideally it would be desirable to show the complete energy spectrum of the proton component in these events as a function of time. Upon consideration of the incomplete information and uncertainties involved in the measurements, however, we see that this can only be done approximately. Regions of time and energy which have not been adequately surveyed can be described only by interpolation and, to some extent, by extrapolation. The goal is to remain within a factor of 2 of the real intensity at all times. Frequently the accuracy attained is very much better.

This survey begins with the event on February 23, 1956 — the first one for which there is an estimate of both the low and high energy flux components. All of the largest events from that date to the present and some of the smaller ones for which particularly complete data are available have been selected for examination. All events for which there was a riometer reading in excess of 10 db (indicating a particle flux greater than about 600 particles/cm^2-ster-sec for particles with energies above 20 Mev) have been included. Also any event with a high energy component sufficiently large to be detected on the neutron monitor has been studied. Events for which less than 10 db of absorption was detected on the riometer and no detectable neutron monitor increase was observed have, in general, been included only if there were other data from detectors flow on balloons and satellites.

The description of the various detectors used to study the solar particles will be followed by a discussion of the individual events in order to emphasize the interesting features and the variety of geophysical effects occurring from time to time. The descriptions will be followed by diagrams giving the integral flux as a function of time above specified energies and energy spectra at various times during the event. Finally, an imaginary event will be presented which is just large enough to include all the types of events observed.

19

DETECTORS

The Riometer

The riometer measures the signal strength of extraterrestrial radio noise (References 15 and 16). During solar particle events the bombardment of the earth by energetic charged particles increases the electron density in the upper atmosphere causing absorption of the extraterrestrial noise and a consequent decrease in the signal measured at the ground (Reference 17). The particles primarily responsible for this absorption are protons in the 20-200 Mev kinetic energy range. Owing to the earth's magnetic field these particles can enter only at high latitudes; hence, this phenomenon is termed polar cap absorption (PCA). Thus at high latitudes, a riometer permits continuous monitoring of the intensity of protons in this energy range.

Magneto-ionic theory shows that, if the riometer observation frequency, ω, is much greater than both the critical frequency of the ionosphere and the longitudinal component of the magnetic gyrofrequency, the absorption for a vertically incident plane wave is found by integrating the following equation over the height of the ionosphere:

$$A = 0.46 \int \frac{N\nu}{\nu^2 + \omega^2} \, dh , \tag{2-1}$$

where A is the absorption in decibels, N the electron density, ν the electron collision frequency, and h the altitude in centimeters. The electron density at any height is related to the electron production rate q by the equation

$$N = q^{1/2} \left[(1 + \lambda)\alpha_e \right]^{-1/2} , \tag{2-2}$$

where α_e is the effective recombination rate for electrons and λ is the negative-ion to electron ratio. By substitution of Equation 2-2 into Equation 2-1, we then get the following equation.

$$A = 0.46 \int q^{1/2} \left[\nu(\nu^2 - \omega^2)^{-1}(1 + \lambda)^{-1/2}\alpha_e^{-1/2} \right] dh . \tag{2-3}$$

During a PCA event, the electron production rate at any altitude is directly proportional to the total rate of energy loss by ionization of solar protons at that altitude. Equation 2-3, then, is a relation between the absorption measured by a riometer and the intensity and energy spectrum of the particles causing the PCA. For spectra of the same shape Equation 2-3 also predicts that the absorption in decibels is directly proportional to the square root of the particle intensity, provided the quantity in the brackets is independent of q.

During the daytime this is indeed the case to a high degree of accuracy, but there is a some-what important dependence of λ on q during times of darkness.

Because of the photo-detachment effect of sunlight on the ionosphere, the absorption during a PCA is much stronger during the day than at night. A calculation by Reid (Reference 18), based on currently accepted values for the atmospheric parameters, yields a value of about 3 for the ratio of day to night absorption at any observing frequency of 30 Mc for a particular spectrum shape. Observations indicate that the average ratio is about 4, but that it can vary considerably and is sometimes as large as 10 or 12. The riometer provides its most useful information during the daylight hours and conversion of nighttime absorption readings to effective daytime absorption readings must be approached with some caution.

By the nature of its response, the riometer absorption is a function of geomagnetic lati-tude. However, the riometer records from College, Alaska; Churchill, Canada; and Thule, Greenland, generally show approximately the same absorption, though the cutoff energies for protons calculated by Quenby and Webber (Reference 19) are 113, 6.4, and approximately 0 Mev., respectively. Here it was assumed that the absorption from these stations was equivalent, and absorption values from stations other than Churchill were used when needed.

In order to calculate the expected absorption during a PCA the particle spectrum, inten-sity, and directionality must be known. The radiation causing the PCA is generally assumed to be isotropic over the upper hemisphere; and this is a good approximation a few hours after the flare causing the event. The electron production rate must be determined from the spec-trum shape and intensity, and Equation 3 integrated. This has been done by a number of authors (References 17, 18, and 20) for specific times in specific events where some spec-tral details have been determined experimentally.

To find the spectral shape and intensities of solar particles from the observed absorp-tion is a more ambiguous process, and several assumptions must be made. A calculation by Brown and Weir (Reference 20) shows that for protons with energies greater than 100 Mev, the predicted absorption is very insensitive to the shape of the energy spectrum and depends primarily upon the particle intensity. A similar calculation by Bailey (Reference 17) indicates that the same is true for particles in the energy range between 20 and 100 Mev. For protons with energies at the top of the atmosphere less than about 20 Mev the effectiveness for pro-ducing absorption is a rapidly decreasing functon of energy, because protons of these ener-gies ionize primarily at altitudes where the electron collision frequency is small.

From a series of rocket shots during PCA's in the fill of 1960 the energy spectra and intensities of protons were obtained down to energies below 20 Mev for a variety of riometer absorption intensities (References 21 and 22). The results indicated that for these events, the shape of the energy spectrum does not remain constant to very low energies. If the shape

22

of the energy spectrum is expressed by means of a power law

$$dN(E) = CE^{-\gamma}dE ,$$

(2-4)

then the exponent γ is a decreasing function of energy. Because of this and the fact that protons with energies below 20 Mev are less effective in producing absorption, it was assumed that the absorption at the times of the rocket shots was determined by the intensity of particles with energies greater than 20 Mev. The proton intensity at energies greater than 20 Mev is plotted against the observed absorption on the 30 Mc riometer at Churchill in Figure 2-1. This curve was subsequently used to obtain the PCA-determined particle intensities for the other events studied here. The extremum lines shown in Figure 2-1 indicate the uncertainty in the riometer readings alone and do not reflect the uncertainty in the resulting particle intensities, which is estimated to be about a factor of 2.

The shape of the energy spectrum for most solar particle events shows that the primary contribution to the absorption is from protons in the energy range below 100 Mev, since the
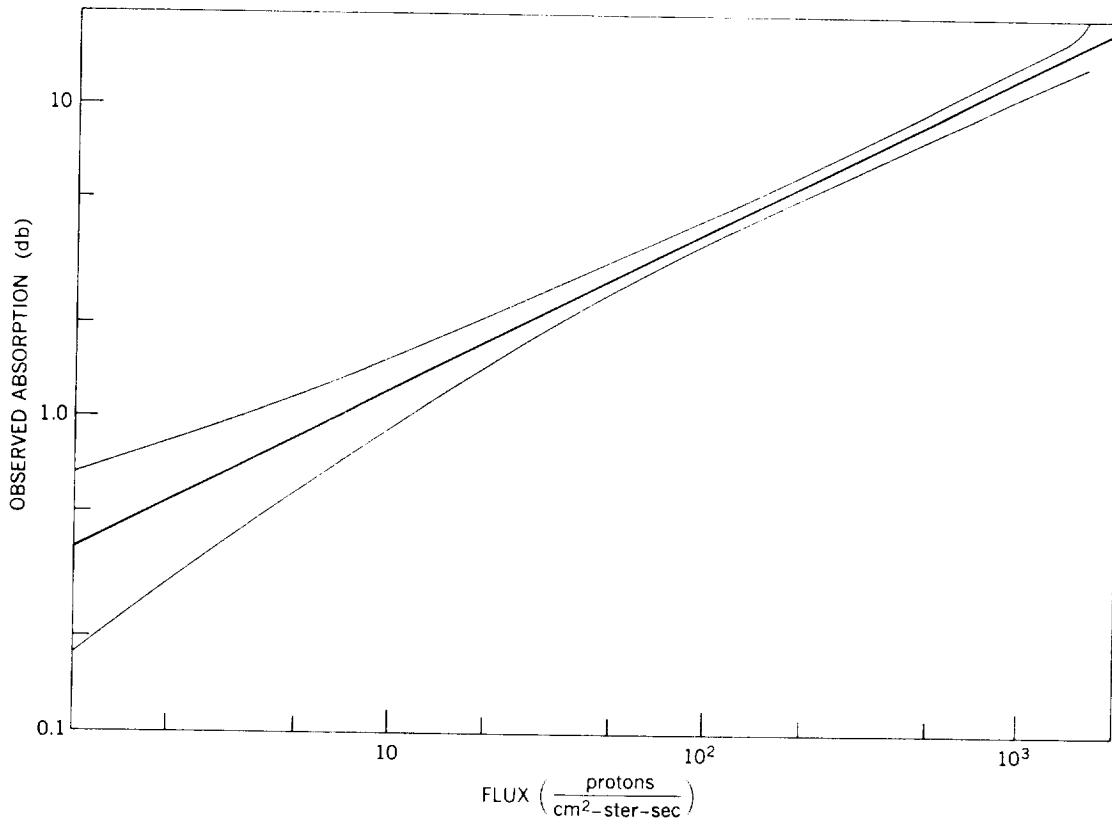
Figure 2-1—Proton flux versus riometer absorption

particle intensity above this energy is negligible by comparison, except for times early in the events. If the energy spectrum at higher energies is known, a knowledge of the absorption data makes it possible to show something of the nature of the spectrum as well as the intensity below 100 Mev. For example, the proton flux was measured during the daylight hours of July 13, 1961 by nuclear emulsions on a balloon flight at Churchill. The intensity with energies above 78 Mev was 1.6 P/cm^2-ster-sec, and between 78 and 230 Mev $= 5.5 \pm 0.3$. Extrapolating this spectrum back to 20 Mev would result in an intensity 7.9×10^{-2} P/cm^2-ster-sec which, from Figure 3, corresponds to an absorption of 11 db. However, the observed absorption on the 30 Mc polar riometer at Churchill was equal to or greater than 15 db during the entire flight, while that on the 27.6 Mc riometer at College varied from 14.5 to 17.5 db. This indicates that the shape of the spectrum did not change appreciably down to energies below 20 Mev. It must be noted that, although particles below 20 Mev become increasingly less effective at producing absorption, there would be 16 times as many particles between 20 and 10 Mev as there are above 20 Mev if γ did not decrease with energy.

The above example shows that the deduction of particle intensities from the curve of Figure 2-1 must be approached with some caution. If the shape of the energy spectrum is such that there is a very high intensity of particles with energies below 20 Mev, the intensities from Figure 2-1 must be looked upon as an upper limit, when interpreted as an integral intensity of particles of kinetic energy greater than 20 Mev. In the section where specific events are discussed, events which are suspected or known to be of this type will be noted.

The interpretation of riometer absorption in terms of particle intensities is complicated by two other problems: the superposition of auroral absorption upon the PCA; and the occurence of anomalous but real changes in absorption.

At stations within the auroral zone riometers show auroral absorption as well as the PCA. College lies near the maximum of the auroral absorption zone, and Churchill at the northern edge. Usually the auroral absorption can be at least partially eliminated since it appears as absorption spikes superposed upon the generally smoothly varying PCA. Leinbach and Reid (Reference 23) suggested that the PCA is best represented by the minimum absorption recorded over a period of several hours when auroral absorption is present.

During a number of PCA events anamalous decreases of absorption have been observed immediately following a sudden commencement. These have been discussed by J. Ortner, et al. (Reference 24). Leinbach (Reference 25) has also noted the occurrence, on some occasions, of *mid-day recoveries* at College, and on at least one occasion this phenomenon was observed at Churchill. These seem best attributed to local changes in the geomagnetic cutoff or local changes of the characteristics of the absorption layer rather than to a change in the intensity of the particles causing the event.

Increases in absorption have also been observed near the time of a sudden commencement (Reference 24). Recently, it was found that the sudden increase in absorption

24

immediately preceding a sudden commencement following the flare of September 28, 1961 was coincident with an increase in the intensity of very low energy particles as observed by the satellites Explorer XII (Reference 27) and Injun I (Reference 3) (1961υ and 1961σ2, respectively).

In general, it is assumed herein that the PCA is a smoothly varying function of time, although a sustained increase in absorption following a sudden commencement is interpreted as an increase in particle intensity. "Spikes" are generally interpreted to be auroral absorption or due to local manipulation of the ionization causing the absorption rather than actual fluctuations in particle intensity.

In calculating particle intensities, the daytime values of absorption from the 30 Mc riometer at Churchill were used whenever possible. During periods of particular interest a factor of 4 was used to convert nighttime absorption to effective daytime absorption unless this procedure seemed unreasonable. At several periods of importance the absorption records from College, Barrow, and Thule were used. These riometers record a higher absorption before saturating than does that at Churchill. In all cases it was assumed that there was no effective cutoff operating at any of these stations.

Webber (Reference 3) has also calculated particle intensities from riometer records for several events. The absorption for a 30 Mc riometer and for a differential rigidity[*] spectrum of the form

$$dN(R) = CR^{-6}dR \qquad (2-5)$$

was calculated in a manner similar to that of Bailey (Reference 17) but with the more recent values for the atmospheric constants. He then used these curves to calculate the particle intensities as a function of time for a number of PCA events. In Figure 2-1, the transformation from db to particle intensities agrees quite well with the values obtained by Webber and the differences in particle intensity are results of differences in interpretation of the absorption. The most notable difference occurs for the event of February 23, 1956. Before the sudden commencement Webber assumed a proton cutoff of 113 Mev at College, Alaska. In this paper, we assume that there is no effective cutoff at College and that the absorption increase following the sudden commencement is attributable to an increase in very low energy particles similar to that observed on September 28, 1961.

The Neutron Monitor

The neutron monitor (Reference 28) consists of an extensive structure in which BF_3 neutron proportional counters are surrounded by an arrangement of lead and paraffin blocks. A high energy proton or neutron passing through this lead has a high probability of undergoing

---

[*]Rigidity is defined by the equation $R = pc/z$, where R is the particle rigidity, p its momentum, z its charge, and c the velocity of light.

an interaction similar to a *star* in a nuclear emulsion; and some of the reaction products
will be neutrons. These neutrons are slowed down in the paraffin by collisions with hydrogen
nuclei, which are then detected by the counters. Thus the detected particles are, for the most
part, secondaries to the nucleonic component of the cosmic radiation at sea level. Conse-
quently, the neutron monitor is more sensitive to primary particles of rigidity in the range 1
to 2 Bv than any other sea level monitor. The neutron method of detecting cosmic ray inten-
sity changes also has the advantage that the necessary corrections for meteorological effects
can be made accurately, as cannot be done, for instance, with a meson detector.

We can write (Reference 29), the following relation between the counting rate of a moni-
tor and the primary spectrum:

$$N\left(R, x, t_0\right) = \int_{R_0}^{\infty} S(p, x) \; \frac{dJ(R, t)}{dR} \; dR \; . \tag{2-6}$$

Here the counting rate — a function of rigidity, time, and the depth of the detector in the
atmosphere — is obtained from the primary differential spectrum J by multiplying dJ for a
rigidity interval dR by a function $S(p, x)$, and integrating over a range of rigidity from R_0 to

infinity. The quantity S, called the specific
yield function, gives the number of second-
ary particles detected in a neutron monitor
at any given atmospheric depth as a func-
tion of primary particle rigidity. It depends
upon the composition of the primary radia-
tion, and henceforth we shall assume that
this remains constant. R_0, the lowest pri-
mary rigidity incident at the top of the at-
mosphere, is a function of the geomagnetic
coordinates of the detector. Atmospheric
absorption causes S to go to zero for R less
than about 1 Bv independently of the influ-
ence of the earth's magnetic field. In Fig-
ure 2-2 S is plotted in terms of R.

Thus, if particles in the rigidity range
from about 1 Bv upwards are isotropically
incident upon the earth, a network of neutron
monitors set up at points with known R_0 per-
mits something to be learned about their
energy spectrum, since S is known. This
situation is complicated by at least two
effects. If the source of the particles is
localized in space in a region surrounding the
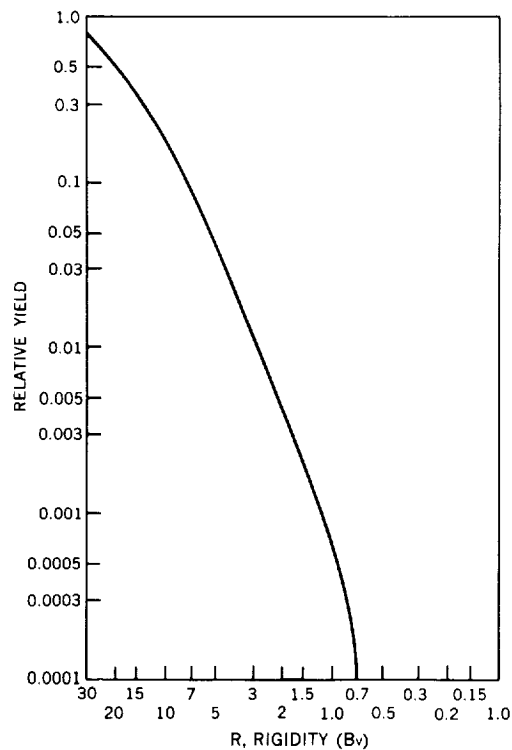
Figure 2-2—The specific yield function

sun, for example, we cannot assume in general that the particles are incident isotrop-
ically. In fact, anisotropic incidence usually occurs early in the solar event; later isot-
ropy can usually be assumed. An intense magnetic storm can change the magnetic thresh-
old rigidity R_0 and this must also sometimes be taken into account.

The motion of particles toward the earth from the sun has been studied by many
authors (References 30 and 31), and we now have a fair knowledge of the effects which
occur. These are discussed in detail in Chapter 3.

In Figure 2-3 the times of these events are superimposed upon a plot of smoothed
sunspot numbers (Reference 32). Even making allowance for the increase in the number
of detecting stations during the past solar cycle it seems, in contrast to the PCA, that
there is a definite tendency for flares producing a large flux of particles in the Bv rigid-
ity range to occur during the increase and decrease of sunspot activity rather than during
the maximum. At present there is no explanation for this tendency.

Using the neutron monitor record we can determine easily the percentage increase in
the rate at any time during an event. The background rate is caused by the galactic cosmic
rays which are always incident upon the earth. If we use the known spectrum of these parti-
cles and the specific yield functions[*], we can obtain from Equation 2-6 a quantity propor-
tional to the rate due to particles having rigidities above R_0. A similar calculation made
with various assumed or measured spectra for the flare particles gives a quantity propor-
tional to the additional rate due to flare particles. A difficulty arises in that the primary
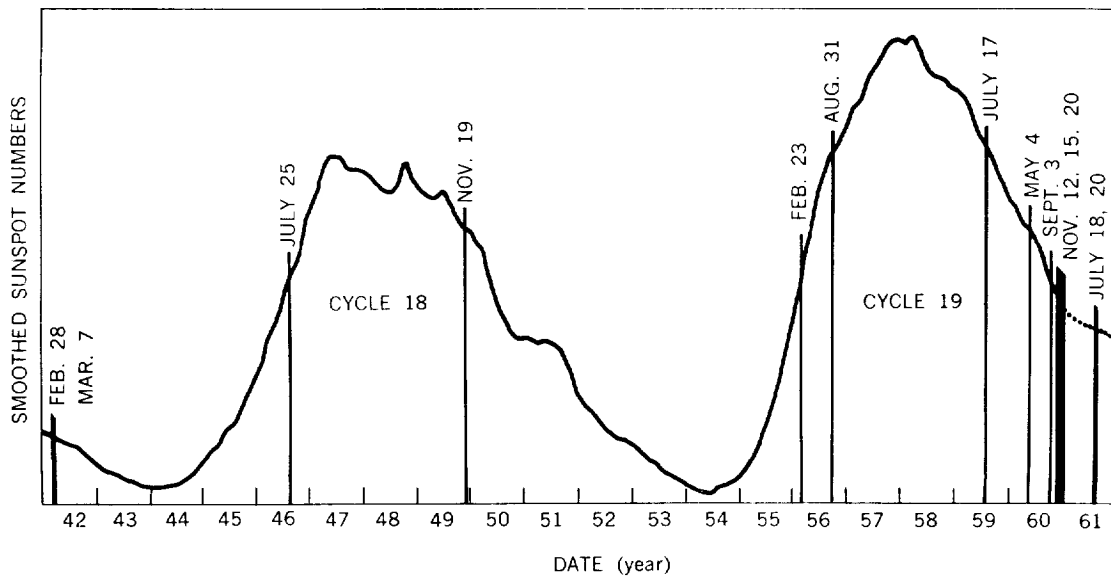
Figure 2-3—Distribution of cosmic ray events detected at sea level as a function of the solar cycle

---

[*]Obtained by using the revised specific yield function shown in Figure 2-2.

spectrum varies with time over the solar activity cycle (References 33 and 34) but an approximate correction can be made for this. Various relevant assumed spectra and threshold rigidities have been employed in Table 2-1 to show the intensity increase required above rigidity R_0 (in units of the normal cosmic ray background above R_0) to double the counting rate of a neutron monitor. We shall use these figures and the primary spectrum variations to deduce intensities in the rigidity range from the observed counting rate increases. By using the figures in the second column for interpreting rate increases of neutron monitors situated at points where the cutoff rigidity is less than 1 Bv, we make the assumption that they are not affected by the additional particles present. Thus a 5 percent increase in the rate of a high latitude neutron monitor $(R_0 = 1 \text{ Bv})$ indicates, if the incident spectrum is $1-p^6$, an incident flux of $0.05 \times 13 \times J_0 = 0.05 \times 13 \times 0.23$ (in February 1956) $= 0.150/\text{cm}^2\text{-ster-sec}$, in addition to the background above 1 Bv. The minimum increase that can be detected with certainty is less than 5 percent, and probably about 2 percent. This figure depends to some extent on the monitor involved and upon geophysical conditions. For example a confusing situation might arise if the increase in flux occurs during a Forbush decrease. At such times the diurnal variation in rate becomes large and irregular in phase and might conceivably obscure a slow change due to solar emitted particles.

The procedure outlined above for determining the intensity of particles away from the earth, requires two approximations. First, there is the question of the primary spectrum referred to above; and second, the specific yield function has been extrapolated from 2 Bv to 1 Bv — a region of critical importance with steep spectra. In deducing the spectra the assumption is made that the intensity of the radiation in the asymptotic cones of acceptance is the same; this is difficult to check, but probably true. It seems likely that the intensities given here are accurate to at least a factor of 2. The largest contribution to the error arises from the uncertainty in the knowledge of the spectral exponent.

Table 2-1

The Radiation Increase Required above Rigidity R_0 (in Units of Normal Cosmic Ray Background above R_0) to Double the Counting Rate of the Neutron Monitor.

Differential Spectral Exponent	Intensity Increase			
	$R_0 = 1$ Bv	$R_0 = 2$ Bv	$R_0 = 3$ Bv	$R_0 = 5$ Bv
4	10	17	24	40
5	12	31	62	160
6	13	45	130	—

Direct Primary Particle Detectors

Some information on solar cosmic rays has been obtained directly from particle detectors flown on balloons, sounding rockets, and satellites. Balloon borne experiments have provided valuable information on the intermediate energy interval (between approximately 80 and 500 Mev) for protons. The lower limit of the energy interval is determined by the air cutoff — usually of the order of 6 gm/cm^2. The upper energy limit is set by the difficulty of obtaining anything but an integral flux above that energy with the detectors used and the fluxes observed.

The detectors used on these flights can be divided into three very broad groups: nuclear emulsions; simple omnidirectional or wide-angle counters; and complex electronic systems including both a small solid angle and fine energy discrimination. Nuclear emulsions have the advantage of yielding an excellent energy spectrum and permitting one to determine the charge composition, but have the disadvantage of not providing time variation information throughout a flight. Simple counters do provide time resolution, when other factors such as balloon altitude variations are not present; but it is difficult to deduce good quantitative flux values because of the absorber variation as a function of solid angle and, in some cases, the lack of sufficient knowledge about the energy spectrum. However, an estimate of the energy spectrum can sometimes be obtained by observing the counting rate as a function of altitude during ascent and by using atmospheric absorption information. In addition, for some flights, nuclear emulsion data exist for a time interval included in the counter record and may therefore be used as an absolute flux calibration for the counting rates. Unfortunately, there have been only a few balloon flights with electronic experiments capable of energy resolution, so information from this source is limited.

For balloons flown where the geomagnetic particle rigidity cutoff is normally greater than that caused by the residual atmosphere, there is the additional problem of time dependent magnetic field effects, which permit varying percentages of the total particle flux to reach the detector. At the present, it is not possible to construct a model, based upon existing data, which gives the actual percentages of transparency as a function of energy and time in the event. In practice, fortunately, at Minneapolis, where many of the measurements were made, the cutoff often seems either to be the same as during geomagnetically quiet times or not to exist for energies greater than the air cutoff. However, this difficulty has limited the degree to which the proton energy spectra of solar cosmic ray events can be described in quantitative detail.

Sounding rockets with recoverable payloads provide a means of studying these events above the earth's atmosphere with both electronic counters and nuclear emulsion techniques. Data from these payloads provide information on the proton energy spectrum down to a fraction of an Mev, and detailed charge composition measurements exist for three of the events to be included in the present analysis. This method provides only a sampling of the radiation at a few times during the event; however, it does help to calibrate those instruments which do record time variations, such as the riometer.

Finally, electronic experiments in satellites outside the Van Allen belts can give a detailed time history of the energy spectrum down to very low energies. However, not until Explorer XII was launched on August 15, 1961 did such a system exist; and at present, data giving the detailed history of the proton energy spectra are available only for the September 28, 1961 event. Previous satellites have provided integral fluxes above an energy cutoff, determined from the counting rate of a single detector under a known amount of material. These results have been used in developing the history of several of the events discussed in this report.

From several of the previously mentioned sources, it has been determined that protons are by far the most abundant nuclei in these events. In the same energy/nucleon interval (and hence the same range interval), helium nuclei are less abundant than hydrogen nuclei by a factor of 20 or more. Nuclei with a charge greater than 3 are more scarce than protons in the same energy/nucleon interval by a factor of a few thousand at low energies (40-100 Mev) and probably by a larger factor at higher energies.

HISTORY AND ENERGY SPECTRA OF EVENTS

In the diagrams of spectra presented here a solid curve indicates that the detailed energy spectrum has been obtained directly. A dashed curve indicates an interpolation between these data and the integral flux at 20 Mev deduced from PCA measurements.* In the time variation curves a solid line represents the particle intensity greater than 20 Mev; a dotted portion of the curve represents an extrapolation, and a blank space represents a portion for which a reasonable interpolation could not be made. This time variation curve normally was obtained from riometer results which were generally in agreement with satellite data at those times when a valid comparison could be made. The only exception is the latter portion of the May 4, 1960 event, for which information from a satellite-borne counter was available, but no riometer data. A dashed curve represents neutron monitor results, giving the integral intensity above 1 Bv rigidity, or about 440 Mev for protons, and a dot-and-dash curve represents the variation of intensity above 100 Mev. The zero of time represents the time of the beginning of the flare, and it should be noted that there is a change of scale at 12 hours.

0331 UT February 23, 1956

The February 23, 1956 flare produced the largest intensity of particles yet observed in the Bv range. However, the riometer observations show that the intensity of low energy particles was an order of magnitude smaller than in many other solar particle events

---

*With respect to the PCA measurements, it must be remembered that a very high intensity of particles with energies below 20 Mev can appreciably increase the riometer absorption. In such cases the particle intensity as deduced from Figure 2-1, interpreted as an integral intensity above 20 Mev, must be considered as an upper limit and may be as much as an order of magnitude too high. For events where this is suspected or known to be the case, it will be noted in the discussion of the particular event.

(Figure 2-4). There is only a single counter measurement (Reference 35) indicating an intensity at Minneapolis (threshold 0.81 Bv) 4-5 times normal at 2030 UT on the 23rd.

A great deal of work has been done on the neutron monitor observations of this event, and we shall summarize these with a view to finding the intensity, the spectrum, and their variation with time. The spectrum of particles at various times has been derived by examination of the latitude effect (Table 2-2).

Pronounced impact zone effects were seen during the first 10 minutes of the event (References 37 and 38) but isotropy may be safely assumed for much later times after 0400, at least in space close to the earth. The first spectrum refers to the direct radiation; that is to say radiation received in the primary impact zone, which covered most of Europe at the time. The storage region was not filled up at that time, but the steeper spectra observed later refer to radiation stored in that region. If we now apply our results to these observations, we arrive at the data given in Table 2-3. Thus an expression for the integral rigidity spectrum containing the best available information for the period from 0400 UT to 1000 UT is $150/p^5 \, t^{-3/2}$ with R in Bv above 1 Bv, and t in hours from 0400 UT. Simpson (Reference 28) has established that the neutron monitor rate at Chicago and other stations decayed according to a $t^{-3/2}$ law between 0430 and 1000 UT ($t \approx 0$ at 0350 UT), and exponentially thereafter with a decay constant of about 8 hours.

The peak intensity for particles with energies greater than 20 Mev, as deduced from the riometer observations at College (Reference 15) by using the curve of Figure 2-1, is radically different from the value at 30 Mev determined by Webber and Malitson;[†] the difference results from a difference in interpretation. Here it is assumed that the geomagnetic cutoff at College is not appreciably different from that at Churchill. This, indeed, seems to be the case during all other events for which comparisons are available. In reference 39, Sauer quotes cutoff values for various stations as computed by particle trajectories in the Finch and Leaton field. He obtains a cutoff rigidity for Churchill of 0.199 Bv in the absence of a ring current; this is approximately 21 Mev for protons. For College he obtains 0.497 Bev (120 Mev), but the presence of a ring current is found to reduce this

Table 2-2

February 23, 1956 High Energy Observations.

Source	Energy Threshold	Time from Flare	Diff. Rigidity Spectrum
Pfotzer	1 Bv	20 min.	p^{-4}
Simpson	1.6 Bv	2 hr. 20 min.	p^{-6}
		20 hr.	p^{-7}

*Reference 36
†Reference 37

†Chapter 1.

Table 2-3

February 23, 1956 High Energy Intensities.

Time from Flare (min.)	Station	Threshold (Bv)	Diff. Spectrum	Integral Intensity above Threshold $\left(\dfrac{particles}{cm^2\text{-ster-sec}}\right)$
20	Leeds	1.77	$1/p^4$	150
40	Chicago	1.6	$1/p^6$	160
50	Ottawa	1.05	$1/p^6$	90*
150	Chicago	1.6	$1/p^7$	34

*The inconsistency between Ottawa and Chicago may be due to the late arrival of particles at low energies.

to a marked degree. For example, a ring current of strength $Mr = 1$, located at 7 earth radii, which gives a cutoff for Churchill of 5 Bev agreeing with an exponential determination, will reduce this value to 0.247 Bv (32 Mev for protons) at College. In view of the reduction in the differential sensitivity of the riometer below 20 Mev, it becomes clear that the effective cutoff at College must often be low enough to produce riometer readings that are comparable to those observed at Churchill. It is a pity that the cutoff at College has not been measured directly. The interpretation here is that the event was large at high energy and small at low energy — similar to that of September 3, 1960 or July 18, 1961.

A small increase in absorption preceded the sudden commencement on February 25th and this was interpreted as an increase in particle intensity similar to that of the Explorer XII observations (Reference 26).

1030 UT August 29, 1957

In the August 29, 1957 event (Figure 2-5) a PCA lasted for 49 hours, reaching a maximum of 8 db at Churchill (Reference 40). There was no neutron monitor increase and also no increase detected at balloon altitudes between 1400 UT (Reference 41) on the 29th, an hour after the start of the PCA, and 0600 UT on the 30th. Such a detector could have found an increase of 10 percent, and from this fact it can be shown that the exponent γ of a spectrum $N = N_0 E^{-\gamma}$ must have been of the order of 6 or more.

32

(a) Time history

FLUX $\left(\dfrac{\text{protons}}{\text{cm}^2\text{-ster-sec}}\right)$

TIME FROM BEGINNING OF FLARE (hours)

ENERGY (Mev)

(b) Energy spectrum at 2030 UT, February 23 (+17 hours)
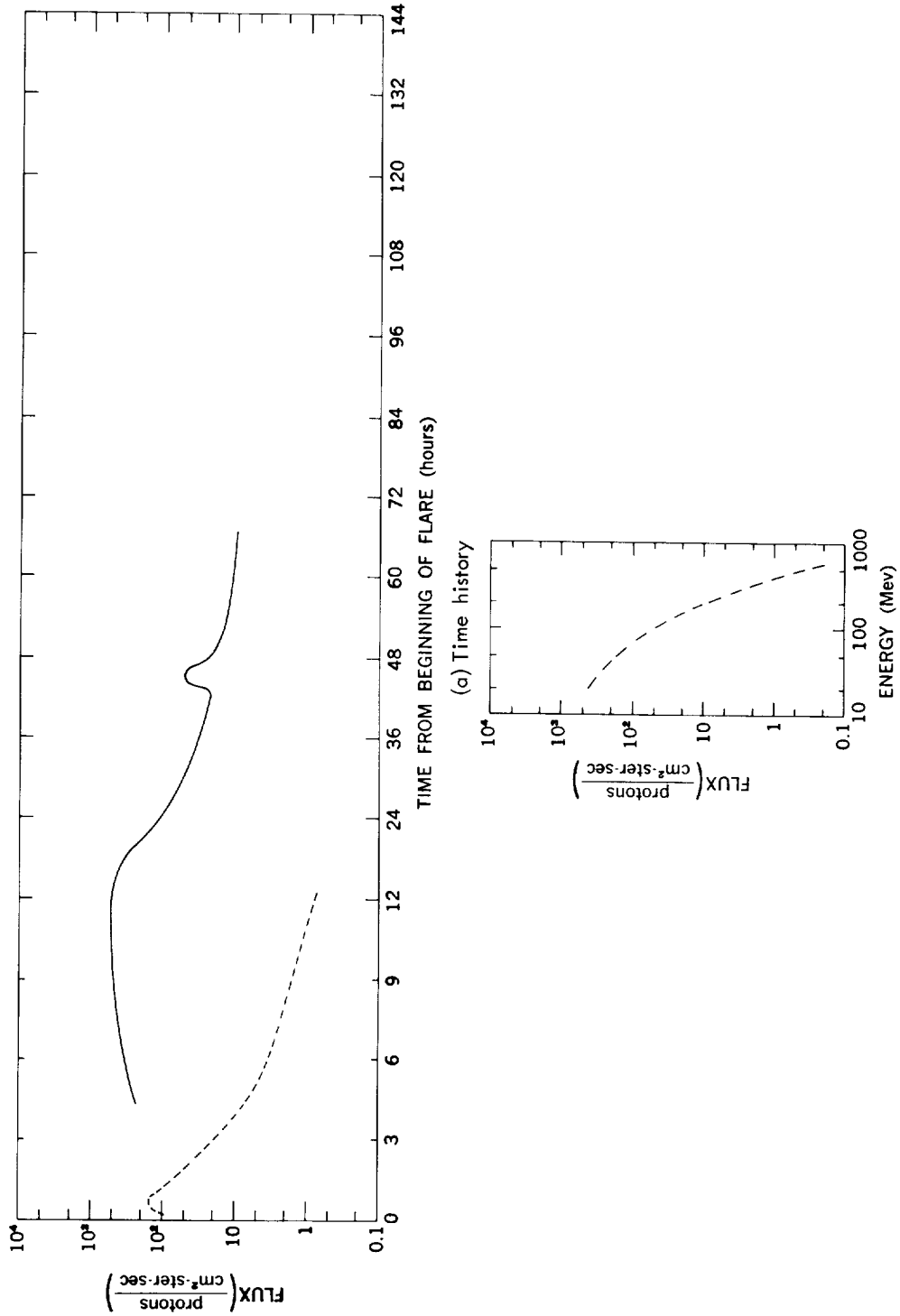
Figure 2-4—The February 23, 1956 event. The various curves are explained on page 29.

It is suspected that this event is one of those for which there was a high intensity of particles with energies below 20 Mev and, hence the intensity profile of Figure 2-5 must be considered as an upper limit.

0947 UT March 23, 1958

The PCA began within a few hours after the flare (Reference 42). At the time of the sudden commencement, 1540 UT on the 25th, there was a rapid increase in the PCA to about 12 db. This was probably a consequence of an intensity increase at low energies of the type observed by Bryant et al. (Reference 26) with instruments flown in Explorer XII on September 28, 1961. There was no detectable neutron monitor increase, but at 0700 UT on March 26th a lower limit of 0.07 ± 0.01 particle/cm^2-ster-sec (between 120 and 180 Mev), was determined by balloon measurements at Minneapolis (Reference 43). Probable variations of the magnetic threshold during the flight prevent anything more than the determination of a lower limit to the flux or an upper limit of 4 to the exponent of the integral energy spectrum in the 20-200 Mev interval.

0020 UT July 7, 1958

The flare produced a PCA reaching as much as 17 db at Kiruna (Reference 44) at 0400 UT on July 8th. No neutron monitor increase was observed, but balloon measurements were made by Russian workers at Kiruna (References 45 and 46). At an atmospheric depth of 10 gm/cm^2 the intensity was 4 times normal at 1000 UT on July 8th, when the riometer absorption was 18 db, and returned to normal by 1500 UT when the riometer absorption was 13 db (Figure 2-6). In this instance it is hard to reconcile the balloon and riometer results, but it is evidence for a very steep spectrum and indicates that the riometer absorption was probably affected by large numbers of particles with energies
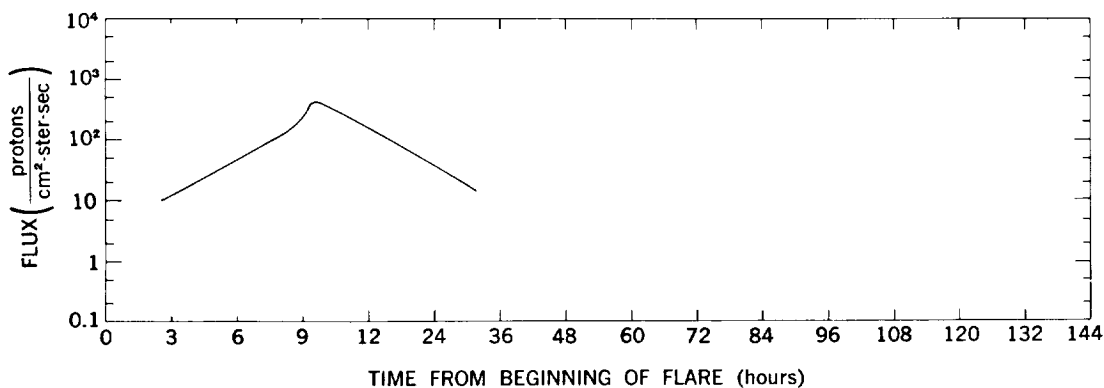
Figure 2-5—The time history for August 29, 1957 event.

below 20 Mev. It is possible that the energy spectrum was so steep that, if the second balloon were under a few gm/cm² more atmosphere than the first, the difference in counting rate could be caused by the differences in the cutoff energy determined by the air above the balloon.
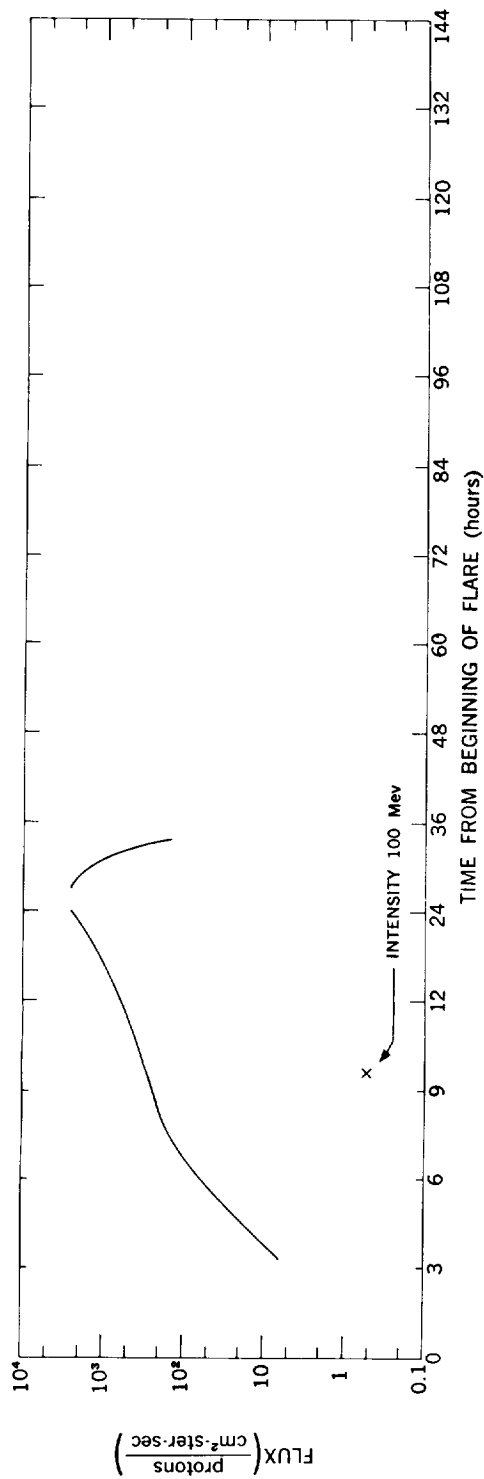
0433 UT August 16, 1958

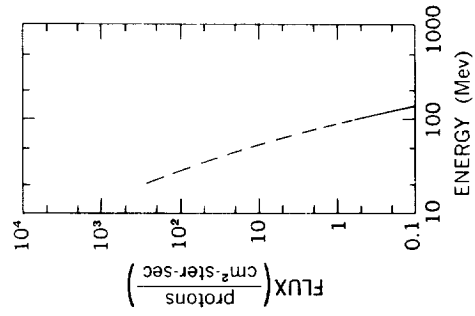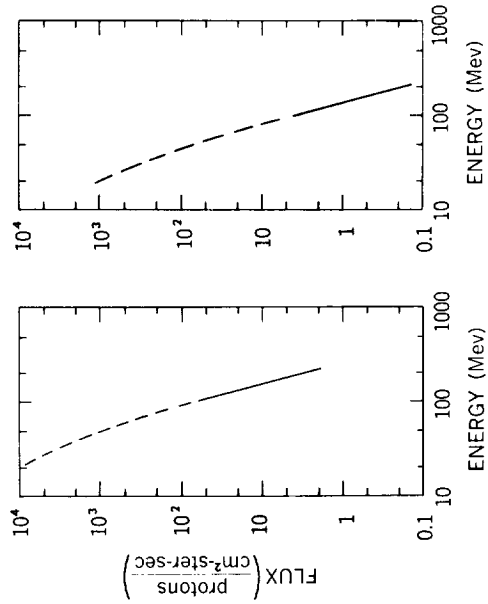For this event only riometer data, showing a maximum absorption greater than 15 db, are available. Because an energy spectrum cannot be constructed from riometer data alone, no figure is presented for this event.

1428 UT August 22, 1958

This event is characterized by a steep spectrum and no detectable neutron monitor increase (Figure 2-7). The solar particles were observed by means of balloons (Reference 47) and by Explorer IV (1958ε) satellite (Reference 48). At Churchill, after only 1 hour, the intensity of protons with kinetic energies above 100 Mev was 20 times normal; and the subsequent rapid fluctuations until 1900 UT were probably due to fluctuations in particle emission. The spectra exhibited are derived from the balloon and satellite observations. A direct determination at 0500 UT on August 23rd gives an approximate integral energy spectrum proportional to $1/E^{3.5}$ above 100 Mev; and the satellite results support the validity of extrapolating this energy spectrum to 30 Mev. Measurements made on Explorer IV (References 48 and 49) give integral fluxes, above 30 and 40 Mev, at three times during the event, which are consistent with the riometer observations (Reference 40).

0005 UT August 26, 1958

For this event only riometer data showing a maximum absorption greater than 15 db, are available.* Because an energy spectrum cannot be constructed from riometer data alone, no figure is presented for this event.

2101 UT May 10, 1959

Energy spectra were obtained at balloon altitudes on May 12, 1959 at Minneapolis, by the University of Minnesota (References 50, 51, and 52). However, balloon observations by Charakhch'yan, et al. (Reference 45) show that during the latter portion of this time only a fraction of the total particle flux reached Minneapolis, so that only the energy spectrum at 0640 UT has been shown (Figure 2-8). The PCA began about 5 hours after the

---

*Chapter 1.

(a) Time history

FLUX $\left(\dfrac{\text{protons}}{\text{cm}^2\text{-ster-sec}}\right)$

INTENSITY 100 Mev

TIME FROM BEGINNING OF FLARE (hours)
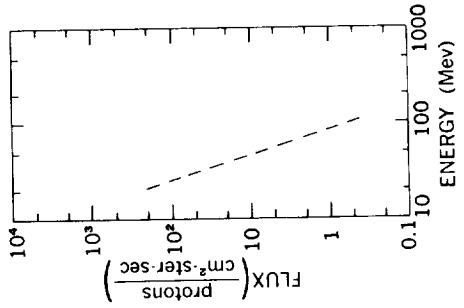
(b) Energy spectrum at 1000 UT, July 7 (9-2/3 hours)

FLUX $\left(\dfrac{\text{protons}}{\text{cm}^2\text{-ster-sec}}\right)$

ENERGY (Mev)

Figure 2-6—The July 7, 1958 event. The various curves are explained on page 29.

(a) Time history

TIME FROM BEGINNING OF FLARE (hours)

$$\text{FLUX} \left(\frac{\text{protons}}{\text{cm}^2 \cdot \text{ster} \cdot \text{sec}} \right)$$

(b) Energy spectrum at 0430 UT, August 23 (·14 hours)

ENERGY (Mev)

$$\text{FLUX} \left(\frac{\text{protons}}{\text{cm}^2 \cdot \text{ster} \cdot \text{sec}} \right)$$
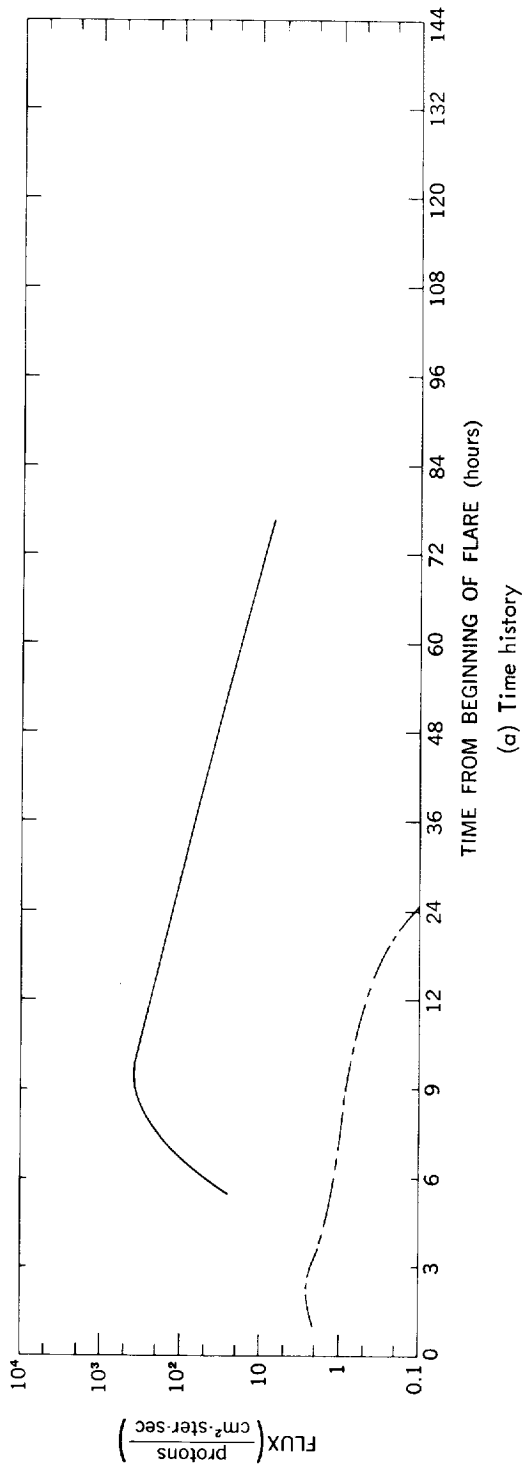
Figure 2-7—The August 22, 1958 event. The various curves are explained on page 29.

(a) Time history

TIME FROM BEGINNING OF FLARE (hours)

FLUX $\left(\dfrac{\text{protons}}{\text{cm}^2\text{-ster-sec}}\right)$

ENERGY (Mev)

ENERGY (Mev)

FLUX $\left(\dfrac{\text{protons}}{\text{cm}^2\text{-ster-sec}}\right)$
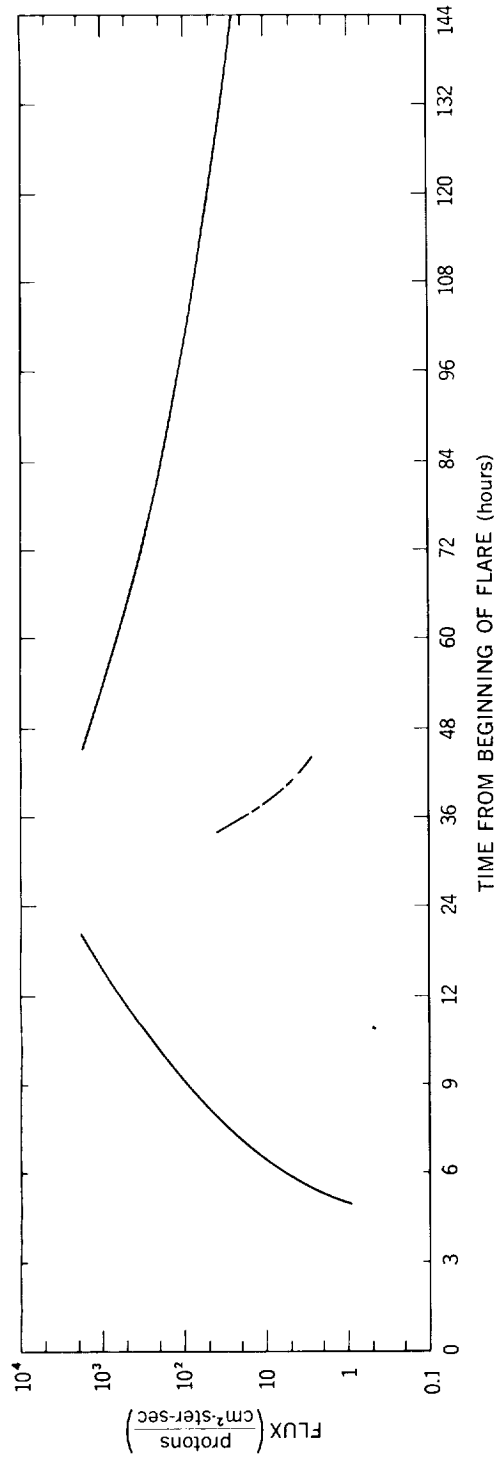
(b) Energy spectra at 0640 UT, May 12 (+ 34 hours) and 2101 UT (+ 42–2/3 hours)

Figure 2–8—The May 10, 1959 event. The various curves are explained on page 29.

flare, reached an absorption maximum in excess of 18 db at College, Barrow and Thule (Reference 42) and recovered over a period of several days. The riometer absorption at Longyearbyen (Reference 53) was also in general agreement with this data.

The July 1959 Events

The complex series of events occurring during July 1959 are the subject of a monograph published by UGGI (Reference 54). In brief, a series of three great solar flares, occurring before 0210 UT July 10th, at 0319 UT July 14th, and at 2118 UT July 16th, caused a series of three large solar cosmic ray events (Figures 2-9, 2-10 and 2-11). The last of the flares also produced particles in a range of energies and in a quantity detectable by neutron monitors. The absorption showed increases to greater than 20 db for all three of the events, as recorded by the 27.6 Mc riometer at College (Reference 23); the riometers at Barrow (Reference 23), Thule (Reference 23), and Churchill (Reference 55), are in general agreement with these maximum values.

The neutron monitor increase has been discussed by McCracken and Palmeira (Reference 14) who point out the very slow rate of rise, and the isotropic nature of the flux at the energies detected by the neutron monitors. High latitude monitors detected an increase at about 0300 UT on the 17th and, between 0800 UT and 1200 UT, recorded an increase of about 6 percent for particles above 1 Bv. If we take a differential spectrum (Reference 54) of the form $1/p^6$, a particle intensity of $0.06 \times 13 \times 0.09 = 0.07$ particles/cm²-ster-sec (P > 1Bv) is implied. This is consistent with the fact that stations with thresholds above 1.2 Bv did not see an increase.

The neutron monitor records show no additional particles – even at the highest latitudes – after about 1800 UT on the 17th. If we assume a steepening of the spectrum of $1/p^6$, and that a 1 percent increase would have been detected, the intensity above 1 Bv was less than $0.01 \times 13 \times 0.09 = 0.0012$ particles/cm²-ster-sec.

A number of balloon flights provided particle data in the intermediate energy range. Information from Frier (References 50 and 52), Winckler, et al. (Reference 55), Webber (Reference 56), Brown and D'Arcy (Reference 57), and Anderson and Enemark (Reference 41), have been combined to give energy spectra at four times during the July 10th event and three times during each of the other two, as well as relatively complete histories of the integral flux above 100 Mev.

0138 UT April 29, 1960

The riometers at College (Reference 42), Thule (Reference 42), and Churchill (Reference 58) were in essential agreement during this event and showed a maximum absorption of about 13 db on April 30th at about 0600 UT (Figure 2-12). Several readings from the Explorer VII (1959 ι 1) (Reference 59) counters during the period 1800 UT April 29th through

39
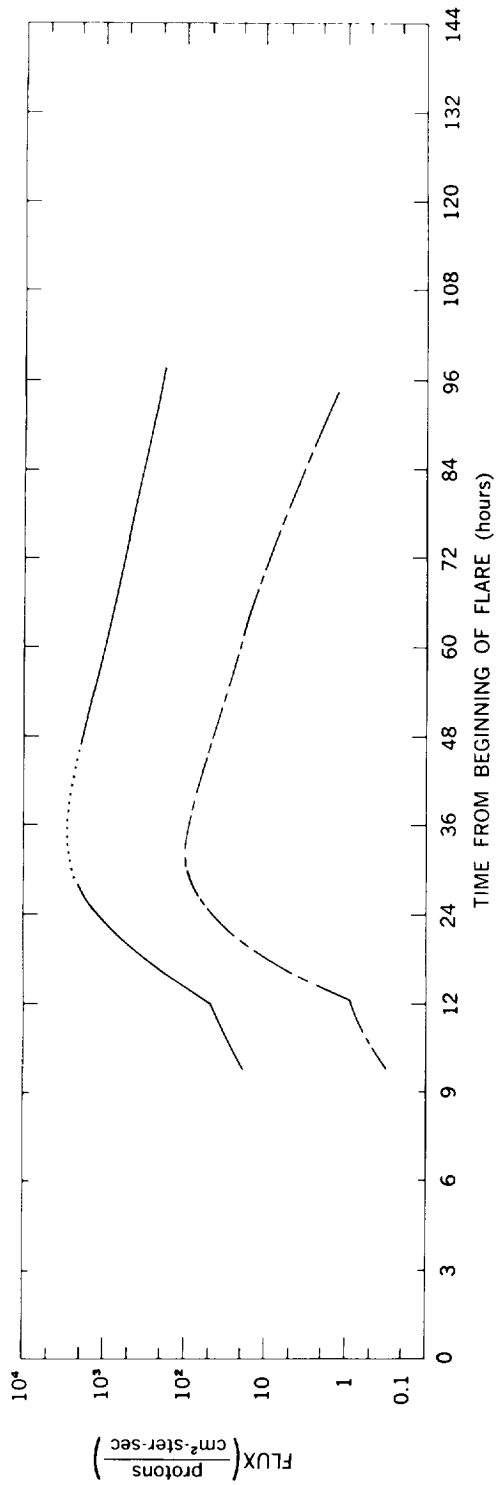
(a) Time history
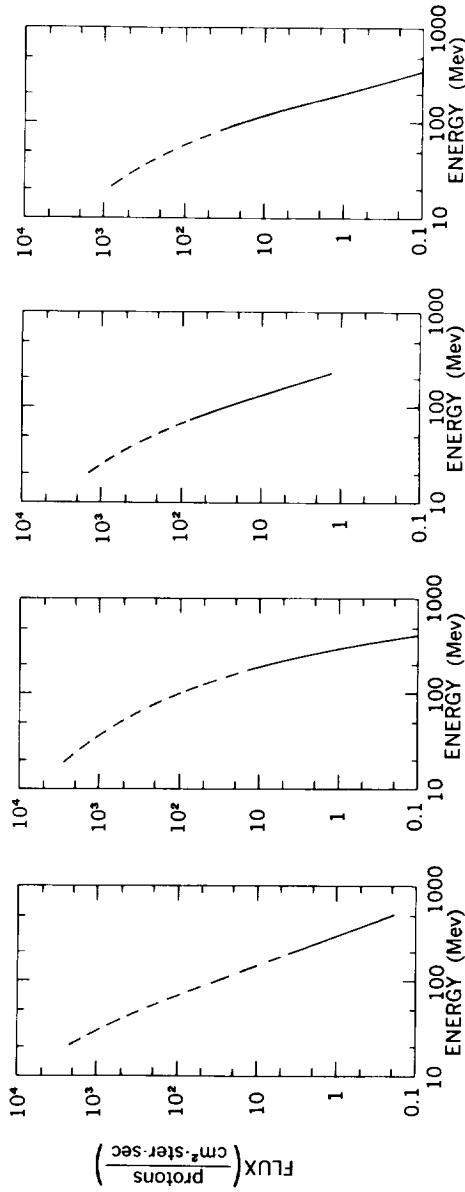
(b) Energy spectra at 0800 UT July 11 (+30 hours); 1200 UT (+34 hours);
0700 UT July 12 (+53 hours); and 1800 UT (+64 hours)

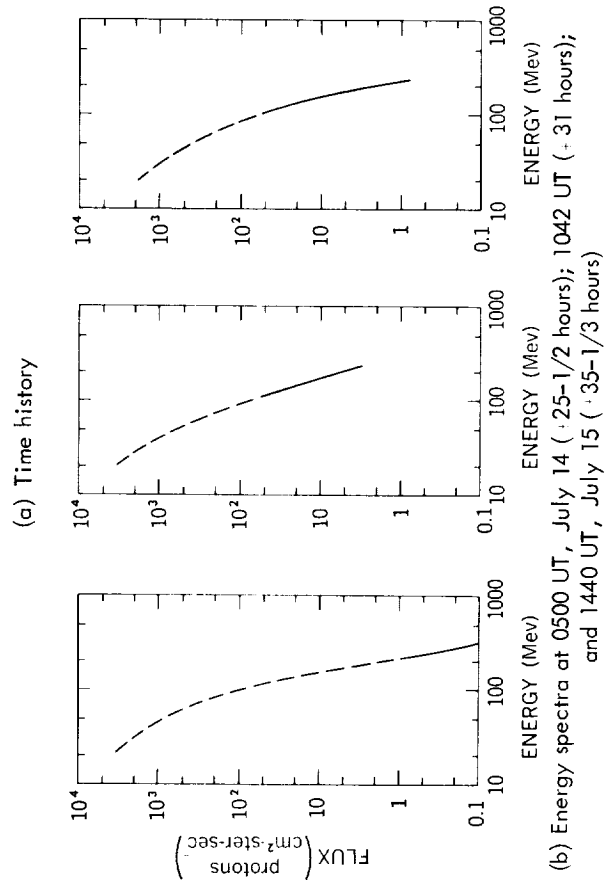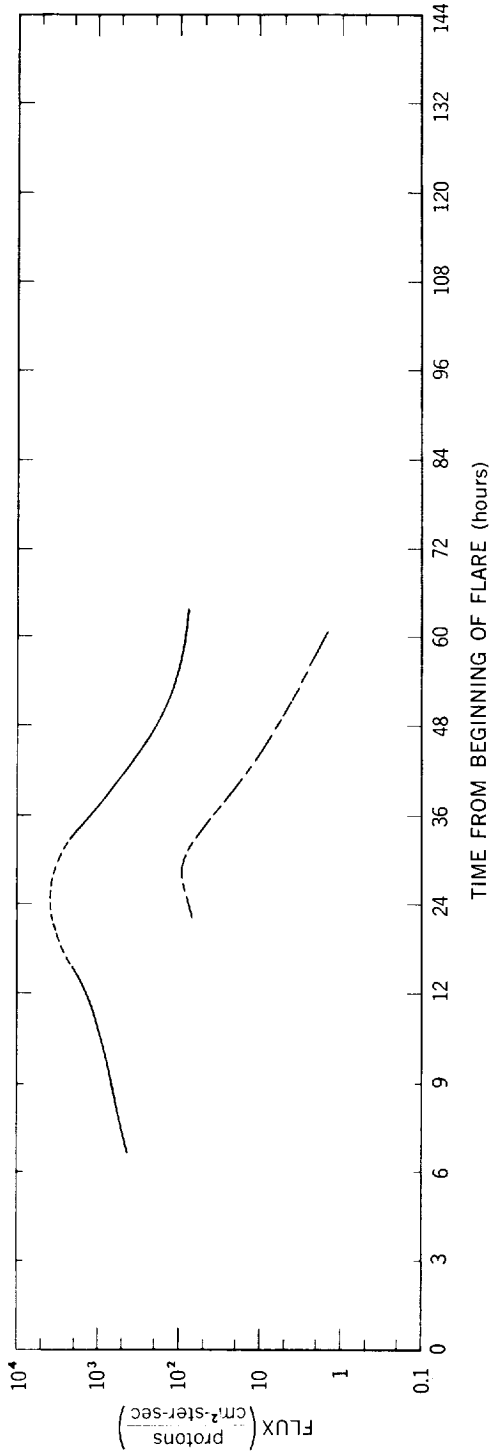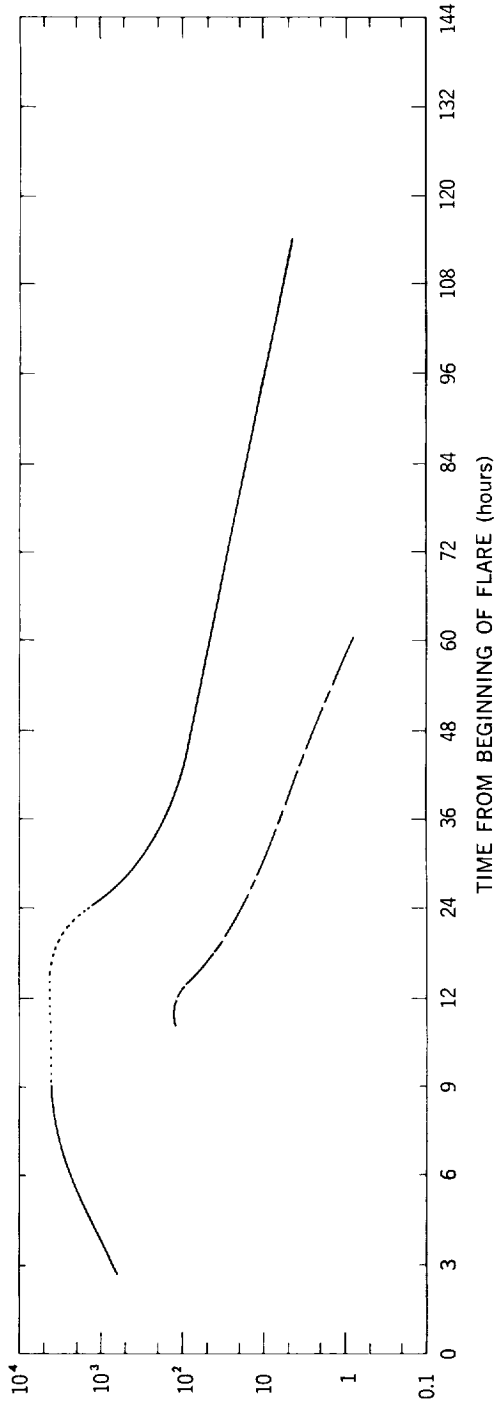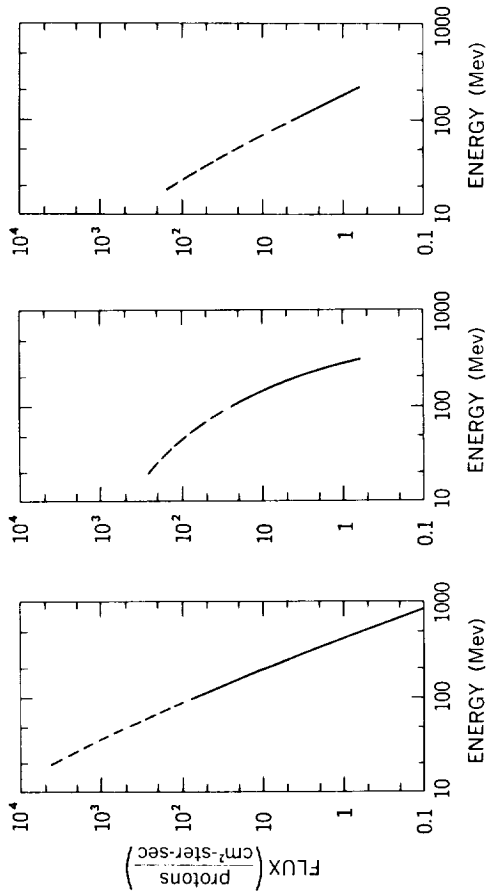Figure 2-9—The July 10, 1959 event. The various curves are explained on page 29.

(a) Time history

(b) Energy spectra at 0500 UT, July 14 (+25-1/2 hours); 1042 UT (+31 hours); and 1440 UT, July 15 (+35-1/3 hours)

Figure 2-10—The July 14, 1959 event. The various curves are explained on page 29.

TIME FROM BEGINNING OF FLARE (hours)

(a) Time history

FLUX $\left(\dfrac{\text{protons}}{\text{cm}^2\text{-ster-sec}}\right)$

ENERGY (Mev)

ENERGY (Mev)

ENERGY (Mev)

(b) Energy spectra at 1200 UT, July 17 (~14-3/4 hours); 1745 UT (~20-1/2 hours); and 1510 UT, July 18 (~42 hours)

Figure 2-11—The July 16, 1959 event. The various curves are explained on page 29.

0100 UT April 30th at L values* where the full intensity was often seen in other events indicated flux values more than an order of magnitude lower than those inferred from the riometer data. This shows that either the satellite was situated in a position where the minimum energy observable due to geomagnetic effects was larger than the nominal threshold energy of the detectors (18 and 30 Mev) or that there was a large component at energies below 18 Mev which affected the riometer absorption.

1000 UT May 4, 1960

This event, observed at sea level by neutron monitors, falls into the category of *rapid risers* and shows pronounced impact zone effects. The intensity in the impact zones started to rise at 1030 - 1 UT, and reached maximum at 1040 - 2 UT, with a differential spectrum of about p^{-4} (Figure 2-13). Outside the impact zones the intensity began to rise at 1035 UT and reached maximum at 1048 - 2 UT, with a differential spectrum varying approximately as p^{-5}. The neutron monitor at Deep River detected particles arriving directly and observed as increase of 3.5 times at maximum, which implies an intensity of $3.5 \times 12 \times 0.1 = 4.5$ particles/ cm^2-ster-sec above 1 Bv. This quantity checks within a factor of 2 with the increase recorded at the Jungfraugoch where the threshold is 3.6 Bv; the agreement provides some confidence in the spectrum. The decay above 1 Bv can be approximated by an expression of the form $N = N_0 e^{-t/t_0}$ with t_0 = 2 hours. J. R. Winckler et al. (Reference 60), at 1630 UT on May 4th, found a flux above 1 Bv with detectors flown on balloons, which is in excellent agreement with the flux inferred by neutron monitor data. Further, Biswas and Frier (Reference 61) measured the energy spectrum between 1700 UT, May 4 and 0200 UT, May 5 with nuclear emulsions carried on a balloon; this spectrum is shown in Figure 2-13.
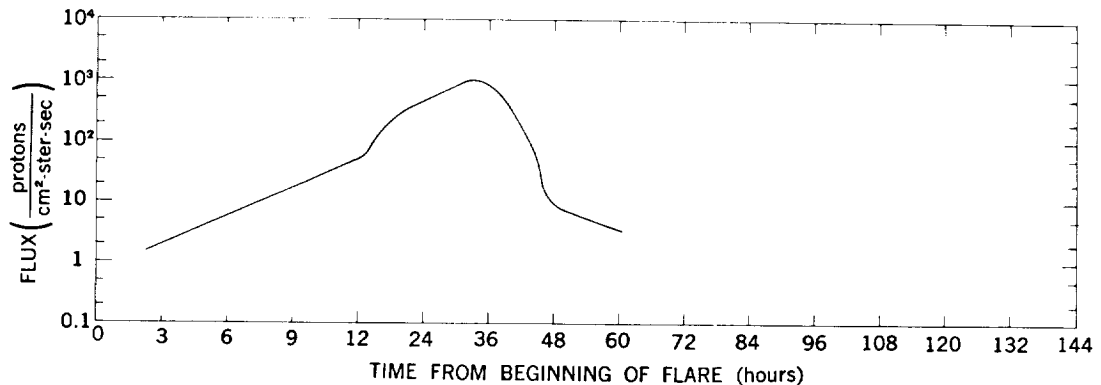
Figure 2-12—The time history of the April 29, 1960 event.
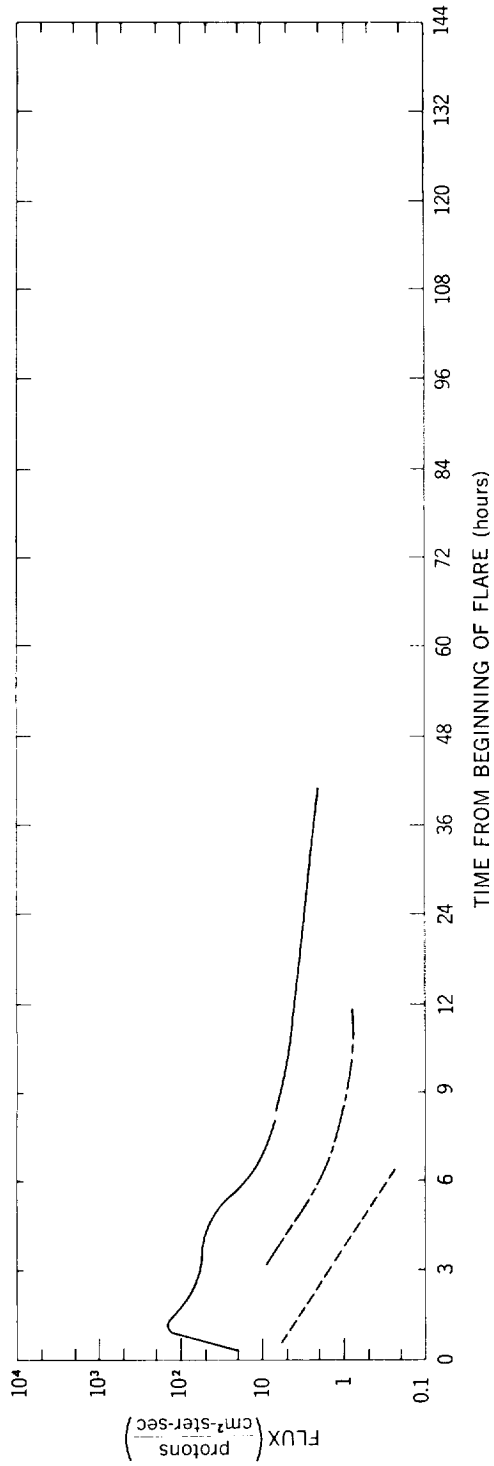
(a) Time history
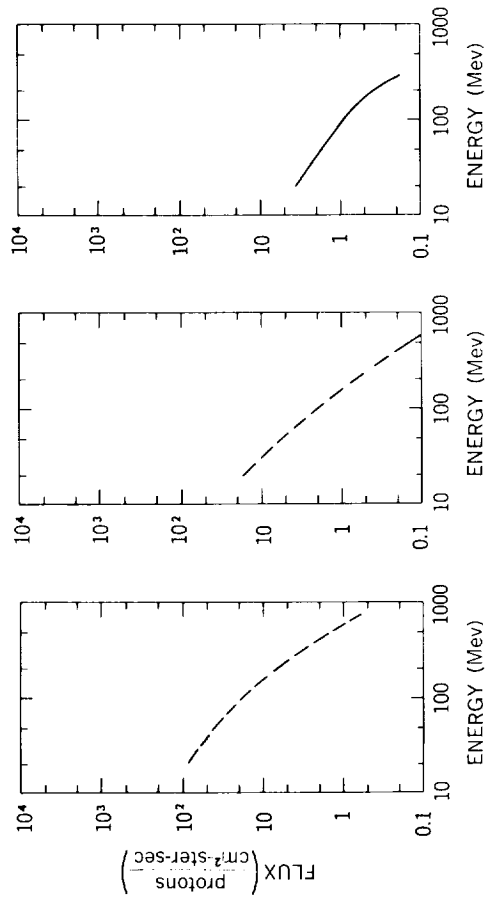
(b) Energy spectra at 1220 UT, May 4 (~2 hours); 1630 UT (~6 hours); and 2130 UT (+11-1/2 hours)

Figure 2-13—The May 4, 1960 event. The various curves are explained on page 29.

The riometer data from Thule (Reference 42) showed a rapid increase to a maximum absorption of about 5 db two hours after the start of the flare. The riometers at College (Reference 42) and Churchill (Reference 58) were in darkness at that time. Following the maximum, the three riometers were in agreement, and the inferred particle intensity agreed with the State University of Iowa (SUI) Explorer VII data (Reference 59) obtained from 10 to 32 hours after the flare.

1404 UT May 6, 1960

The riometers at College (Reference 42), Churchill (Reference 58), and Thule (Reference 41) showed agreement for this event, with a maximum absorption of about 13 db, forty hours after the flare (Figure 2-14). Again there is disagreement with the SUI Explorer VII data (Reference 59), probably for the same reasons discussed in connection with the event of April 29, 1960.

0037 UT September 3, 1960

In this interesting event the solar emission, due to a class 3 flare at 17°N 87°E on the sun, occurred during the transit to the earth of disturbances from two previous flares. A slowly rising isotropic flux was detected, which caused an increase of about 2 percent in the neutron monitor rate at Deep River at 0900 UT (Reference 32). Rockets launched from Churchill at 1400 UT and 1700 UT measured a spectrum steepening towards high energies (Reference 21), which could be approximated in differential form $1/p^{3.3}$ between 0.15 and 0.7 Bv (Figure 2-15). If we assume that $1/p^6$ is appropriate above 1 Bv, then the intensity at the time of maximum was about 0.05 particles/cm^2-ster-sec. Winckler (References 55 62, and 63) deduced an integral spectrum $2 \times 10^7 \, E^{-3.1}$ (E in Mev) from balloon measurements at Minneapolis and Churchill at about 1730 UT. This is in fair agreement with the
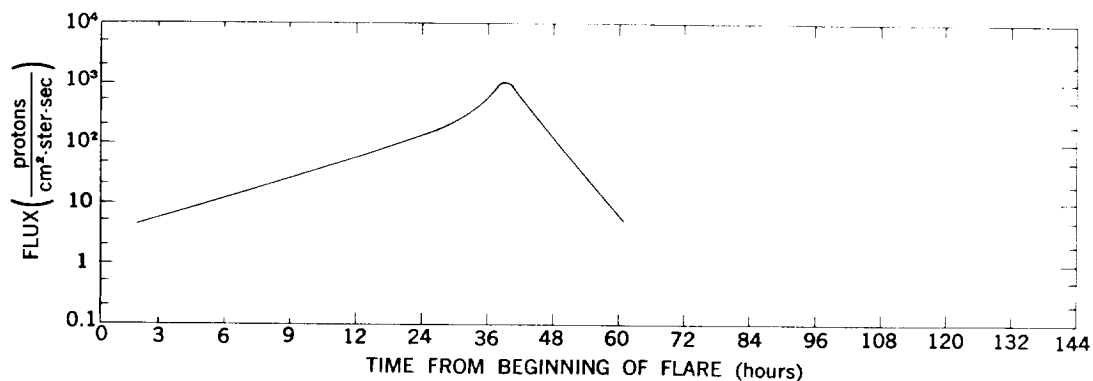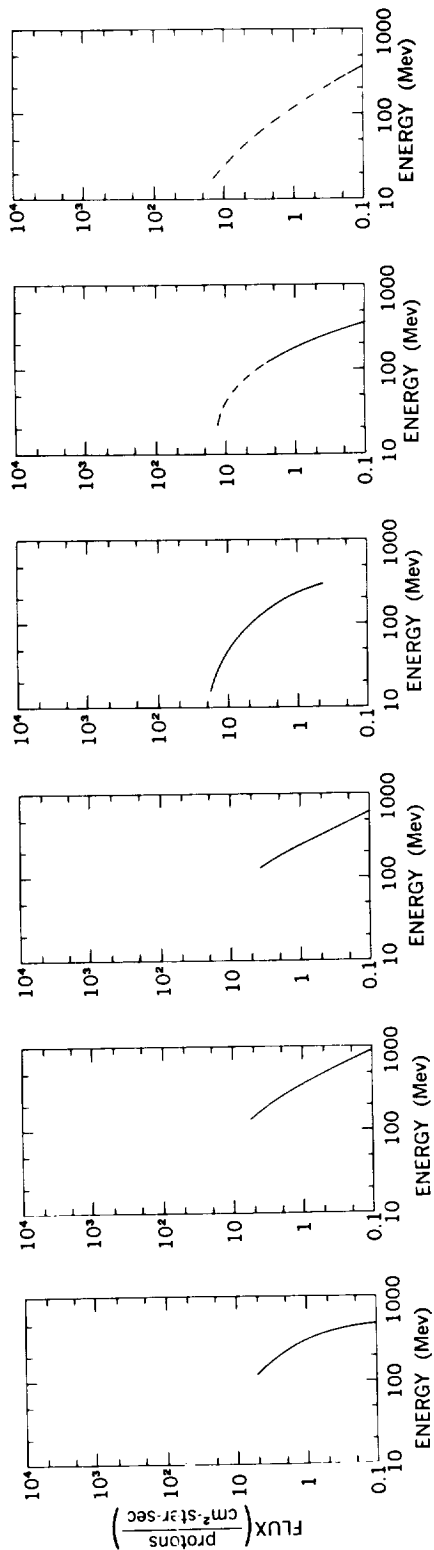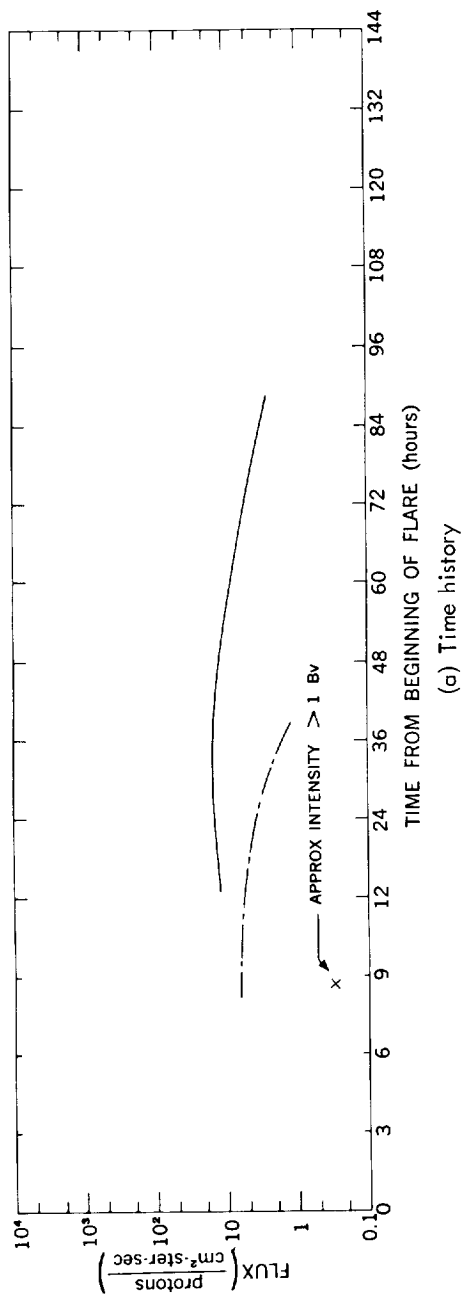

Figure 2-14—The time history of the May 6, 1960 event.

(a) Time history

(b) Energy spectra at 0900 UT, Sept. 3 (+8 hours); 1000 UT (+9 hours); approximately 1230 UT (+12 hours); 1408 UT (+13-1/2 hours); 0000 UT, Sept. 4 (+23 hours); and 1615 UT (+39-1/2 hours).

Figure 2-15—The September, 1960 event. The various curves are explained on page 29.

intensity value given above, as are the results of Biswas et al. (Reference 5). In the energy region from 22 to 67 Mev the intensity remained the same between 1400 and 1700 UT. We know from the behavior of the low energy particles producing the cosmic noise absorption that the decay of the event at these energies was very slow; and examination of the emulsion measurements at 1 Bv at Minneapolis showed that the high energy flux decayed by a factor of almost 10 in about 30 hours.

The PCA observations indicated a very flat spectrum, consistent with that found by the rocket emulsion measurements. In addition the measurements of Explorer VII (Reference 59) are in agreement with the intensities inferred from riometer absorption.

1322 UT November 12, 1960

This event was a complicated one in which two separate maxima are displayed at high latitudes by the neutron monitor records. Figure 2-16 shows the records of the Deep River neutron monitor for the month of November 1960 showing the coordinates of the important flares. It has been postulated (References 64 and 65), that the flares occurring on the 10th and 11th produced plasma fronts, and these were in transit towards the earth when the flare on the 12th produced an injection of high energy particles. Thus, detectors on the earth sampled the intensity of solar particles for six hours before and several hours after the passage of a front which generated a large magnetic storm and a very rapid Forbush decrease. In addition to the neutron monitor and riometer data, detailed energy spectra were
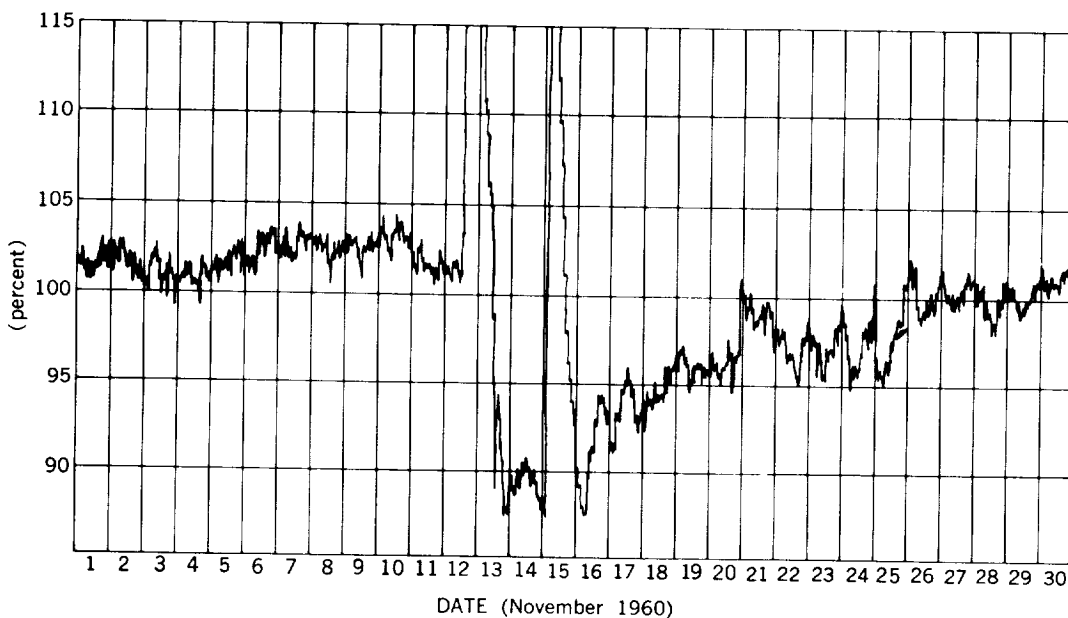

Figure 2-16—November 1960 neutron monitor data from Deep River.

obtained at three times during this event by the reduction of data from sounding rockets fired from Churchill (References 65 and 66) and from balloon data of Winckler (Reference 55). These spectra for the November 12 event are shown in Figure 2-17. The low energy component between 20 and 80 Mev was seen to increase markedly between 1840 and 2330 UT in agreement with the riometer data. Between 2330 UT on November 12 and 1603 UT on November 13, the high energy component continued to decline as indicated by the curve deduced from neutron monitor data between about 2000 UT on November 12 and 0400 UT on November 13.

For this event Lockwood and Shea (Reference 67) have performed calculations similar to those reported here; and this permits a check on our procedure for finding the flux above the atmosphere corresponding to a given neutron excess. Lockwood and Shea find a spectrum of the form p^{-6} between 1600 and 1630 UT on November 12, and deduce a differential spectrum for protons which corresponds to 2.9 particles/cm^2-ster-sec above 1.25 Bv. Our calculations leads to $0.85 \times 21 \times 0.11 = 2.0$ particles/cm^2-ster-sec above 1.25 Bv.

Further confirmation can be found from the results of the measurements made at 1840 UT by a NASA rocket launched from Churchill just before the earth entered the trapping region (Reference 67). From the emulsion measurements, Fichtel and Guss found an intensity above 680 Mv of 24 particles/cm^2-ster-sec, and a slope of about -6 for the integral rigidity spectrum. Assuming this slope to continue, the intensity above 1 Bv would be 3.5 particles/cm^2-ster-sec. It is difficult to obtain a rate of decrease with time which has much meaning over a wide rigidity range. After 1900 UT Manzano et al. (Reference 68) found a decrease proportional to $t^{-2.3}$ and a sudden increase in the decay rate at 1000 on November 13th.

0200 UT November 15, 1960

After the first hour, during which particles were incident principally from a direction about 50° west of the earth-sun line and the intensity rose rapidly, a regular decline set in at high energies. The maximum of the neutron monitor increase at high latitudes indicates an intensity of approximately 3 particles/cm^2-ster-sec above 1.25 Bv, assuming a $1/p^6$ differential rigidity spectrum. Lockwood and Shea deduced a differential rigidity spectrum of $10^2 p^{-6}$ for P in the range 1.7 Bv. This leads to an intensity above 1.25 Bv of 6.5 particles/cm^2-ster-sec at the time of the maximum, which is in fair agreement with the calculation made here.

The riometer data indicate that the maximum flux of particles above 20 Mev occurred about twenty hours after the flare (Reference 42), and was almost 10^4 particles/cm^2-ster-sec (Figure 2-18). Detailed energy spectra were available early in the event from balloon borne equipment (References 6 and 52) and later in the event from sounding rockets (References 65 and 66). The Explorer VII (Reference 59) data agree with the other data obtained to within a factor of 2. A relatively fast decline is observed late in the event, with the

48

(a) Time history

TIME FROM BEGINNING OF FLARE (hours)

SUDDEN DECREASE IN HIGH ENERGY FLUX

(b) Energy spectra at 1840 UT, Nov. 12 (+5 hours); 2330 UT (+10 hours); 1630 UT, Nov. 13 (+26–1/2 hours); and 0500 UT, Nov. 14 (+39–2/3 hours)
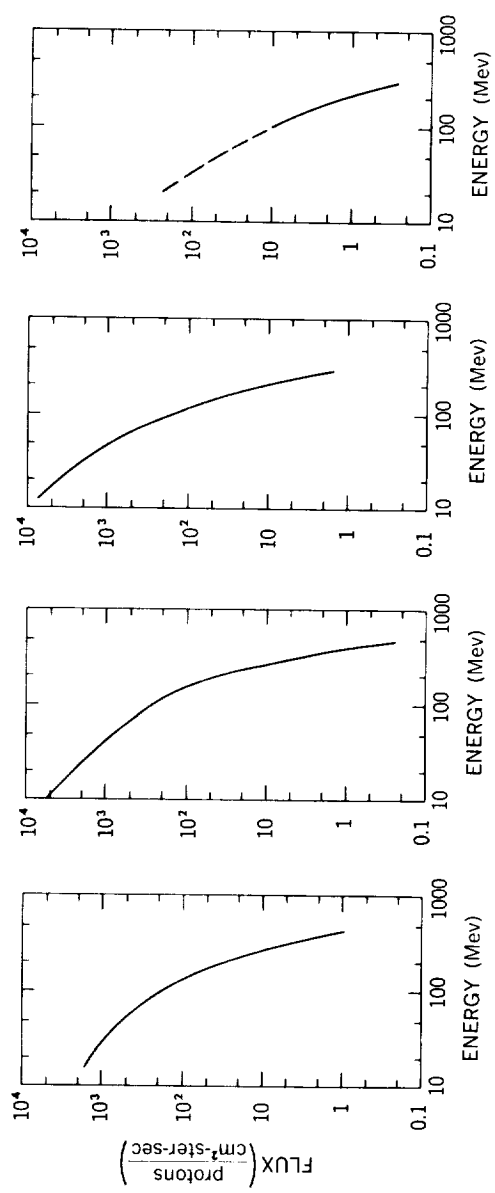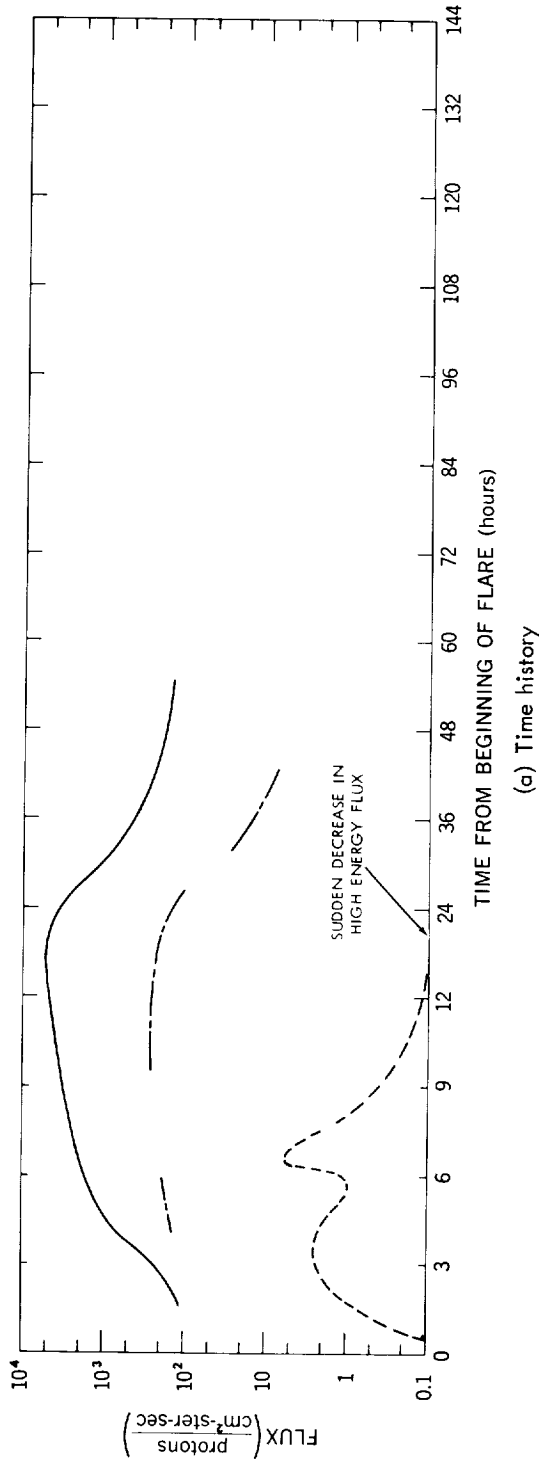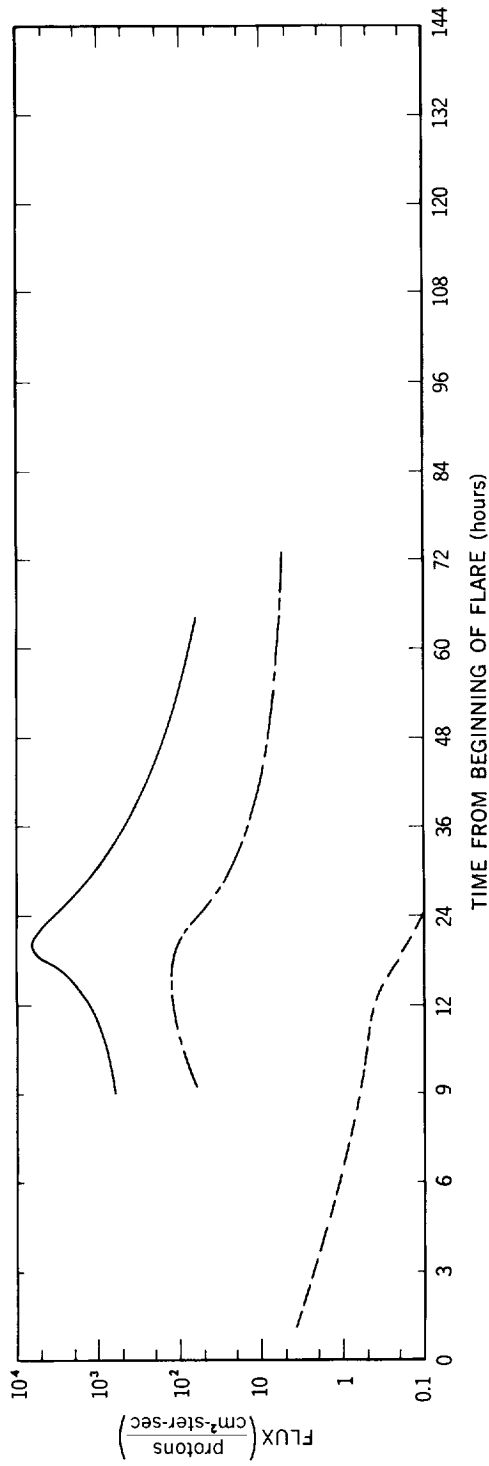
Figure 2-17—The November 12, 1960 event. The various curves are explained on page 29.

(a) Time history

(b) Energy spectra at 0500 UT, Nov. 15 (+3 hours); 1130 UT (+9-1/2 hours); 2145 UT (+19-3/4 hours);
1600 UT, Nov. 16 (+38 hours); and 0340 UT, Nov. 18 (+74 hours)
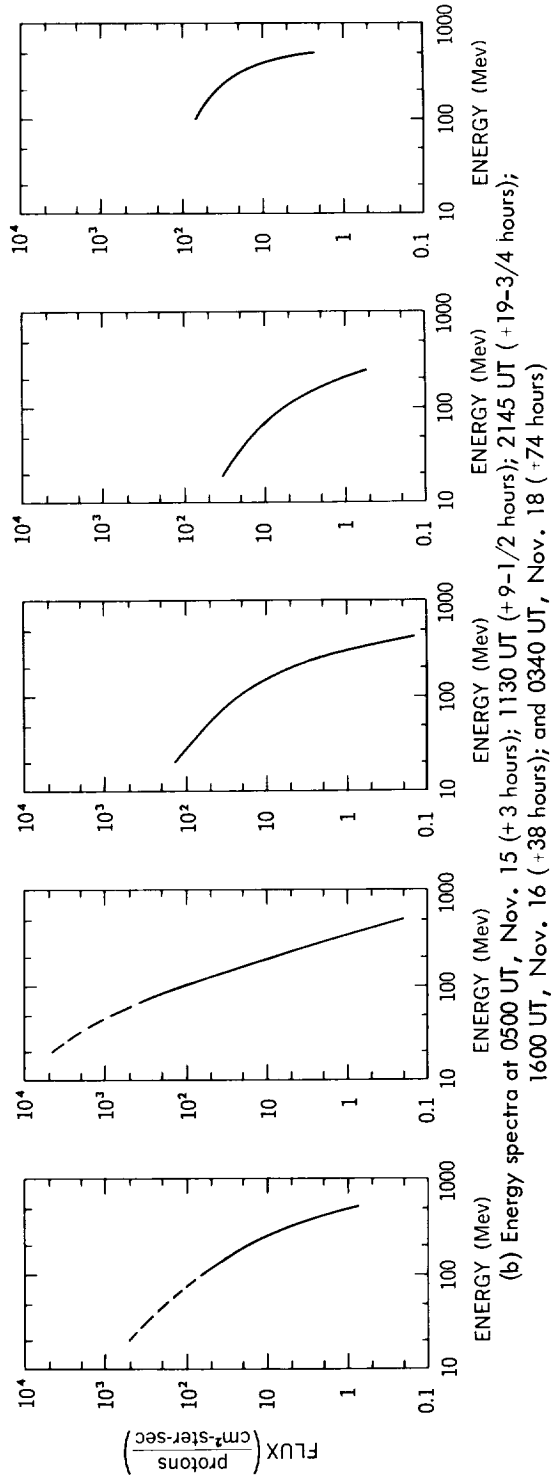
Figure 2-18—The November 15, 1960 event. The various curves are explained on page 29.

decay following a law of the form $1/T^n$, with $T = 0$ at the time of the flare and n perhaps as large as 3 (Reference 69).

November 20, 1960

On November 20th there was another solar event; the flare was from the same region as the flares associated with the November 12th and 15th events which, by then, was just around the western limb of the sun. The increase at neutron monitor energies was small and took about one hour to reach its maximum value, 5 percent above background, at Deep River (Reference 20). An increase of the order of 1/2 to 1 percent occurred at points with a threshold rigidity of 3 Bv, indicating a very flat spectrum. The riometer increase was also relatively small, indicating that the integral intensity of particles above 20 Mev did not exceed 100 particles/cm^2-ster-sec.

July 12, 1961

The integral flux of particles greater than 20 Mev, as determined by the absorption detected on the riometer (References 42 and 58), increased relatively slowly early in the July 12, 1961 event and reached a maximum shortly after the sudden commencement — 24 hours after the flare (Figure 2-19). From nuclear emulsions flown on a balloon near Churchill, Guss and Waddington (Reference 70) obtained an energy spectrum averaged over a 10 hour period centered about 26-1/2 hours after the flare,* when the intensity was greatest. From Figure 2-19, we see that the integral proton energy spectrum is very steep at this time, of the order of $1/E^{4.5}$, in the energy range from 78 to 140 Mev. The unpublished results of Freier and Hofmann (quoted in Reference 52) confirm the steep spectra and permit a reasonably good determination of the integral flux above 100 Mev during the period from 24 to 42 hours after the flare.
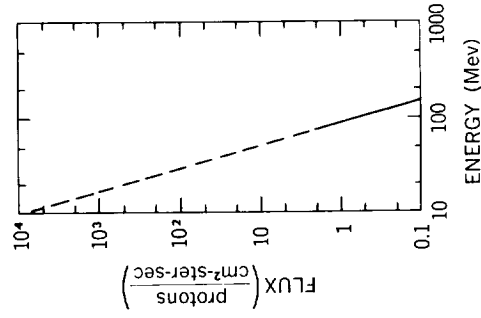
0930 UT July 18, 1961

This event is presumed to be associated with the 3+ flare at 0930 UT on July 18, 1961 because of the relatively rapid flux increase shortly thereafter as detected by neutron monitors and the riometers at various northern stations. There were, however, two major flares shortly before this time, a class 3 flare at 0505 UT and a class 2 flare at 0805 UT, which may have contributed particles to the event. Unlike the previous event on July 12, the riometer absorption for this event shows a rapid rise almost to the maximum value within about two hours (Figure 2-20). In addition, there was a detectable particle flux in excess of about 450 Mev as shown by the neutron monitor increase. There were several

---

*Data obtained from the Injun satellite (Reference 70) is in general agreement with this interpretation.
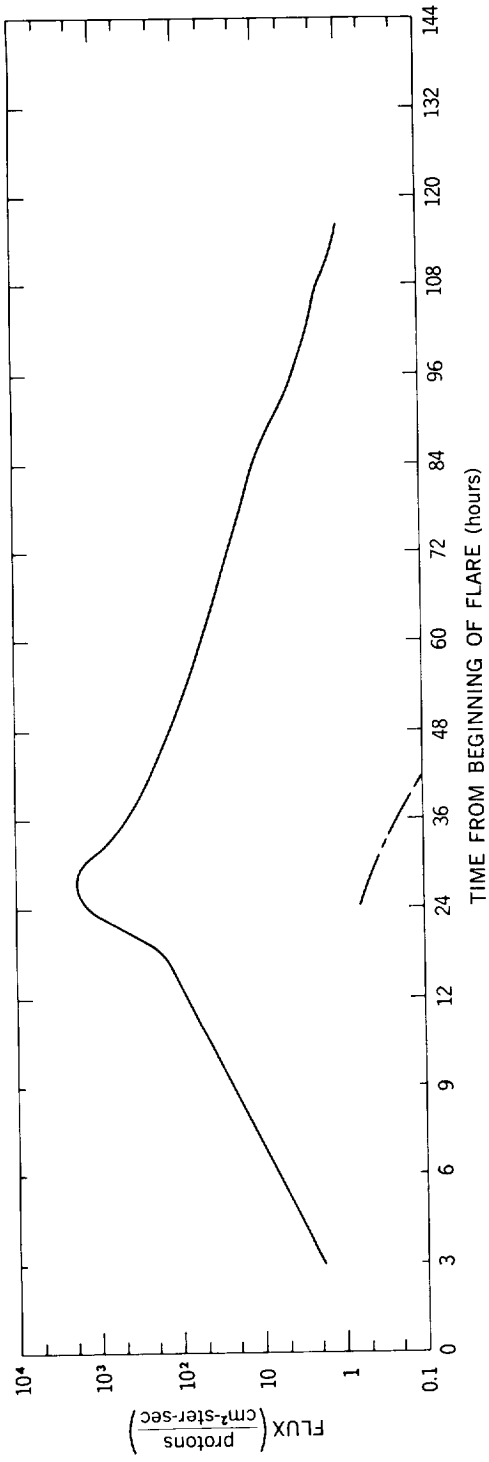
(a) Time history

(b) Energy spectrum at 1300 UT, July 13 (+27 hours)

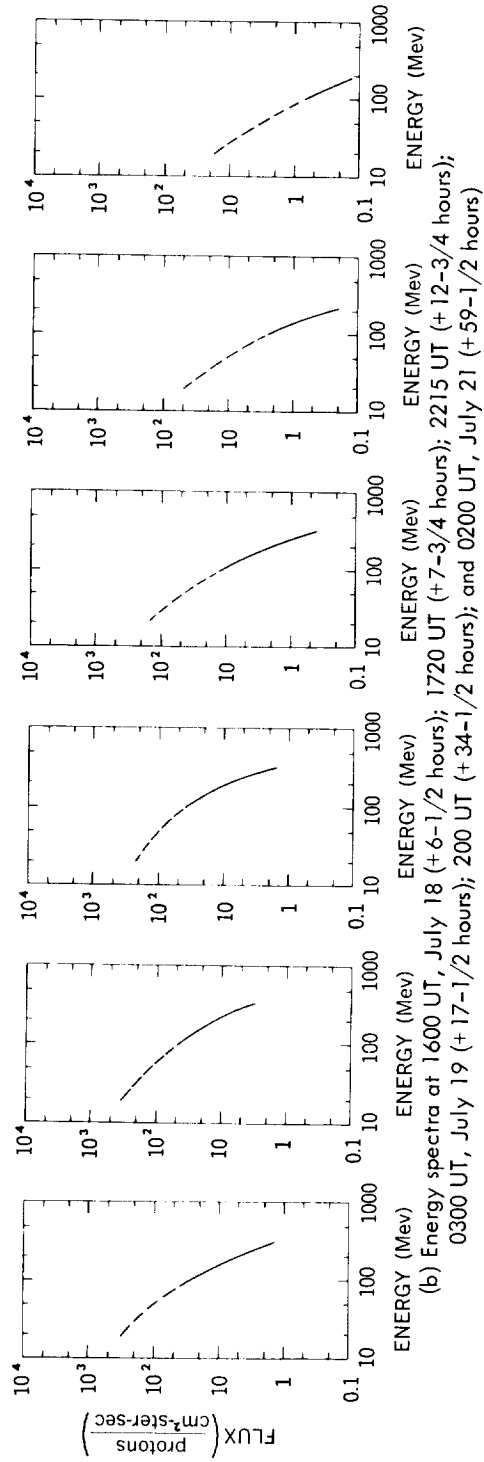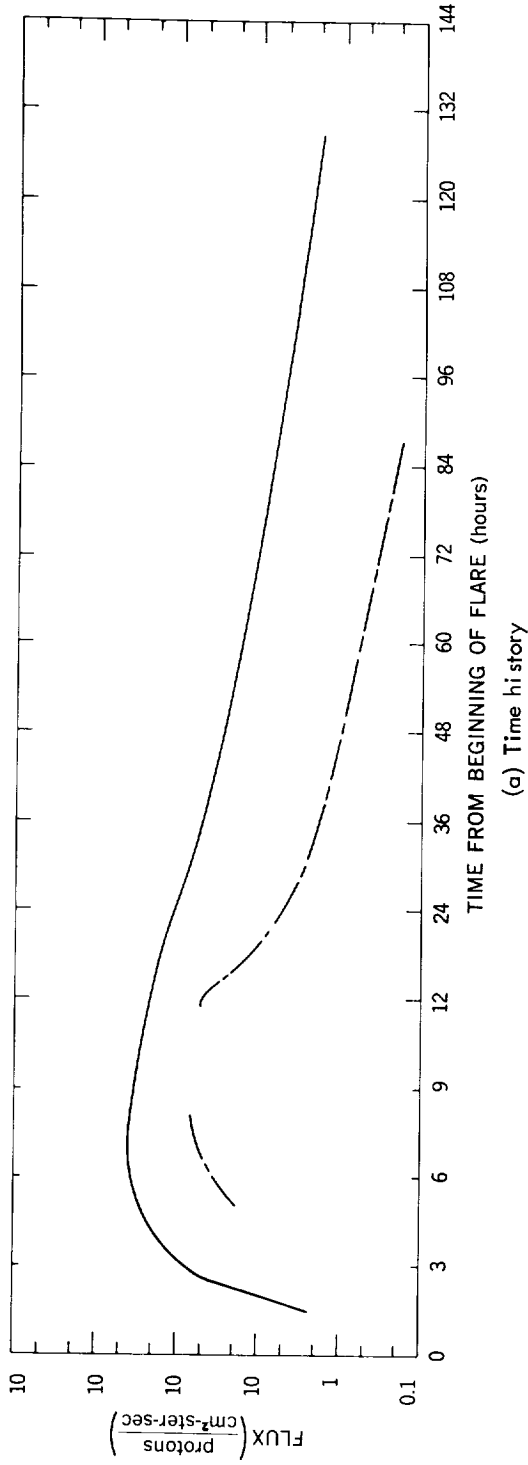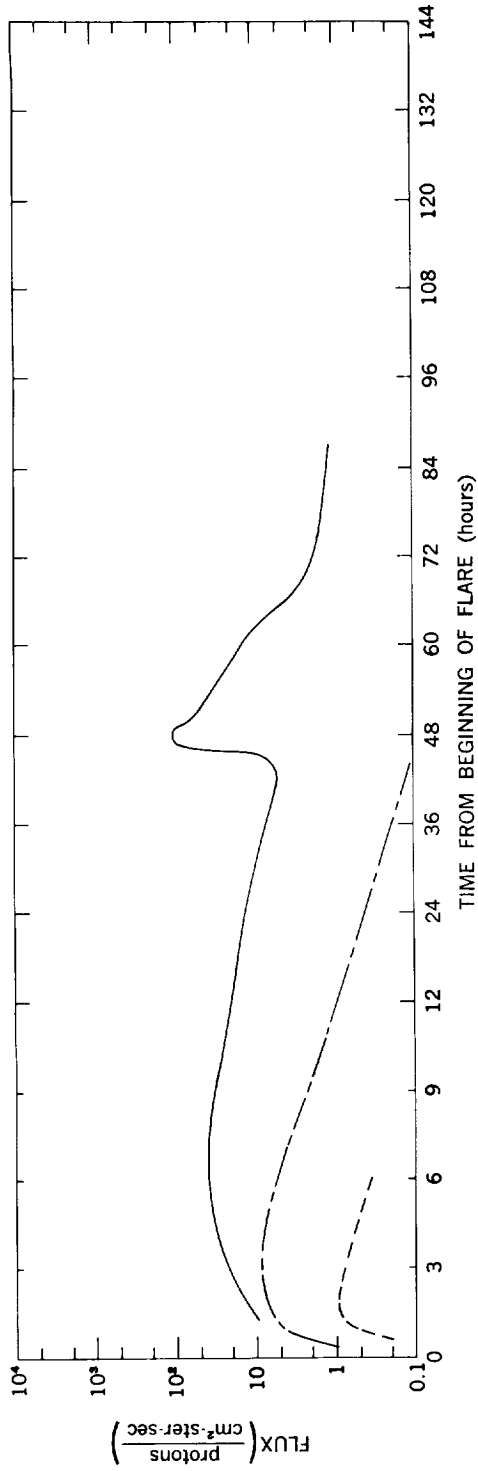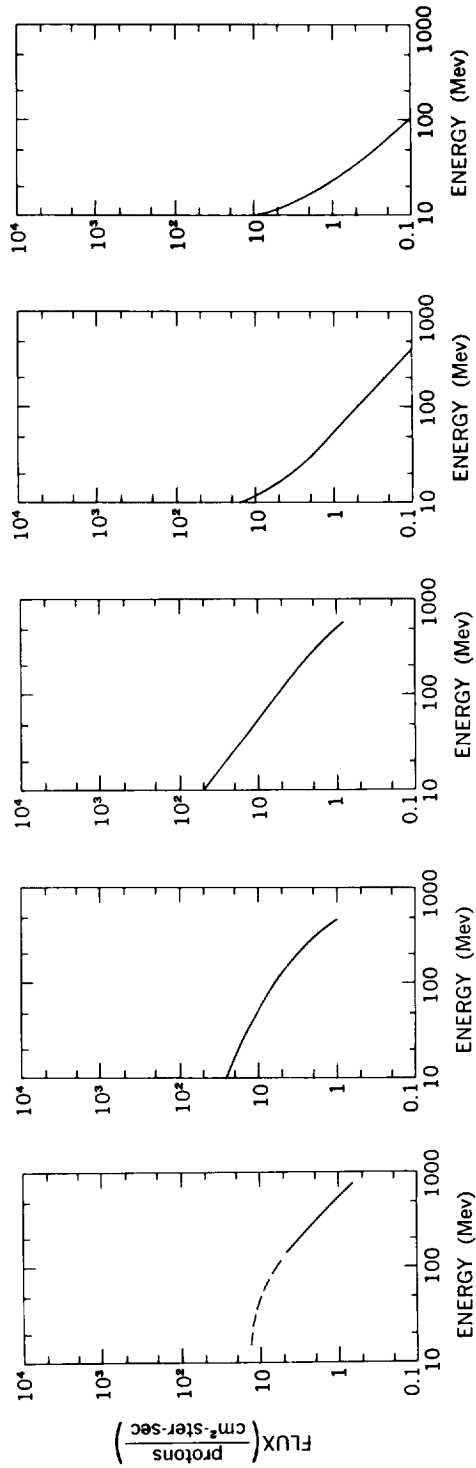Figure 2-19—The July 12, 1961 event. The various curves are explained on page 29.

FLUX $\left(\dfrac{\text{protons}}{\text{cm}^2\text{-ster-sec}}\right)$

TIME FROM BEGINNING OF FLARE (hours)

(a) Time history

FLUX $\left(\dfrac{\text{protons}}{\text{cm}^2\text{-ster-sec}}\right)$

ENERGY (Mev)

(b) Energy spectra at 1600 UT, July 18 (+6-1/2 hours); 1720 UT (+7-3/4 hours); 2215 UT (+12-3/4 hours); 0300 UT, July 19 (+17-1/2 hours); 200 UT (+34-1/2 hours); and 0200 UT, July 21 (+59-1/2 hours).

Figure 2-20—The July 18, 1961 event. The various curves are explained on page 29.

(a) Time history

(b) Energy spectra at 2330 UT, Sept. 28 (+2-1/2 hours); 0140 UT, Sept. 29 (+4-1/2 hours); 0410 UT (+7 hours); 1730 UT (+20 hours); and 1902 UT, Sept. 30 (+46 hours)

Figure 2-21—The September 28, 1961 event. The various curves are explained on page 29.

energy spectra measured during this event with balloon borne detectors (References 52 and 71) at various times from about 6 to 82 hours after the flare. A combination of this, the riometer, and the neutron monitor data permits the determination of an energy spectrum several times during the event.

2115 UT September 28, 1961

The September 28, 1961 event is the first for which there is a detailed energy spectrum as a function of time from 10-1000 Mev, for a large fraction of the event (Figure 2-21). The data was obtained from instruments flown on Explorer XII by D. A. Bryant et al. (Reference 26). The flare presumed to be associated with the event began at approximately 2215 UT, September 28 and reached its maximum intensity at about 2230 UT. The slope of the integral energy spectrum progressively increased with time in the low energy region until it was approximately as steep as that at high energies. Then there was a general decay with relatively little change in spectral shape above about 30 Mev. In the energy region from 1.5-30 Mev the flux was seen to increase markedly around the time of the sudden commencement and remain at a high level for several hours (References 26 and 72). The fluxes obtained by D. A. Bryant et al. (Reference 26) and O'Brien et al. (Reference 72) in the low energy region are found to be in agreement, within expected uncertainties with each other and with the fluxes deduced from the riometer absorption curve. Until 0500 UT, September 29, 1961 interesting anisotropies were observed by Bryant et al. (Reference 26) and these are still being investigated

Imaginary Envelope Event

In Figure 2-22 the curves of proton flux as a function of time were drawn so that the integral flux above the indicated energy level would be just slightly larger than in any event ever observed at the corresponding time from the beginning of the flare. This imaginary event is based on a number of large events as detailed below. The magnitude of the flux above 1 Bv at early times is similar to that observed on February 23, 1956, but the rate of decay of flux is similar to that observed on November 15, 1960. The flux above 100 Mev is obtained by combining observations of the November 12, 1960 event with those of July 10, 1959, in which the intensity above 100 Mev decayed very slowly. The flux above 20 Mev is seen to behave at early times similarly to that observed on November 12, 1960, but to decay at a rate similar to that observed on July 16, 1959.

While an event represented by a curve such as that shown would be exceptional in every respect, both as regards intensity and duration, there is no guarantee that larger events have not occurred in the past and will not in the future.
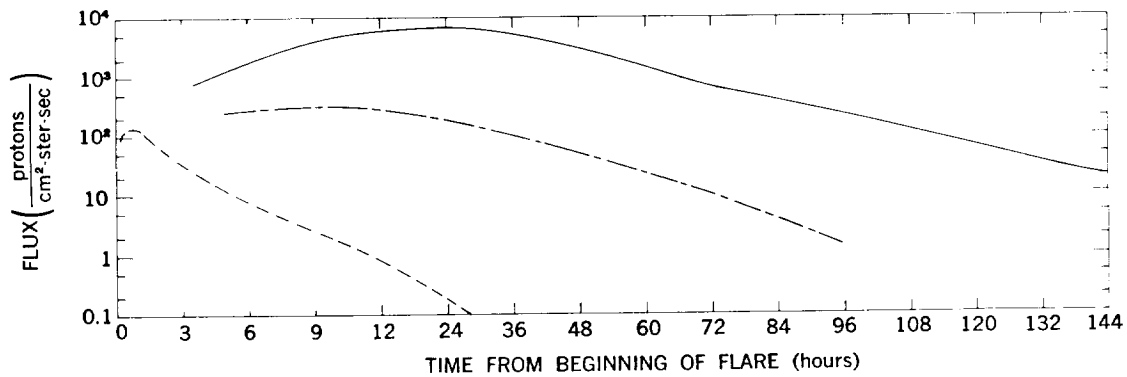
Figure 2-22—The time history of an imaginary envelope event which includes
all the types of events observed.

ACKNOWLEDGMENTS

CHAPTER 3

ANISOTROPIES IN COSMIC RADIATION OF SOLAR ORIGIN

by

Kenneth G. McCracken*

INTRODUCTION

On rare occasions, cosmic rays generated by large solar flares are observed by cosmic ray detectors situated upon the earth's surface. Sometimes the particle fluxes are very great. It has been shown that the energy spectrum of the solar cosmic radiation is very steep; the unidirectional particle fluxes (particles/cm²-sec-ster) increasing rapidly with decreasing particle energy. Owing to absorption in the atmosphere, particles with energies less than 450 Mev are not detected near sea level; however, recently introduced high altitude techniques have shown that the particle flux continues to increase rapidly below 450 Mev. Furthermore, it has been shown that many solar flares which produce no appreciable effect at sea level do result in very intense fluxes of particles of energies less than 450 Mev. It is now recognized that the copious production of cosmic radiation is a common feature of large solar flares.†

The very great particle fluxes present in the solar system after a solar flare are a potential hazard to manned space flight, and a space vehicle is likely to require radiation shielding. It has been observed, however, that the solar cosmic ray fluxes are sometimes markedly anisotropic; i.e., the fluxes from some directions are greater by as much as a factor of ten than those from other directions. Therefore the most economical utilization of shielding material might be obtained if the vehicle were more heavily shielded on one side than on the other. It is the purpose of this chapter to document the current experimental and theoretical knowledge of these flux anisotropies in order to assist in developing criteria for space vehicle design.

This chapter is organized as follows: First there is a brief section on nomenclature, and on the nature of the experimental data used to investigate the anisotropies. The second section gives a detailed discussion of the anisotropies associated with three flare effects.

---

*University of Tasmania; now at Graduate Research Center of the Southwest.
†Chapter 1.

57

The third section describes a model for the magnetic fields within the solar system in good agreement with all the current experimental data pertaining to the cosmic ray effects of solar flares. The model makes it possible to predict the flux anisotropies which would be observed at low particle energies, and at points far distant from the earth (neither of these situations having been observed to date). The fourth section details the method currently available for investigating the flux anisotropies. This section has been included to facilitate future investigations of flare effects; thereby adding to the body of experimental data, and leading to more accurate predictions of future situations.

NOMENCLATURE AND THE EXPERIMENTAL TECHNIQUES

A direction in free space is usually specified by two angles, the declination, and the right ascension (RA). The declination is the angle the direction makes with the equatorial plane of the earth. For the purposes of this paper, the right ascension will be replaced by another quantity L the longitude relative to the sun. Figure 3-1 illustrates the inter-relation of these quantities. The longitude relative to the sun is the angle between the earth's meridional plane containing the sun, and the meridional plane parallel to the direction in question. Clearly RA = S + L, where S is the right ascension of the sun.

The instruments most commonly used to monitor the cosmic radiation at sea level are the ionization chamber, the meson telescope, and the neutron monitor. Of these the neutron monitor is the most sensitive to low energy cosmic rays; hence a flare effect as observed on the ground is always much more pronounced in neutron data than in the records from the other detectors. Furthermore, the correction of neutron data for atmospheric effects is relatively simple, but rather difficult for the other detectors. For these reasons neutron data have been used almost exclusively in detailed derivations of anisotropies in particle fluxes of high energy events. Furthermore, it has been shown that if the cosmic radiation is isotropic, then the increments observed by different neutron detectors of a standard construction (Reference 73) are all equal (Reference 32). Hence we can be confident that differences in neutron monitor amplitudes are due to anisotropies, and we may analyze the data accordingly.

There is always a relatively time-invariant flux of cosmic rays arriving at the earth. This will be referred to as the *galactic cosmic radiation,* since it is believed to arise outside the solar system. The cosmic rays produced in a solar flare will be called *solar cosmic rays.*

The motion of a cosmic ray in the earth's magnetic field is exceedingly complex; the particle often undergoes very great deflections before reaching the earth; for example, see Jory (Reference 74) and references therein. Nevertheless, it is possible to calculate the deflections, and to state the direction from which any given cosmic ray was travelling prior to its entry into the geomagnetic field.
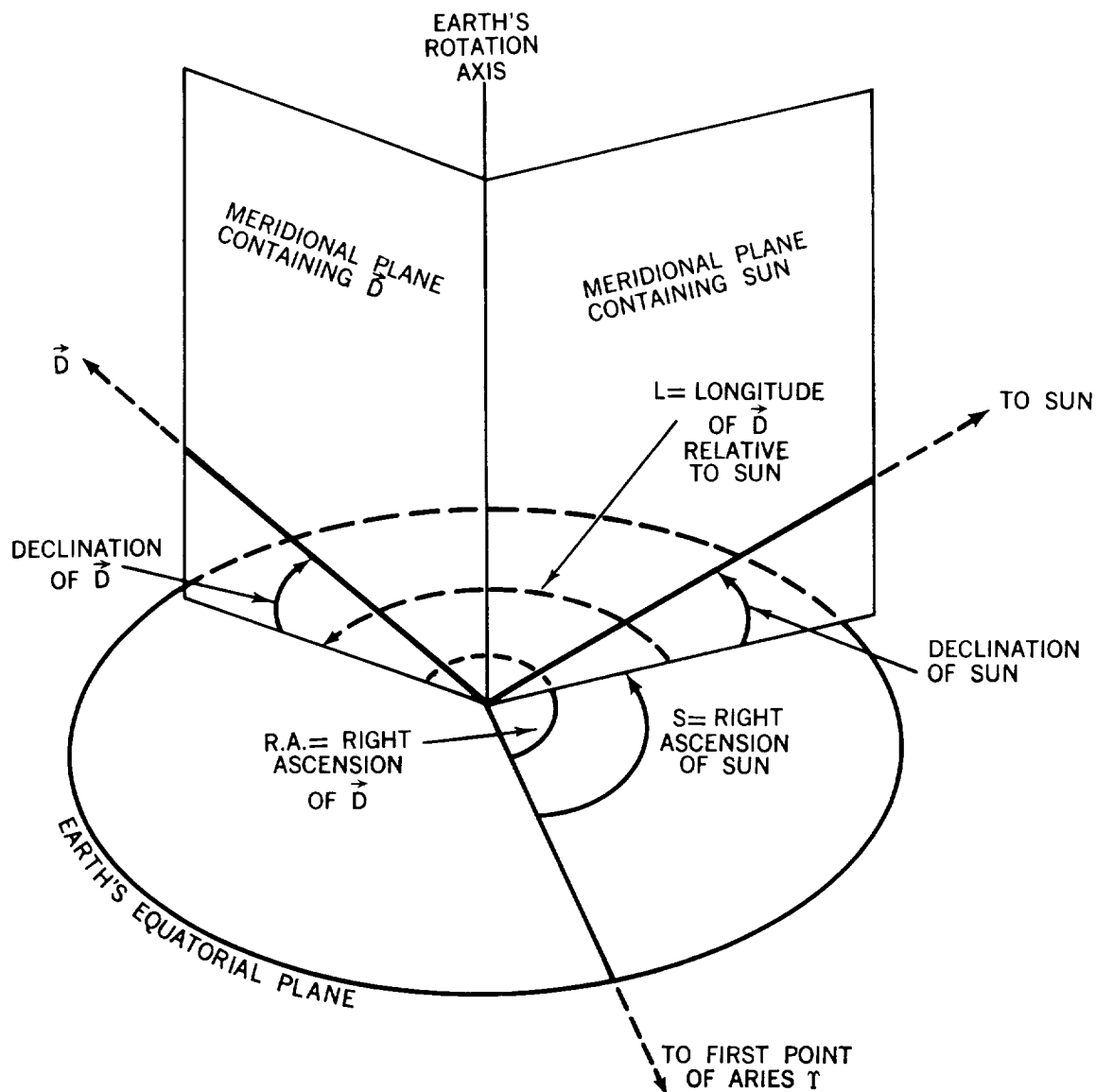
Figure 3-1—Illustrating the definitions of declination; S, the right ascension and longitude relative to the sun applicable to a direction D.

By considering the totality of cosmic rays (all energies and all directions of arrival) arriving at a given cosmic ray detector, it is found that although detectors at low and medium latitudes (less than 60° geomagnetic latitude) sample the radiation from directions all over the celestial sphere, a detector at a high latitude samples the radiation from directions included within a small solid angle. That is, this latter "looks" in an essentially unique direction (Reference 32). The "directions of viewing" of a number of cosmic ray detectors are shown in Figure 3-2. The simultaneous observation of a flare effect by a number of stations permits the preparation of a "map" in which the cosmic ray enhancements as

60
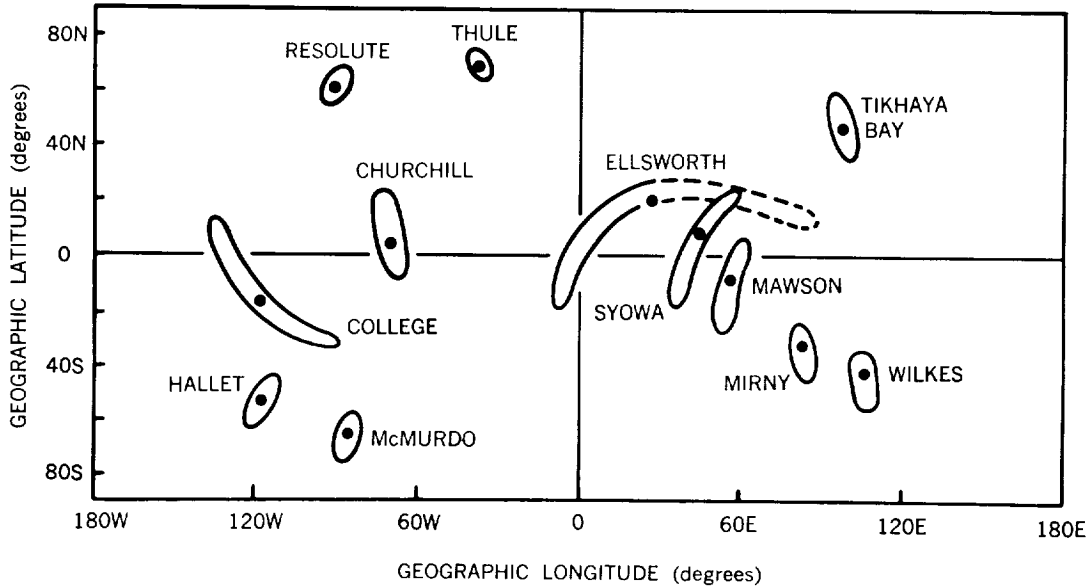
Figure 3-2—The totality of directions from which cosmic rays can reach twelve high-latitude neutron monitors. The mean directions of viewing are indicated by dots. The dashed curve for Ellsworth indicates some uncertainty as to the detailed nature of the direction of viewing.

measured by each detector at some given time are assigned to the detectors' directions of viewing. The map therefore shows the manner in which the solar cosmic ray flux varied with direction at any given time during the flare effect, and a succession of such maps indicates the manner in which the anisotropy varied with time. For an adequate description of the anisotropies, data must be obtained by a large number of detectors situated on the earth's surface in such a way as to give complete coverage of the celestial sphere. In Chapter 1 it was pointed out that many flare effects observable at low energies (using riometer, or direct primary particle detectors) are not observed by neutron monitors. Unfortunately the existing data pertaining to these additional flare effects contribute very little to our knowledge of the anisotropies in the solar cosmic radiations, for two reasons: (1) Riometers and detectors in balloons or low altitude satellites sample the cosmic radiation which, prior to entry into the geomagnetic field, was coming from within a solid angle extending essentially 360 degrees in right ascension. Consequently these detectors do not "look" in any unique direction; instead they measure a weighted average of the cosmic ray fluxes arriving from within a large part of the celestial sphere. (2) The continuity in time of the balloon and satellite data is poor. Balloons are usually launched once the flare effect has started, and many satellite borne detectors are only useful for the study of solar cosmic rays when the satellite is outside the Van Allen belts.

Much could be learned through study of the anisotropies of low energy cosmic rays, and instruments designed for this purpose offer great promise for the future when flown in high-apogee satellites.

THE OBSERVED ANISOTROPIES

Although the anisotropic nature of the solar flare cosmic radiation has been recognized for more than a decade (Reference 75), the scarcity of detectors precluded a definitive study prior to 1957. Since that time, however, an adequate network of detectors has been in existence; and careful studies have been made of the flare effects of May 4, November 12, and November 15, 1960. A number of other flare effects since 1957 have been too small to permit a detailed study of the anisotropies. We will discuss the aforementioned three events in detail, and then state some general conclusions reached from study of the totality of observed flare effects.

May 4, 1960

The data obtained by seven stations at the time of the flare of May 4, 1960 are presented in Figure 3-3. It has been shown that when the solar cosmic radiation is isotropic, these seven detectors all observe the same percentage increment in the counting rate. Hence the amplitude differences evident in Figure 3-3 must be the result of the stations' sampling of radiation from different directions in space. The great disparity in increments in Figure 27 indicates that the flux was very anisotropic; for example, the flux sampled by Churchill was more than ten times that sampled by Mawson.

The flare on the sun was observed over a large sunspot on the west limb of the sun at 1014 UT. Simultaneously, intense radio noise was observed at centimeter wavelengths. The first indication of an increase in the cosmic ray flux occurred at 1029 UT and thereafter the fluxes rose rapidly with the maximum intensity observed at 1038 UT at Churchill.

We should note that the 15 minute delay, between the optical and radio observations of the flare and the initial arrival of solar cosmic rays at the earth, is quite characteristic of flares near the western limb of the sun: 5 such events show time delays between 12 and 17 minutes. The reason for these time delays is not known with certainty.

A "map" of the cosmic ray flux during the interval 1045-1100 UT (soon after the maxima were attained at the various stations) is given in Figure 3-4a and for the period 1115-1130 UT in Figure 3-4b. For each station and interval the observed counter rate enhancement (essentially a measure of the flux of particles with energies greater than 450 Mev) is assigned to the direction of viewing of the station. It is immediately clear that during both intervals the greatest particle fluxes were observed from a direction to the west of the sun. Analysis of the data represented in Figure 3-4a showed that during the period 1045-1100 UT the cosmic ray fluxes were symmetrical about a direction $\vec{D}$, specified by declination 10° north, and longitude 55° west of the sun; this direction is known within ±5° The flux of cosmic rays arriving from any direction $\vec{S}$ depended solely upon the angle δ between $\vec{D}$ and $\vec{S}$ (Figure 3-5).
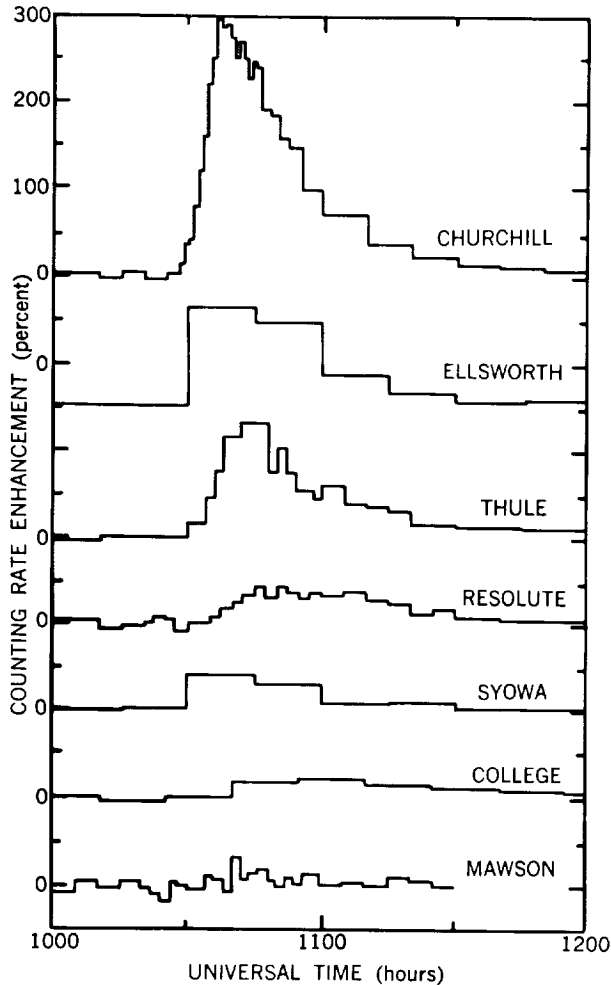
Figure 3-3—The neutron counting rate enhancements observed during the flare effect of May 4, 1960. The ordinate scales are identical for all seven curves.

The data represented by Figure 3-4b, and those pertaining to other intervals during the flare effect, have also shown that the particle fluxes exhibited a direction of symmetry (Reference 32). The direction of symmetry applicable to the period 1115-1130 UT is shown in Figure 3-4b and differs from that derived for the period 1045-11-- UT by 7.5 in longitude; this difference is statistically insignificant. An extremely important result derived from these maps, and from balloon data obtained at 1900 UT by Winckler, et al. (Reference 59) is that, throughout a period of nine hours (starting at the time of the flare), the direction of symmetry showed no significant change but remained consistent with the direction for the 1045-1100 UT period (declination 10° North; longitude 55 West of the sun). The dependence of particle flux upon δ (as defined above) at various times during the flare effect is shown in Figure 3-6. In summation we can state that:

1. During the entire event, the particle fluxes were symmetrical about a direction 55° west of the sun, and 10° north of the equatorial plane.

2. The radiation was extremely well collimated initially; with time, however, the angular distribution became progressively broader, and tended towards isotropy (Figure 3-6). The flux anisotropies of this event were long lived compared to some other flare events. Two hours after the start of the flare effect the ratio of the maximum to minimum flux was still 2:1, while the particle flux was still anisotropic nine hours after the flare. For directions such as sampled by Mawson, the average flux of particles of energies greater than 450 Mev was some 0.05 times that sampled by Churchill. This increase represents an extremely great anisotropy of the radiation.

3. When the greatest fluxes were observed (1036-1038 UT, Figure 3-6), the angular distribution of the radiation was very steep. The Mawson data indicate that at this

time the flux from a direction inclined at an angle of about 85 to the direction of symmetry was not significantly different from the pre-flare value; i.e., the whole flux of solar cosmic radiation was incident from one hemisphere. This situation persisted for the first nine minutes of the flare effect (1029-1038 UT).

4. The derived angular distributions pertaining to early times (Figure 3-6) are increasing steeply as δ decreases to the smallest value for which data are available. It is therefore conceivable that from some direction the maximum flux was considerably greater than that sampled by Churchill.

5. The fluxes mentioned above and implicit in Figures 3-5 and 3-6 are all unidirectional fluxes. To calculate the radiation dosage represented by this flare we must estimate the omnidirectional flux, (i.e., the total number of particles passing through a sphere of unit cross section in unit time). This estimate could be made from the curves of Figure 3-6; however, the extrapolations into the region of small δ introduces rather large errors. But it is qualitatively clear that the rate of decrease of the omnidirectional flux will be slower than the rate of decrease of the intensity observed by Churchill because of the trend towards isotropy.

6. For some investigations it may be useful to estimate the fluxes incident from directions for which observations are not available. This

(a) 1045 to 1100 UT

(b) 1115 to 1130 UT
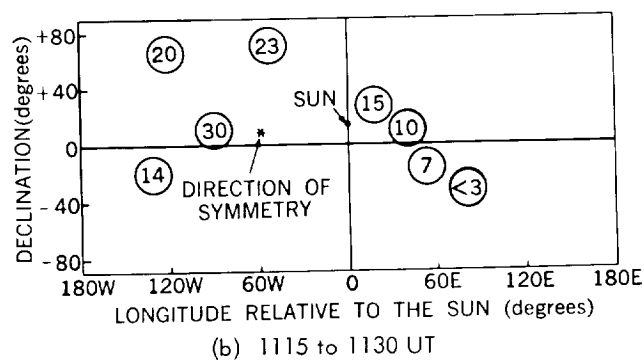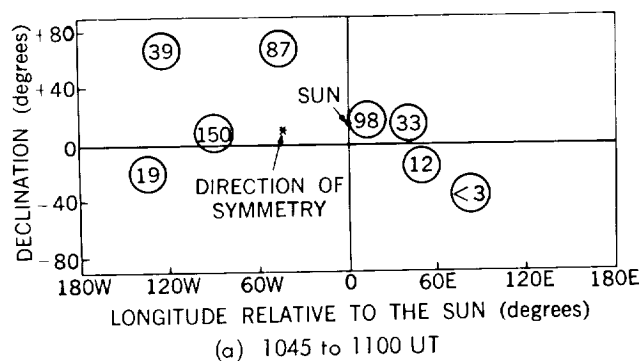
Figure 3-4—Maps showing the dependence of a cosmic ray flare upon direction for two intervals during the flare effect of May 4, 1960.
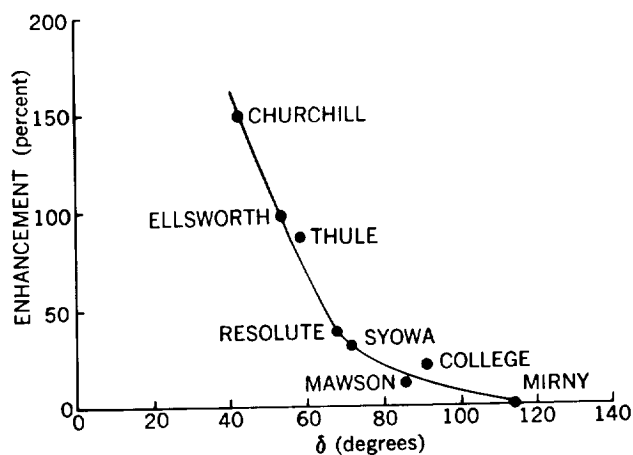
Figure 3-5—The dependence of counting rate enhancement (and hence of cosmic ray flux) upon direction for the interval 1045-1100 UT on May 4, 1960. δ is the angle between the axis of symmetry and the direction in question. The axis of symmetry is shown in Figure 3-4a.
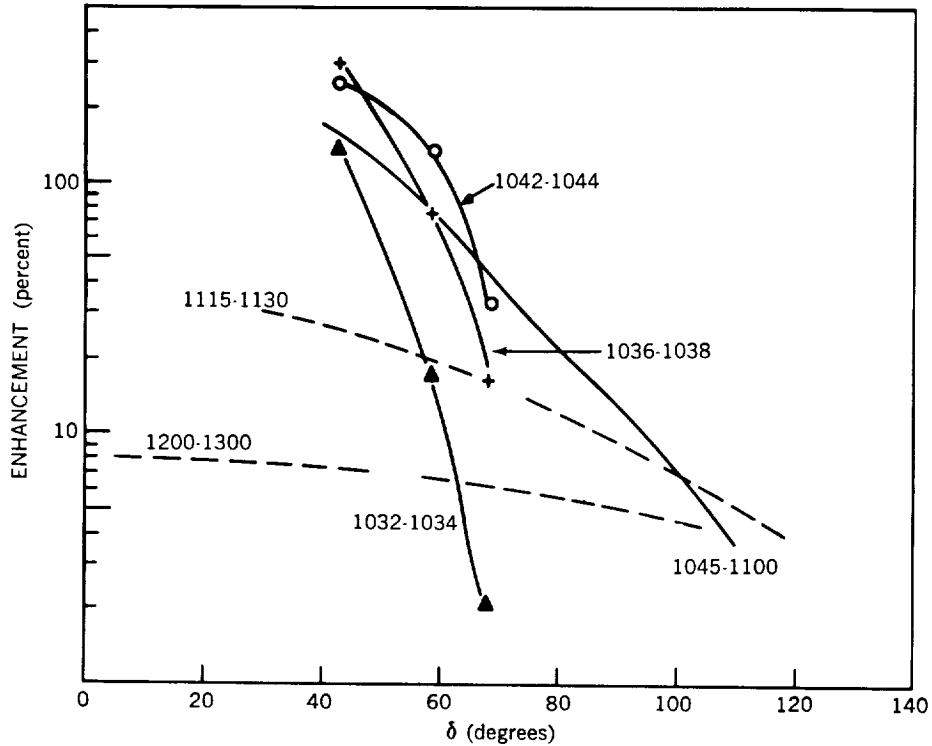
Figure 3-6—The dependence of counting rate enhancement (and hence of cosmic ray flux) upon direction of viewing at various times during the flare effect of May 4, 1960. δ is the angle between the axis of symmetry and the direction in question. The axis of symmetry is shown in Figure 3-4a.

requires extrapolation or interpolation based upon the observed data and is possible if the fluxes are symmetrical about a known, single direction in space. With these facts, diagrams such as Figure 3-7 can be prepared for various times during a flare effect. Figure 3-7 has been derived from Figure 3-6 for the interval 1045-1100 UT on May 4, and here the curves are "contour lines" of constant cosmic ray intensity, which show the variation of intensity with direction.

7. It has been shown in Reference 32 that the differential energy spectrum of the flare radiation approximated E^{-5} at early times (about 1045 UT), and increased to $E^{-6.5}$ by 1100 UT (where E is the particle energy). Within a precision of 0.5, the exponent of the spectrum has been shown to be invariant with respect to direction. The spectral exponent at the high energy end of the flare spectrum, however, may be different from that observed at lower energies.
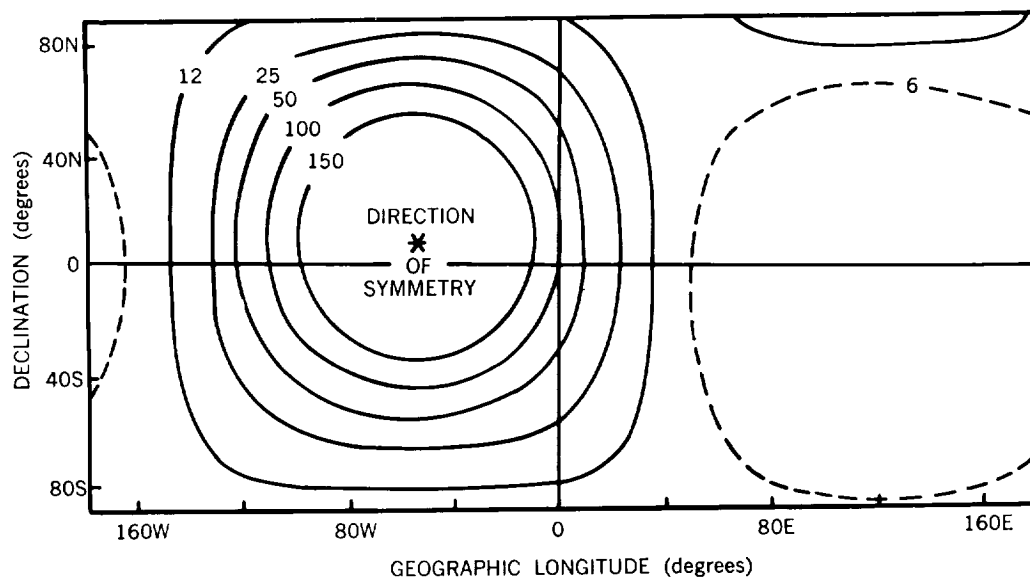
Figure 3-7—The cosmic ray flux variation with direction during the interval 1045-1100 UT on May 4, 1960. The "contour lines" join the directions of equal cosmic ray flux. The unit of intensity is not known at present, and this diagram should only be used to compare relative flux values.

November 15, 1960

On November 15, 1960, a solar flare was observed to commence over a large sunspot group situated 33° west of the central solar meridian at 0207 UT. About 0238 UT the cosmic ray intensity at Mawson increased rapidly, reaching a maximum at about 0305 UT. By referring to Figure 3-8a, we see that there are marked differences between the Mawson and Churchill data: in particular, the solar flare effect started at Mawson at 0238 UT, and did not commence at Churchill until after 0310 UT. This indicates a strong anisotropy of the radiation at early times. Analysis (Reference 32) has shown that, during the anisotropic phase, the particle fluxes were symmetrical about a direction $50° \pm 20°$ to the west of the sun. Note the similarity to the May 4, 1960 event, for which the axis of symmetry was 55° to the west of the sun.

The graphs of Figure 3-8a show that the differences between the various data had largely disappeared by 0330 UT, and completely so by 0400 UT. This indicates that the anisotropy was small at 0330 UT and that complete isotropy prevailed by 0400 UT. The degree of isotropy is indicated by the "map" (Figure 3-8b), which shows that various stations sampling the cosmic ray fluxes from entirely different directions were recording essentially equal cosmic ray intensities during the hour 05-06 UT.* A detailed analysis

*Compare Figure 3-8b with Figure 3-4a for which the anisotropy is marked.
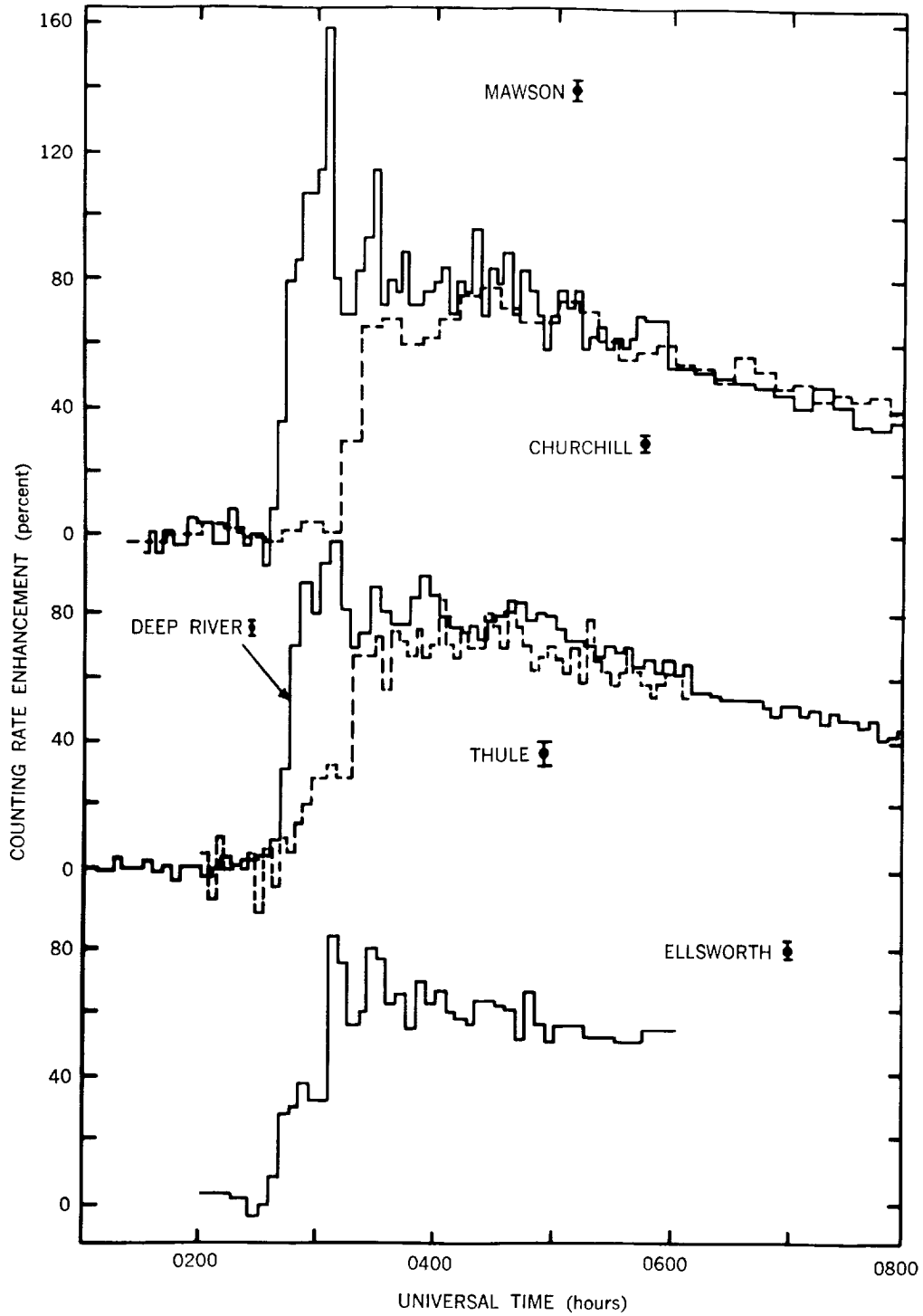
Figure 3-8a—The neutron counting rate enhancements observed during the flare effect of November 15, 1960. The enhancements are relative to the mean counting rate for the period 2200-0200 UT prior to the flare. ⚕ indicates the statistical accuracy appropriate to each value of the enhancement.

showed that by 0400 UT, any anisotropy was less than 2 percent of the total radiation flux. Therefore the anisotropic phase of the event lasted no more than 80 minutes and essentially was over after 50 minutes (0330 UT). Solar particles continued to be detected until after 2400 UT, and the radiation remained isotropic throughout the whole interval 0400-2400 UT.
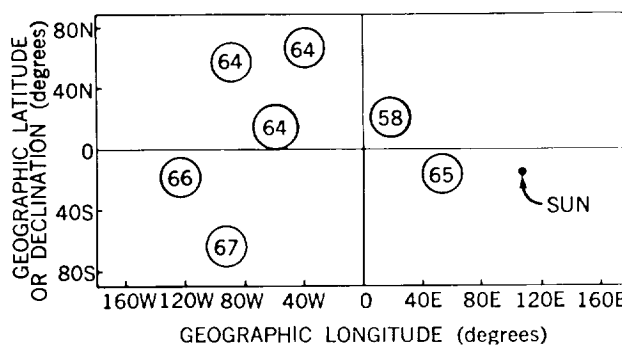
Figure 3-8b—The "map" of the solar cosmic ray flux for the interval 0500-0600 UT on November 15, 1960.

For this event the anisotropic phase was only a small portion of the total solar cosmic ray event, and the major part of the event exhibited complete isotropy. On November 15, the time-averaged flux from the direction of the maximum flux sampled by Mawson was only 1.2 times the minimum sampled by Churchill. This is in distinct contrast to the May 4 event, for which the comparable ratio was 16.0, and for which the anisotropy was long lived.

When compared with the totality of flare effects observed to date, the May 4 and November 15 events are both found to belong to one distinct class of flare effects. There are, in fact, rather marked similarities between the two events:

1. Both flare effects were produced by flares on the western portion of the solar disk.

2. The cosmic ray intensity rose rapidly (in less than 30 minutes) to a maximum; the rate of rise was very great for the fluxes from some directions (about 10 min.).

3. There was a strong anisotropy at early times. It would appear that the decay of the anisotropy varies from event to event.

4. The greatest cosmic ray fluxes were observed from a direction approximately 50° to the west of the sun.

The totality of flare effects observed to date leads us to believe that these properties will be observed for any flare effect produced by a flare occurring between 30° and 90° on the solar disk.

November 12, 1960

Data for the November 12, 1960 event are presented in Figure 3-9. Apart from the presence of the second maximum at about 1900 UT, this event differs from the previously
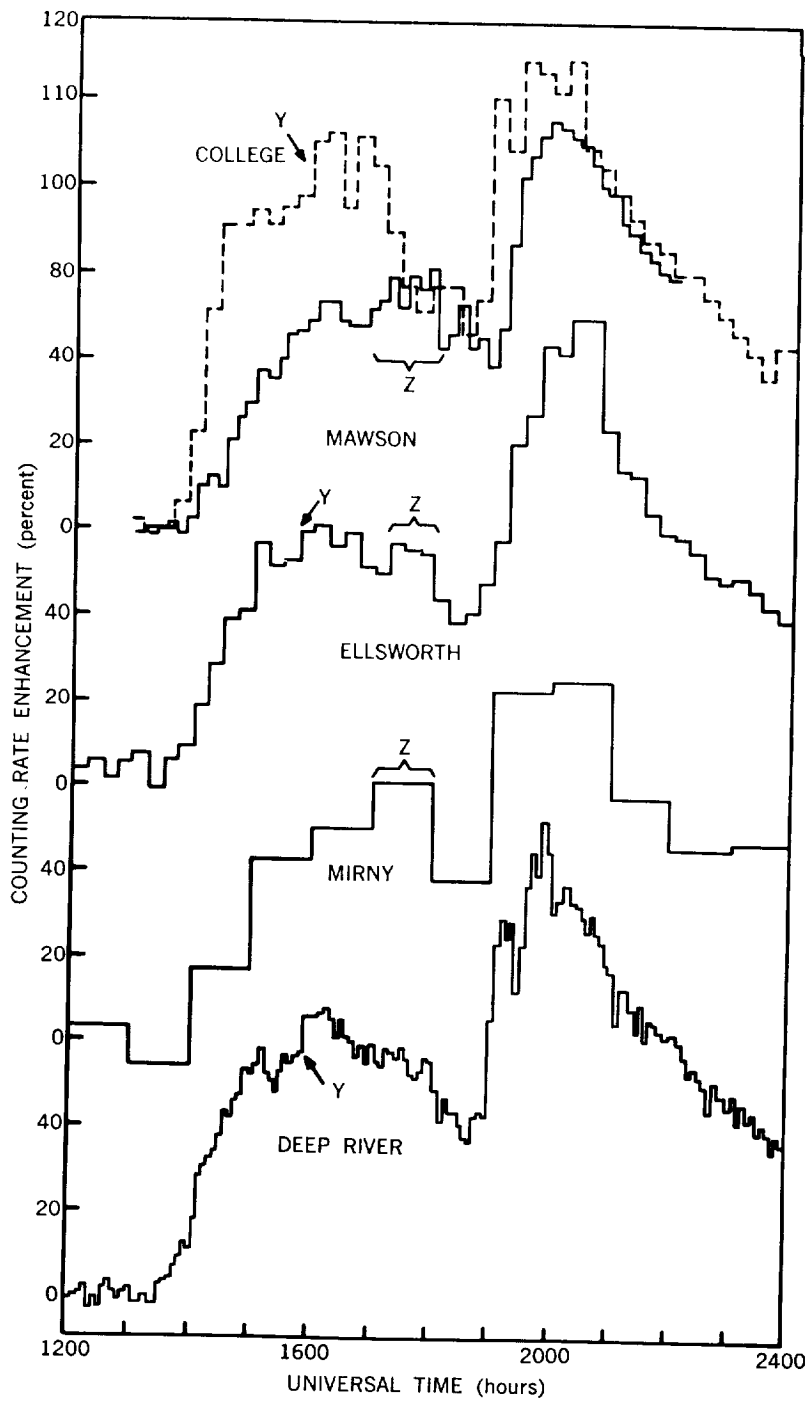
Figure 3-9—The neutron counting rate enhancements observed during the flare effect of November 12, 1960. The enhancements are relative to the mean counting rates for the period 0800-1200 UT.

discussed events in that the intensity rose to a maximum very slowly (approximately 2 hours). A "map" of the cosmic ray fluxes shows that, until 1900 UT (the start of the second increase in intensity), the radiation was mildly anisotropic, with the maximum intensity from a direction specified by a declination of $-20°$ and a longitude of $40°W$. A "map" of the cosmic ray intensity during the interval 1400-1500 UT is given in Figure 3-10a. Figure 3-10b shows the angular distribution of the particle fluxes about this direction during the same interval. The angular distributions are basically similar for all times prior to 1900 UT.

A quantity W has been defined to measure the degree of anisotropy of the incident radiation. W is essentially the root-mean-square deviation of the flux from the mean value, divided by the mean value. Table 3-1 lists the values of W for the November 12 flare effect. It can be seen that W was essentially constant until 1800 UT, i.e., until shortly before the commencement of the second enhancement in intensity. After 2000 UT, when the second maximum in intensity was reached, the values of W are consistent with isotropy.
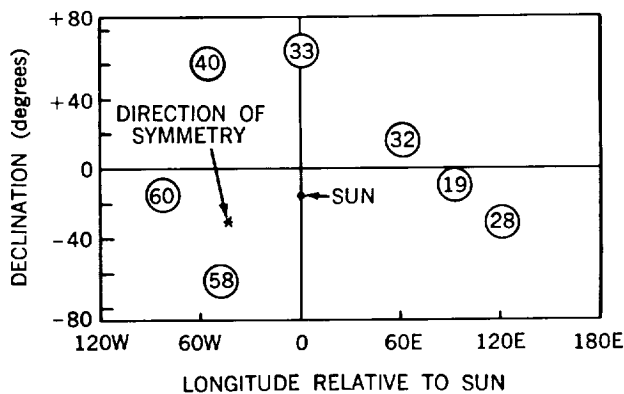

Figure 3-10a—The "map" of the solar cosmic ray flux for the interval 14-15 UT on November 12, 1960.
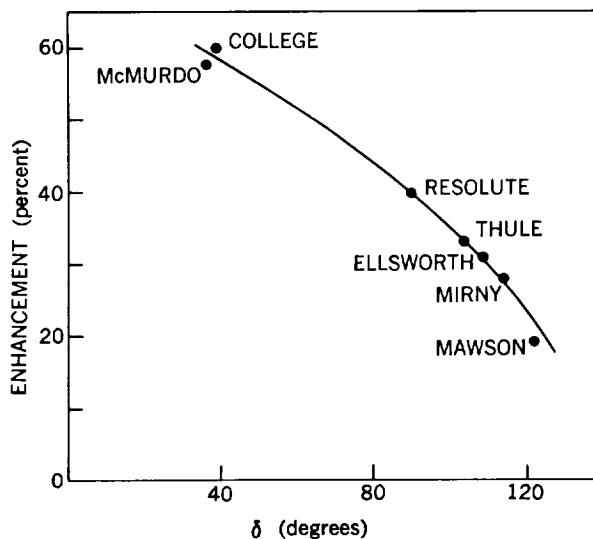

Figure 3-10b—The angular dependence of cosmic ray flux during the interval 1400-1500 UT on November 12, 1960. δ is relative to the axis of symmetry of the solar radiation (as shown in Figure 3-4a).

Thus the character of the radiation changed suddenly from mildly anisotropic to completely isotropic at the time of the second enhancement.

A thorough discussion of this event is unnecessary in this paper; however, Reference 62 considers it in detail. Here the current interpretation of this event is sufficient: Prior to 1900 UT the situation was one which usually exists when cosmic rays are produced near the center of the solar disk. On this occasion, however, at 1900 UT, the earth entered the

Table 3-1

The Degree of Anisotropy of Incident Radiation Calculated from
Observations of the November 12, 1960 Flare. A Value of
Approximately .030 for W Indicates Isotropy of the
Incident Cosmic Radiation.

Universal Time	W	Universal Time	W
1400-1500	.392	1900-2000	.101
1500-1600	.183	2000-2100	.011
1600-1700	.216	2100-2200	.017
1700-1800	.213	2200-2300	.045
1800-1900	.138	2300-2400	.031

region of the solar system where the situation was typical of cosmic ray production on the western portion of the solar disk. Events such as these are uncommon.

The Totality of Solar Flare Data

Except for the three flare effects discussed, it has not been possible to investigate the anisotropies of solar flare radiation in any detail. It is possible, however, to say in broad terms whether other flare effects exhibited anisotropies. This information is given in Table 3-2 for all the flare effects observed to date. The flares are listed in order of increasing rise time (i.e., the time required for the intensity of high energy particles (E > 450 Mev) to reach a maximum value.) The position on the solar disk of the flare which generated the cosmic rays is also presented.

From a study of this table, and the three well documented flare effects described previously, the following phenomenological statement of the properties of solar flare radiation can be made:

(1) The probability of observing a flare effect at high particle energies (E > 450 Mev) is greatest if the flare generating the cosmic radiation is on the western portion of the solar disk. Furthermore, the most intense flare effects (see Table 1, Chapter 1) have been those associated with flares on the western portion of the solar disk; this suggests that the propagation conditions experienced by the high energy cosmic rays tend to prevent access to the earth if the parent flare is not in the western hemisphere of the solar disk.

Table 3-2

Data on All Flares Exhibiting Anisotropies; the Data are Too Scarce and the Events
Too Small to Permit Determinations of The Rise Times for The Last Four Events.

Date of Event	Relative Rise Time*	Position of Parent flare on Solar Disk	Anisotropy
May 4, 1960	1	90° W	very marked
February 23, 1956	4	80° W	marked
November 15, 1960	6	45° W	very marked
November 19, 1949	6	70° W	very marked
March 7, 1942	7	90° W	marked
February 28, 1942	13	4° W	poorly defined
July 25, 1946	17	15° E	not noticeable
November 12, 1960	20	10° W	poorly defined
July 17, 1959	36	30° W	none
September 3, 1960	50	90° E	none
August 31, 1956	—	15° E	—
November 20, 1960	—	90° W	—
July 18, 1961	—	50° W	—
July 20, 1961	—	90° W	—

*Defined as the interval between the commencement of the intensity enhancement and the time of maximum
intensity in comparison to that of the May 4, 1960 event.

Large solar flares are observed equally often on the eastern and western portions of
the solar disk. If we make the reasonable assumption that the production of cosmic rays
is equally likely at all points on the solar disk, the observations will provide an estimate
of the probability that the solar cosmic ray flux at the earth will exceed the threshold im-
posed by a ground level cosmic ray detector. The observations and a smoothed probability
curve are given in Figure 3-11. The probability that radiation produced near the western
limb will reach the earth is arbitrarily taken as 1. This curve gives the relative proba-
bilities for the observation of a solar flare effect for different points on the solar disk.

It should be noted that the above east-west effect is not so well defined at the lower
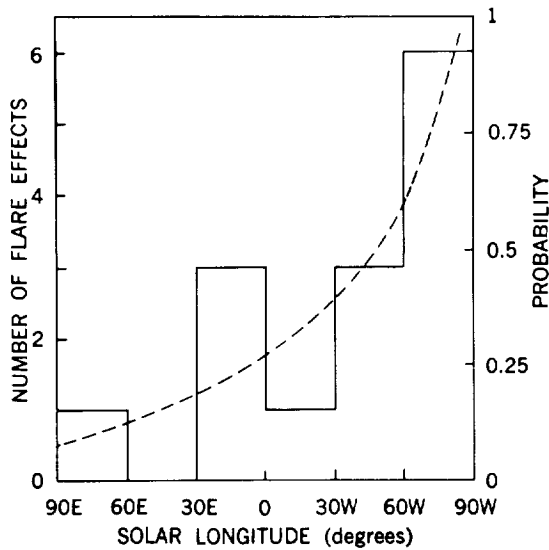energies of about 100 Mev (Reference 77). A possible cause is that although the particle

Figure 3-11—Plotting the number of flare effects produced by flares in each 30° of longitude of the visible solar disk. A smoothed curve, to be understood as the probability of observation of a flare effect, is superposed.

energy is low, the particle density great, and the total energy density is sufficient to markedly influence the magnetic fields which guide the higher energy particles to the earth.

2. Flares producing cosmic rays on the far western portion of the solar disk result in flare effects for which the particle flux rises rapidly to a maximum (rise time ≤ 30 minutes), and for which the flux is initially markedly anisotropic. The anisotropy may be as great as 10:1 at early times. With the passage of time, the radiation rapidly tends towards isotropy. In the majority of cases, the radiation is essentially isotropic (to within 10 percent) within about 90 minutes of the commencement of the flare effect. The flare enhancement of cosmic ray intensity may then continue for many hours. During the anisotropic phase, the greatest particle flux comes from the general direction of the sun. The events for which a detailed analysis is possible indicate that the greatest flux is from a direction about 50° to the west of the sun, and roughly in the plane of the ecliptic.

3. For flares producing cosmic rays near the center or on the eastern portions of the solar disk, the particle flux of the flare effects rises slowly (in about 2 hours) to a maximum. The radiation may be mildly anisotropic (fluxes differing by as much as 2:1). In the November 12, 1960 event the anisotropy persisted unchanged for many hours, in sharp contrast to the ephemeral nature of the anisotropy associated with the majority of flares on the western portion of the solar disk.

The above are the observed properties of the high energy (> 450 Mev) cosmic radiation at the earth. Observations at low energies and far from the earth are very fragmentary at present, and data on the flux anisotropies are non-existent. It is therefore desirable to see whether the foregoing above can be explained by a model described in terms of some physical property of the solar system; for if this is so, the model can be used to extrapolate the earthbound observations into the regions presently inaccessible to measurement. Such a model has been formulated, and will now be outlined (for a more complete discussion, see Reference 32).

THE MODEL OF THE INTERPLANETARY MAGNETIC FIELD

Because of the great distances involved, very weak magnetic fields will greatly affect the motion of cosmic rays in their passage from the sun to the earth. For example, a 1 Bev particle (a typical energy for solar flare radiation) has a gyro-radius of 5×10^{11} cm in a 10^{-5} oersted magnetic field. This is a large distance by earthbound standards, but small by comparison to the sun-earth distance of 1.5×10^{13} cm. Thus, knowledge of the structure of the interplanetary fields is vital for determining whether cosmic rays generated in a flare can ever reach any given point in the solar system; the direction from which they will arrive at that point; and the degree of isotropy to be expected at that point.

Evidence pertaining to the interplanetary magnetic fields has been obtained from solar flare cosmic ray effects and from other phenomena. To discuss the proposed model adequately, we must briefly discuss these other phenomena.

About 24 to 48 hours after a large flare, there is often a marked perturbation of the geomagnetic field (a geomagnetic storm), and the galactic cosmic ray intensity sometimes decreases abruptly (a Forbush decrease). The geomagnetic perturbation usually persists for 1 or 2 days, while the Forbush decrease persists somewhat longer, the intensity gradually returning the pre-event level. The time sequence and typical effects are shown in Figure 3-12.

The geomagnetic storm and Forbush decrease are both believed to result from the arrival of either a plasma cloud or a hydromagnetic shock wave at the earth, these phenomena having been originated by the flare 24-48 hours previously. The velocity of travel of the "plasma disturbance" is calculated to be 500 to 1500 km/sec. Evidence suggests that the geomagnetic storm is the result of a pressure exerted by the plasma on the earth's magnetic field, while the Forbush decrease is due to magnetic fields carried along by the plasma disturbance and screening galactic cosmic rays away from the earth.

We may now describe the theoretical model, which now has a very substantial experimental foundation. Figure 3-13 illustrates the model for the magnetic regime created by the plasma disturbance originating in a large solar flare (not necessarily a flare that produces cosmic rays). The plasma ejected by the flare carries the lines of force of the sun spot with it, the lines of force being stretched outward from the sunspot in a quasi-radial fashion. The sun's rotation causes the lines to curve westward. The configuration of the lines of force near the leading edge of the plasma disturbance is not yet known; however, it is known to exclude cosmic rays from outside, and to inhibit the escape of cosmic rays injected at points inside the magnetic regime.

In the Forbush decrease the arrival of the leading edge of the plasma disturbance at the earth initiates the magnetic storm, and once the earth is inside the magnetic regime some galactic cosmic rays are screened away from the earth. This phenomenon now
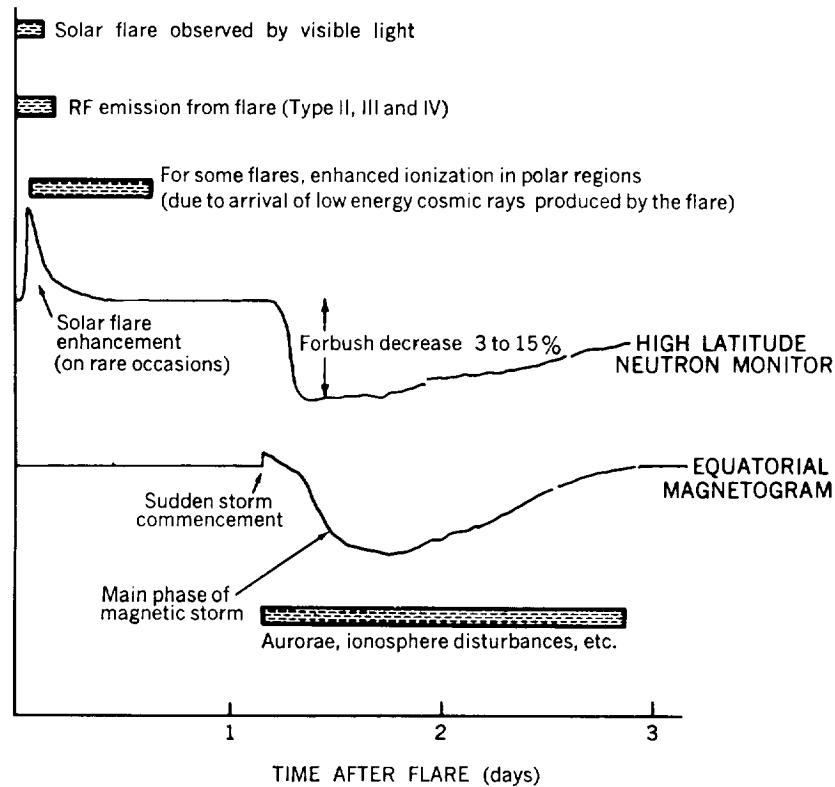
74

Figure 3-12—A typical time sequence of solar and geophysical phenomena.

provides a direct magnetic connection from the earth to the sunspot group. Consequently, if another flare were now to produce cosmic rays, they would travel rapidly along the magnetic lines of force to the earth. They would, therefore, arrive at the earth soon after the occurrence of the flare (about 20 minutes), and maximum intensity would rapidly be reached. The divergent nature of the magnetic lines of force implies that the cosmic rays would tend to become collimated, eventually traveling roughly parallel to the lines of force. Also the particles would be partially trapped within the magnetic configuration; and so after a period of anisotropy, a period of isotropy may be observed. The period of time required to reach isotropy will depend on the number and magnitude of small irregularities in the otherwise quasi-radial field. This will depend on many fine details of the injection of plasma from the sun, and will vary considerably from event to event. Consequently the time required to attain isotropy varies from event to event.

At a point outside the magnetic regime (Figure 3-13a) there is no direct connection to the sunspot, and hence cosmic rays cannot arrive rapidly at the earth. They can only arrive by diffusion across the lines of force — a process that tends to delay and isotropize them. Therefore, an appreciable time delay exists between particle production and arrival at the earth (30-120 minutes), and the intensity rises slowly to a maximum some hours after the flare. The maximum omnidirectional intensity of radiation is less than that which

would be observed if the earth had a direct magnetic connection to the sunspot. The radiation may be mildly anisotropic, with the maximum intensity oriented along the lines of force leading to the sun, but not to the sunspot group in which the flare occurred. It is believed that on November 12 the earth was initially outside the magnetic field regime connected to the sunspot region generating the cosmic rays; and that the first maximum is due to radiation diffusing out of this field regime; and that the plasma disturbance carrying the field regime overran the earth at 1900 UT, producing a geomagnetic storm and Forbush decrease and permitting the earth to sample the more intense solar cosmic radiation trapped in the magnetic regime (see Figure 3-13c). Crude calculations indicate that if a direct magnetic connection from earth to sun had existed at the time of the November 12 flare, the maximum particle fluxes would have been 20 to 40 times greater than those observed.

We therefore can summarize the 3 situations of practical interest. The following statements apply to energies in the range 100 Mev to 10 Bev. No attempt has been made to present quantitative predictions. Although such predictions could be made on the basis of a completely specified model for the interplanetary fields, our knowledge is not sufficiently detailed and the chronology of solar events is too varied to make such predictions worthwhile. The qualitative results, with the addition of some observed quantitative
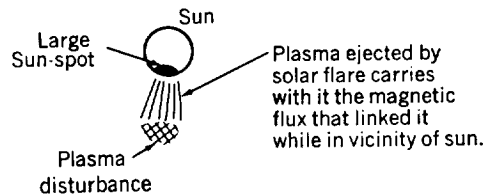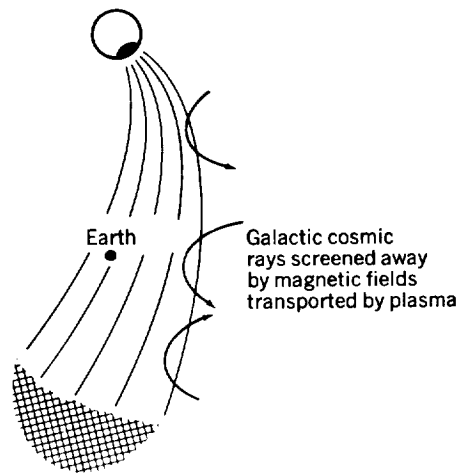

(a) 6 hours after flare
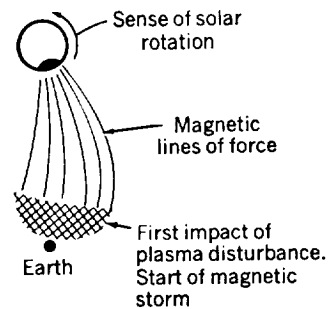
(b) About 24 hours after flare

(c) About 48 hours after flare

Figure 3-13—Changes of the interplanetary magnetic field regime model with time. We are looking down onto the north pole of the earth.

results, seem a much more reliable though less precise guide to what may be expected in future.

Situation 1

A large sunspot is behind the disk, or on the east limb, or in the interval 90 E to 30 E. No great geomagnetic disturbances or Forbush decreases have been produced by flares in this sunspot group.

Prediction: Flare activity in this group has not set up a magnetic regime linking the earth to the sunspot. Hence in the event of a flare in the sunspot region producing cosmic rays,

1. The intensities observed at the earth will be small compared to those observed inside the magnetic regime linked to the sunspot. The integrated skin dose will be of the same order of magnitude as that of the event of September 3, 1960 (0.6 rem for energies greater than 100 Mev).

2. The radiation at the earth may be mildly anisotropic (about 2:1). The anisotropy would persist throughout the whole flare effect.

3. The maximum intensity will occur 2-5 hours after the flare.

Situation 2

A large sunspot is near the center of the solar disk (±30). No great geomagnetic disturbances or Forbush decreases have been produced to date.

Prediction: This situation is similar to that in the above case, except here the particle intensities may be greater, and also a finite probability exists that the magnetic regime due to some previous flare will overrun the earth soon after another flare has filled the magnetic regime with cosmic rays. This situation is that of the November 12, 1960 flare effect. Hence while the intensity of cosmic rays might be fairly small while the earth remains outside the trapping magnetic regime, it would increase considerably once the earth was overrun by the moving plasma disturbance. Inside the regime the radiation would be essentially isotropic.

Situation 3

A large sunspot group is on the western portion of the solar disk (30 W to 90 W), or behind west limb. Flare activity has resulted in marked geomagnetic storms and Forbush decreases. Hence the model indicates that the earth and the sunspot are connected by well ordered lines of force.

Prediction: In the event of another flare generating cosmic rays,

1. The radiation will reach the earth quickly, and maximum intensity will be reached within 10-30 minutes.

2. The omni-directional intensities will be greater than those observable at other points in the solar system the same distance from the sun.

3. At early times the fluxes will be markedly anisotropic, the maximum fluxes being oriented some 50° to the west of the sun-earth line.

Although the above models were derived from observations of particles in the energy range 0.45-10 Bev, the nature of the models implies that qualitatively similar results will be obtained at lower particle energies. The model properties are summarized in Table 3-3.

Table 3-3

Prediction of Flare Effects from the Position of the Solar Flare.

Sunspot Position	Geomagnetic History	Forbush Decreases	Flare produced cosmic radiation			
			Intensity	Direction of Maximum	Time Delay to Maximum	Isotropy
Situation 1: Behind east limb; eastern solar disk (30°-90°E)	No storms	No	Small	Not known (possibly about 50° W)	2-5 hrs	Isotropic or mild, long-lived aniso-tropy
Situation 2: Central solar disk (30°E-30°W)	No storms	No	Moderate (liable to change to great)	50°W	30-120 min.	Isotropic, or a moderate, persistent an-isotropy
Situation 3: Behind west limb; western solar disk (30°-90°W)	Storms	Yes	Great	50°W	30 min.	Marked aniso-tropy at early times. Isotropy commencing after 60-90 min.

On the basis of sunspot positions, and Forbush decrease and geomagnetic activity, it is possible to make rather definite predictions regarding likely radiation conditions near the earth. Clearly, in the above discussion "earth" may be replaced by "observer in free space", where the sunspot positions and Forbush decrease activity are now reckoned relative to the observer. For this case geomagnetic activity would have no meaning; however, a continuous measurement of the interplanetary plasma would probably be entirely equivalent.

Clearly the radiation conditions are potentially worst when a large sunspot group is near the western limb, where the intensities are greatest and the warning least. Anisotropic shielding might be of advantage in this case, although the advantage might not be great when the fluxes are integrated over time (e.g., November 15, 1960). The hazard becomes less the closer the sunspot group is to the east of the central solar meridian. For this case the radiation intensities are small, and, while not markedly anisotropic, tend to retain their anisotropic nature throughout the event. Hence anisotropic shielding might be of value.

THE INVESTIGATION OF THE ANISOTROPY OF SOLAR COSMIC RAYS

We shall now describe, in some detail, how the anisotropies in the solar cosmic radiation can be inferred from ground level observations. Further information will be found elsewhere (Reference 32).

There is no simple relationship between the direction of arrival of a cosmic ray at the top of the atmosphere and the direction in which the particle was moving prior to entry into the magnetic field of the earth (the latter direction is called the "asymptotic direction of approach" of the particle). However, by numerical integration of the equations of motion of the particle in the geomagnetic field, the asymptotic directions corresponding to a number of stations and cosmic ray energies have been calculated. The Finch and Leaton (Reference 76) simulation of the geomagnetic field was employed in these calculations. This simulation employs spherical harmonics up to the sixth degree, and consequently provides a reasonably faithful reproduction of the observed magnetic field.

Some of the asymptotic directions which give access to one specific recorder are plotted in Figure 3-14. Each point in the diagram indicates the asymptotic direction corresponding to a given energy and given direction of arrival at the top of the atmosphere. The coordinates are geographic latitude and longitude. Energies between 450 Mev and 10 Bev are shown, since these are most significant for a neutron monitor during a solar flare effect. Trajectories entering the atmosphere with zenith angles of 0° and 32° are shown. Particles with energies less than 450 Mev, or making angles greater than 40° with the zenith, contribute very little to the counting rate at ground level and can safely be
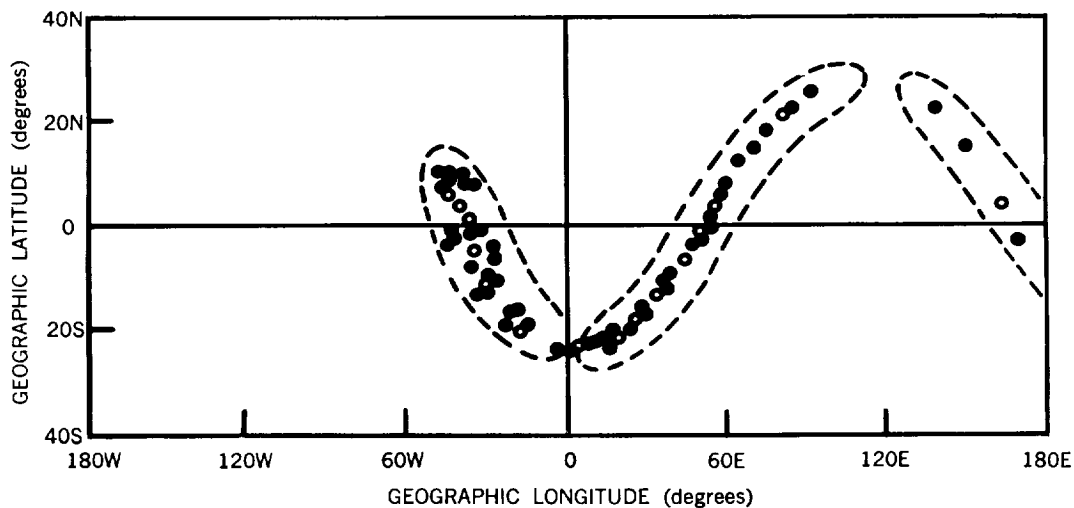
Figure 3-14—The asymptotic directions of approach for particles which ultimately arrive at Deep River, Canada. The particle energies considered lie between .45 and 10 Bev.

ignored. The solid angle containing all the above asymptotic directions will be called the asymptotic cone of acceptance of the detector.

It will be seen that the asymptotic cone of acceptance corresponding to the Deep River neutron monitor is wide in longitude and, therefore, that the Deep River detector does not sample the radiation from any single, unique direction. By way of contrast, consider the asymptotic cone of acceptance for Churchill (Figure 3-15). While the same energies and directions of atmospheric entry are plotted, it can be seen that the asymptotic directions occupy only a small solid angle (about 0.02π steradians) which spread over small ranges of latitude and longitude. Churchill therefore, can be thought of as sampling the radiation from what is essentially a single direction in space.

It has been shown (Reference 32) that there are about 12 neutron monitors in the world which have small asymptotic cones of acceptance and which can be considered to be looking in a unique direction at any given instant. The angular extent of each of the cones of acceptance is shown in Figure 3-2. The solid dots indicate the mean directions of viewing when the various asymptotic directions are weighted according to the counting rate contributions made by the various energies. The mean directions are listed in Table 3-4. The weighting factors are those appropriate to solar flare cosmic radiation. Each of these 12 detectors is analogous to a radio telescope in that it looks at the radiation arriving from within a small solid angle in space, and with the passage of time, the rotation of the earth causes the detector to scan a strip of the celestial sphere.

Figure 3-2 shows that at any instant the various detectors look in different directions in space. Although the coverage of the celestial sphere at any given time is rather
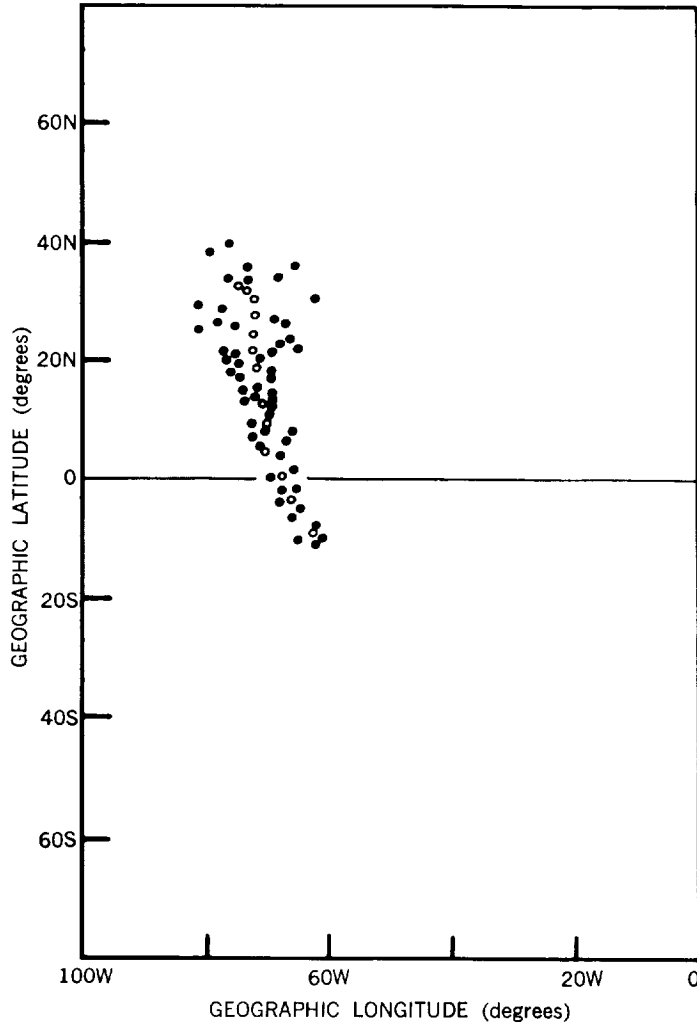
Figure 3-15—The asymptotic directions of approach for particles which ultimately arrive at Churchill, Canada. The particle energies considered lie between .45 and 10 Bev.

incomplete, a number of new neutron monitors have been proposed which will significantly improve the coverage. Once the geographical position of a new detector is known, the details of its asymptotic cone of acceptance can be calculated. The digital computer programs necessary to perform these calculations are available from the author upon request.

The features of Figure 3-2 depend almost completely upon the nature of the geomagnetic field. Providing that the field does not change, this Figure can be applied to the study of any solar flare effect which may occur in the future. However, the figure might be somewhat in error if the cosmic radiation of solar origin were to arrive at the earth during a violent magnetic storm. Fortunately, the magnetic perturbations at the time of a flare are usually very small, and current knowledge of the geomagnetic field indicates that the directions shown on Figure 3-2 are correct to within 2 degrees.

Consider now that the data for a cosmic ray flare effect are available from a number of the detectors indicated in Figure 3-2. At each instant during the flare effect each detector samples the radiation from within its own small cone of acceptance. The angular dependence of the radiation at each instant may therefore be derived by assigning the observed solar cosmic ray fluxes to the appropriate directions of viewing; the resulting diagram is a map of the cosmic ray flux. In practice the observed counting rates must be normalized to allow for differences in the instruments and the atmosphere at the different detector locations. Since the galactic cosmic radiation is essentially isotropic, the most convenient method of normalization is to express the counting rate enhancement

Table 3-4

The Mean Asymptotic Directions of Viewing of a Number of Neutron Monitors with
Small Asymptotic Cones of Acceptance for a Flare Type Cosmic Ray Spectrum.

Station	Station Coordinates		Asymptotic Direction of Viewing	
	Latitude North	Longitude East	Latitude North	Longitude East
Churchill	58° 45'	265° 55'	+4.9°	290.1°
College	64° 51'	212° 10'	-15.7°	241.1°
Ellsworth	-77° 43'	318° 53'	+15.5°	23.3°
Hallet	-72° 25'	170° 15'	-54.6°	243.5°
Mawson	-67° 36'	62° 53'	-8.0°	55.3°
McMurdo	-77° 51'	166° 37'	-66.6°	275.1°
Mirny	-66° 33'	93° 00'	-32.9°	82.4°
Resolute	74° 41'	265° 06'	+59.7°	269.1°
Syowa	-69° 00'	39° 35'	+7.6°	45.5°
Tikhaya Bay	+80° 20'	52° 48'	+44.2°	97.0°
Thule	+76° 33'	291° 10'	+68.7°	321.9°
Wilkes	-66° 25'	110° 27'	-44.0°	108.0°

as a percentage of the galactic counting rate. The correction for atmospheric differences will be outlined later. Figure 3-10a is the map of the solar cosmic ray flux derived in this manner for the interval 1400-1500 UT on November 12th, 1960. Although observations are sparse, it is abundantly clear that the radiation was anisotropic. From this diagram the graph of the angular dependence of the solar cosmic radiation has been derived (Figure 3-10b).

By way of contrast, Figure 3-8a is a map of the cosmic ray flux during the interval 0500-0600 UT on November 15th. From this map it is clear that the solar cosmic radiation was essentially isotropic. Figures 3-4a, 3-10a, and 3-8b are therefore the maps of cosmic ray fluxes exhibiting strong, moderate and zero anisotropy, respectively.

The method of correction for the differences in atmospheric absorption at the different stations must be discussed. It has been shown that the counting rate C of a neutron monitor increases exponentially as the atmospheric pressure $\mathcal{P}$ decreases; the relation between C and $\mathcal{P}$ is $dC/C = -d\mathcal{P}/\lambda$, where λ is the attenuation length of the nucleonic component of the cosmic radiation. It has been shown that the attenuation length applicable to cosmic rays of solar origin is considerably less than that applicable to the galactic radiation

82

(Reference 32). To remove differences of an atmospheric nature from the observed solar flare effect data, observed attenuation lengths are used to calculate the counting rate enhancement above the pre-event value which would have been observed if the pressure had been $\bar{\mathcal{P}}$ throughout the whole event. To normalize for differences in the instruments, this corrected enhancement will then be expressed as a percentage of the counting rate prior to the flare effect (this pre-event value having been corrected to the $\bar{\mathcal{P}}$ pressure level using the attenuation length applicable to the galactic cosmic radiation).

Let λ_g and λ_s represent the attenuation lengths corresponding to the galactic and solar components of the cosmic radiation respectively. The accepted values of λ_g and λ_s are 138 g/cm^2 and 100 g cm^2. If C_0 and $\mathcal{P}_0$ are the mean counting rate and pressure (measured in gm/cm^2) prior to the flare effect, and if C_c and $\mathcal{P}_0 + S\mathcal{P}$ are the same quantities at some time during the event, then the normalized pressure-corrected percentage increase in counting rate is

$$\left\{ \frac{C_c}{C_0} \exp\left(\frac{S\mathcal{P}}{\lambda_s}\right) - \exp\left(\frac{S\mathcal{P}}{\lambda}\right) \right\} \exp\left(\frac{\mathcal{P}_0 - \mathcal{P}}{\lambda}\right),$$

where $1/\lambda = 1/\lambda_s - 1/\lambda_g$. It has been shown that if this correction procedure is used the detectors listed in Figure 3-2 are strictly comparable, that is, if the solar cosmic radiation is isotropic, the enhancements are identical after correction.

ACKNOWLEDGMENTS

REFERENCES

1. Forbush, S. E., "Three Unusual Cosmic-Ray Increases Possibly Due to Charged Particles from the Sun," *Phys. Rev.* 70(9 and 10):771-772, November 1 and 15, 1946.

2. Adams, N., "A Temporary Increase in the Neutron Component of Cosmic Rays," *Phil. Mag.* 41:503-505, May 1950.

3. Webber, W. R., "Time Variations of Low Energy Cosmic Rays during the Recent Solar Cycle," in: *Progress in Elementary Particle and Cosmic Ray Physics,* ed. by J. G. Wilson and S. A. Wouthuysen, Amsterdam: North-Holland Publ. Co., Vol. 6, 1962 (In Press).

4. Fichtel, C. E. and Guss, D. E., "Heavy Nuclei in Solar Cosmic Rays," *Phys. Rev. Letters* 6(9):495-497, May 1, 1961.

5. Biswas,S.,Freier, P.S., and Stein, W., "Solar Protons and α Particles from the September 3, 1960 Flares," *J. Geophys. Res.* 67(1):13-24, January 1962.

6. Ney, E. P. and Stein, W., "Solar Protons in November 1960," in: *Proc. Internat. Conf. on Cosmic Rays and the Earth Storm, Kyoto, September 1961. II. Joint Sessions,* Tokyo: Physical Society of Japan, 1962, pp. 345-353.

7. Dodson, H. W., "Observation of Loop-Type Prominences in Projection Against the Disk at the Time of Certain Solar Flares," *Proc. Nat. Acad. Sci.* 47(7):901-905, July 15, 1961.

8. Kundu, M. R. and Haddock, F. T., "A Relation Between Solar Radio Emission and Polar Cap Absorption of Cosmic Noise," *Nature* 186(4725):610-613, May 21, 1960.

9. Hachenberg, O. and Krüger, A., "The Correlation of Bursts of Solar Radio Emission in the Centimetre Range with Flares and Sudden Ionospheric Disturbances," *J. Atmos. Terrest. Phys.* 17(1/2):20-33, December 1959.

10. Bachelet, F., Conforto, A. M., and Iucci, N., "Solar Flares with Type IV Radioburst and Transient Phenomena of Cosmic Rays," in: *Space Research, Proc. 1st Internat. Space Sci. Sympos., Nice, January 1960,* Amsterdam: North-Holland Publ. Co., 1960, pp. 662-664.

11. Thompson, A. R. and Maxwell, A., "Solar Radio Bursts and Low-Energy Cosmic-Rays," *Nature* 185(4706):89-90, January 9, 1960.

12. Boischot, A. and Denisse, J.-F., "Les Émissions de Type IV et l'Origine des Rayons Cosmiques Associés aux Éruptions Chromosphériques," *Comptes Rendus, Academie des Sciences* (Paris) 245(25):2194-2197, December 16, 1957.

13. Peterson, L. E. and Winckler, J. R., "Gamma-Ray Burst From a Solar Flare," *J. Geophys. Res.* 64(7):697-707, July 1959.

14. McCracken, K. G. and Palmeira, R. A. R., "Comparison of Solar Cosmic Ray Injections Including July 17, 1959, and May 4, 1960," *J. Geophys. Res.* 65(9):2673-2683, September 1960.

15. Little, C. G. and Leinback, H., "Some Measurements of High-Latitude Ionospheric Absorption Using Extraterrestrial Radio Waves," *Proc. IRE* 46(1):334-348, January 1958.

16. Little, C. G. and Leinback, H., "The Riometer — A Device for the Continuous Measurement of Ionospheric Absorption," *Proc. IRE* 47(2):315-320, February 1959.

17. Bailey, D. K., "Abnormal Ionization in the Lower Ionosphere Associated with Cosmic-Ray Flux Enhancements," *Proc. IRE* 47(2):255-266, February 1959.

18. Reid, G. C., "A Study of the Enhanced Ionization Produced by Solar Protons during a Polar Cap Absorption Event," *J. Geophys. Res.* 66(12):4071-4085, December 1961.

19. Quenby, J. J. and Webber, W. R., "Cosmic Ray Cut-Off Rigidities and the Earth's Magnetic Field," *Phil. Mag.* 4(37):90-113, January 1959.

20. Brown, R. R. and Weir, R. A., "Ionospheric Effects of Solar Protons," *Arkiv för Geofysik* 3:523-529, 1961.

21. Davis, L. R., Fichtel, C. E., et al., "Rocket Observations of Solar Protons on September 3, 1960," *Phys. Rev. Letters* 6(9):492-494, May 1, 1961.

22. Ogilvie, K. W., Bryant, D. A., and Davis, L. R., "Rocket Observations of Solar Protons during the November 1960 Event," in *Proc. Internat. Conf. on Cosmic Rays and the Earth Storm, Kyoto, September 1961. II. Joint Sessions,* Tokyo: Physical Society of Japan, 1962, pp. 317-319.

23. Leinbach, H. and Reid, G. C., "Polar Cap Absorption During the Solar Cosmic Ray Outbursts of July 1959," in: International Union of Geodesy and Geophysics, *Symposium on the July 1959 Events and Associated Phenomena, Helsinki, July 1960,* Paris: Institut Géographique National, 1960, pp. 145-150.

24. Ortner, J., Leinbach, H. and Sugiura, M., "The Geomagnetic Storm Effect on Polar Cap Absorption," *Arkiv för Geofysik* 3:429-434, 1961.

25. Leinbach, H., "Some Observations of Daytime Recoveries During Polar Cap Absorption Events," *Arkiv för Geofysik* 3:427, 1961 (Abstract).

26. Bryant, D. A., Cline, T. L., et al., "Results from the Goddard Cosmic Ray Experiments on Explorer XII," Presented at Explorer XII Symposium, Goddard Space Flight Center, January 1962.

27. Van Allen, J. A., Frank, L. A., et al., "Coordinated Injun I — Explorer XII Observations of Solar Cosmic Rays, 28 September to 4 October 1961," Presented at Explorer XII Symposium, Goddard Space Flight Center, January 1962.

28. Simpson, J. A. and Fenton, K. B., "The Neutron Monitor," Univ. Chicago, 1955 (unpublished).

29. Webber, W. R. and Quenby, J. J., "On the Derivation of Cosmic Ray Specific Yield Functions," *Phil. Mag.* 4(41):654-664, May 1959.

30. Schlüter, A., "Störmer Orbits of Low Energy," *Supplemento al Nuovo Cimento* 8(2):349-357, 1958.

31. Carmichael, H. and Steljes, J. F., "Review of Recent High Energy Solar Particle Events Including November 1960," Atomic Energy of Canada Ltd., AECL-1387 (CRGP-1056) October 30, 1961; Also *Proc. Internat. Conf. on Cosmic Rays and the Earth Storm, Kyoto, September 1961. II. Joint Sessions,* Tokyo: Physical Society of Japan, 1962, pp. 337-344.

32. McCracken, K. G., "The Cosmic-Ray Flare Effect. 1. Some New Methods of Analysis," *J. Geophys. Res.* 67(2):423-434, February 1962.

    _____, "The Cosmic-Ray Flare Effect. 2. The Flare Effects of May 4, November 12, and November 15, 1960," *ibid.,* pp. 435-446.

    _____, "The Cosmic-Ray Flare Effect. 3. Deductions Regarding the Interplanetary Magnetic Field," *ibid.,* pp. 447-458.

33. McDonald, F. B. and Webber, W. R., "The Variation of the Cosmic Ray Intensity During a Solar Cycle," in: *Space Research: Proc. 1st Internat. Space Sci. Sympos.,* Nice, January 1960, ed. by H. K. Bijl, Amsterdam: North-Holland Publ. Co.,1960, pp.968-981.

34. Fenton, A. G., Fenton, K. B., and Rose, D. C., "The Variation of Sea Level Cosmic Ray Intensity Between 1954 and 1957," *Can. J. Phys.* 36(7):824-839, July 1958.

35. Winckler, J. R., "Cosmic-Ray Increase at High Altitude on February 23, 1956," *Phys. Rev.* 104(1):220, October 1, 1956.

36. Pfotzer, G., "On the Separation of Direct and Indirect Fractions of Solar Cosmic Radiation on February 23, 1956 and on the Difference in Steepness of Momentum Spectrum of These Two Components," *Supplemento al Nuovo Cimento* 8(2):180-187, 1958.

37. Meyer, P., Parker, E. N., and Simpson, J. A., "Solar Cosmic Rays of February 1956 and Their Propagation through Interplanetary Space," *Phys. Rev.* 104(3):768-783, November 1, 1956.

86

38. Dorman, L. I., "Cosmic Ray Variations," Moscow: State Publishing House for Technical and Theoretical Literature, 1957; Translation prepared by Technical Documents Liaison Office, Wright-Patterson Air Force Base, 1958.

39. Sauer, H. H., "A New Method of Computing Cosmic Ray Cutoff Rigidity for Several Geomagnetic Field Models," *J. Geophys. Res.* 68:957, 1963.

40. Jelly, D. H., "Compiled Data for Polar Cap Absorption Events Observed at Churchill, June 1957 to June 1960," Canada, Defence Res. Telecommunications Establ. Rept. No. 1062, May 1961.

41. Anderson, K. A. and Enemark, D. C., "Observations of Solar Cosmic Rays Near the North Magnetic Pole," *J. Geophys. Res.* 65(9):2657-2671, September 1960.

42. Leinbach, H., Private Communication.

43. Freier, P. S., Ney, E. P., and Winckler, J. R., "Balloon Observation of Solar Cosmic Rays on March 26, 1958," *J. Geophys. Res.* 64(6):685-688, June 1959.

44. Hultqvist, B., Aarons, J., and Ortner, J., Effects of the Solar Flares of 7 July 1958," *Tellus* 11(3):319-331, August 1959.

45. Charakhch'yan, A. N., Tulinov, V. F., and Charakhch'yan, T. N., "Large Cosmic-Ray Intensity Fluctuations in the Stratosphere," *Zhurnal Eksperimental'noi i Teoreticheskoi Fiziki* 38(4):1031-1036, April 1960 (in Russian); Translation in *Soviet Physics—JETP* 11(4):742-746, October 1960.

46. Rymko, N. P., Tulinov, V. F., and Charakhch'yan, A. N., "A Case of a Sharp Increase in Cosmic-Ray Intensity in the Stratosphere," *Zhurnal Eksperimental'noi i Teoreticheskoi Fiziki* 36(6): 1687-1689, June 1959 (in Russian); Translation in *Soviet Physics—JETP* 9(6):1202-1203, December 1959.

47. Anderson, K. A., Arnoldy, R., et al., "Observations of Low-Energy Solar Cosmic Rays from the Flare of 22 August 1958," *J. Geophys. Res.* 64(9):1133-1147, September 1959.

48. Van Allen, J. A., McIlwain, C. E., and Ludwig, G. H., "Radiation Observations with Satellite 1958 ε," *J. Geophys. Res.* 64(3):271-286, March 1959.

49. Rothwell, P. and McIlwain, C., "Satellite Observations of Solar Cosmic Rays," *Nature* 184(4681): 138-140, July 18, 1959.

50. Freier, P. S., Private Communication

51. Winckler, J. R. and Bhavsar, P. D., "Low-Energy Solar Cosmic Rays and the Geomagnetic Storm of May 12, 1959," *J. Geophys. Res.* 65(9):2637-2655, September 1960.

52. Freier, P. S. and Weber, W. R., "Exponential Rigidity Spectra for Solar Flare Cosmic Rays," *J. Geophys. Res.* (To be published).

53. Eriksen, K. W., Holt, O., and Landmark, B., "A Note on the Polar Absorption Event of 11-18 May 1959," *J. Atmos. Terrest. Phys.* 18(1):78-81, April 1960.

54. International Union of Geodesy and Geophysics, "Symposium on the July 1959 Events and Associated Phenomena, Helsinki, July 1960," Paris: Institut Géographique National, 1960.

55. Winckler, J. R., Bhavsar, P. D., and Peterson, L., "The Time Variations of Solar Cosmic Rays during July 1959 at Minneapolis," *J. Geophys. Res.* 66(4):995-1022, April 1961.

56. Webber, W. R., Private Communication.

57. Brown, R. R. and D'Arcy, R. G., "Observations of Solar Flare Radiation at High Latitude During the Period July 10-17, 1959," *Phys. Rev. Letters* 3(8):390-392, October 15, 1959.

58. Hartz, T. R., and Vogan, E. L., Private Communication.

59. Lin, W. C. and Van Allen, J. A., Private Communication; Also, Lin, W. C., "Observation of Galactic and Solar Cosmic Rays from October 13, 1959 to February 17, 1961 with Explorer VII (Satellite 1959 Iota)," State Univ. of Iowa SUI-61-16, August 1961 (Thesis submitted for M.S. degree).

60. Winckler, J. R., Masley, A. J., and May, T. C., "The High-Energy Cosmic-Ray Flare of May 4, 1960. 1. High-Altitude Ionization and Counter Measurements," *J. Geophys. Res.* 66(4):1023-1027, April 1961.

61. Biswas, S., and Freier, P. S., "The High Energy Cosmic Ray Flare of May 4, 1960 - 2 Emulsion Measurements," *J. Geophys. Res.* 66:1029, 1961.

62. Winckler, J. R., Bhavsar, P. D., et al., "Delayed Propagation of Solar Cosmic Rays on September 3, 1960," *Phys. Rev. Letters* 6(9):488-491, May 1, 1961.

63. Winckler, J. R., Bhavsar, P. D., et al., Private Communication.

64. Steljes, J. F., Carmichael, H., and McCracken, K. G., "Characteristics and Fine Structure of the Large Cosmic-Ray Fluctuations in November 1960," *J. Geophys. Res.* 66(5):1363-1377, May 1961.

65. Ogilvie, K. W., Bryant, D. A., and Davis, L. R., "Rocket Observations of Solar Protons during the November 1960 Events, 1," *J. Geophys. Res.* 67(3):929-937, March 1962.

66. Biswas, S., Fichtel, C. E., and Guss, D. E., Private Communication.

67. Lockwood, J. A. and Shea, M. A., "Variations of the Cosmic Radiation in November 1960," *J. Geophys. Res.* 66(10):3083-3093, October 1961.

68. Manzano, J. R., Santochi, O. R., et al., "Cosmic Ray Phenomena during the November 1960 Solar Disturbances," *Notas de Fisica* 7(3):25-43, 1961.

69. Davis, L. R. and Ogilvie, K. W., "Rocket Observations of Solar Protons during the November 1960 Events; 2," *J. Geophys. Res.* 67(5):1711-1716, May 1962.

70. Guss, D. E., and Waddington, C. J., "Observations of the Solar Particle Events of July 1961," *J. Geophys. Res.* (To be published).

71. Fichtel, C. E., Guss, D. E., and Waddington, D. J., Private Communication.

72. O'Brien, B. J., and Van Allen, J. A., Private Communication.

73. Simpson, J. A., "Cosmic-Radiation Neutron Intensity Monitor," in: *Annals of the International Geophysical Year*, London: Pergamon Press, 1957, Vol. IV, pp. 351-373.

88

74. Jory, F. S., "Selected Cosmic-Ray Orbits in the Earth's Magnetic Field," *Phys. Rev.* 103(4):1068-1075, August 15, 1956.

75. Firor, J., "Cosmic Radiation Intensity-Time Variations and Their Origin. IV. Increases Associated with Solar Flares," *Phys. Rev.* 94(4):1017-1028, May 15, 1954.

76. Finch, H. F. and Leaton, B. R., "The Earth's Magnetic Field — Epoch 1955.0," *Monthly Not., Roy. Astronom. Soc. Geophys. Suppl.* 7(6):314-317, November 1957.

77. Warwick, C. S., "Propagation of Solar Particles and the Interplanetary Magnetic Field," *J. Geophys. Rev.* 67(4):1333-1346, April 1962.

Solar Active Regions Associated with some Individual Events

by

Harriet H. Malitson

[handwritten: In its Solar Proton Manual   Dec. 1963 / p 89-107   see N64-17889 10-28) OTS: $2.75   A5]

The solar regions to be discussed here are of particular interest because the particles emitted by them have been recorded and studied in the greatest detail.* The particle information is presented in detail in Chapter 2; primarily optical observations will be covered here.

February 23, 1956—Region 56-AA

For many years it has been known that certain restricted longitude regions on the sun tend toward activity over a period of many months, while others tend to be undisturbed (Reference A1). The active region connected with the February 23, 1956 event was one of several occurring over a long period near latitude 20°N, longitude 190°. Each region lasted for a few rotations and then disappeared, with another coming to take its place after one or more additional rotations.

The first disk passage of Region 56-AA in January, 1956 was marked by the usual indications of considerable activity: coronal emission in the yellow line of Ca XV at the east limb; surge prominences; many flares; large, bright plage; continued growth of spots; and two sudden commencement (SC) geomagnetic storms. Surges and loops were also observed at the west limb.

The second disk passage, in February, again began with Ca XV coronal emission accompanied by tightly looped prominences; knots of gas ejected from the prominence region reached speeds of over 1500 km/sec. As the sunspot group and plage rotated onto the visible disk, it became apparent that they had grown to enormous size. Together with an adjoining region, the whole group extended over 65° of longitude, and had an area of about 5,000 millionths of the visible solar hemisphere – the largest such area seen in several solar cycles of activity. The plage, the largest in several years, was the first in that cycle

---

*Much of the information on active regions was obtained from the High Altitude Observatory Reports (Reference A2), and HAO designation numbers are used.

to produce importance 3 flares. In all, there were 98 flares during the three most active disk passages of the region. The plage reached its maximum size on February 20 and afterwards began to decrease, although it remained bright. The spot area reached maximum at about the same time.

The 3+ flare on February 23 occurred at 23°N, 80°W and was observed by the Tokyo Astronomical Observatory (Reference A3) to begin at 0331 UT, with a maximum at 0342, and to end at 0415. The Kodaikanal Observatory estimated the end to be around 0510. Figure A1 shows sketches made by Ellison (Reference A4) from information obtained from Tokyo, Kodaikanal (Reference A5), and Mount Wilson (Reference A6). The bright filamentary structure of the H-alpha flare is shown in black. Comparison of the two parts of Figure A1 shows the positions of the flare filaments with respect to the visible structure and magnetic field intensities and polarities of the spot group. It is evident that the five separate sunspot groups involved had a very complicated structure. Several of the principal umbrae were covered by the flare emission (shown by dashed lines on the magnetic map). This covering of the umbrae seems to be characteristic of flares producing the larger cosmic ray events. Other flares tend to avoid the umbrae, and often occur over the penumbral regions of a spot group.

A rapid rise in flare emission occurred between 0332 and about 0340. This initial sharp increase – called the flash phase of the flare – is often observed. It is during this phase that particle acceleration is believed to occur. The southern end of one of the flare filaments was observed in white light at Tokyo for about five minutes around 0345. Also a high-velocity spray prominence was emerging from the southern end of the region at around 0335, during the flash phase (Figure A1).

On the sunlit hemisphere of the earth, there were severe ionospheric effects of long duration (about seven hours); intense bursts of solar radio emission were measured on
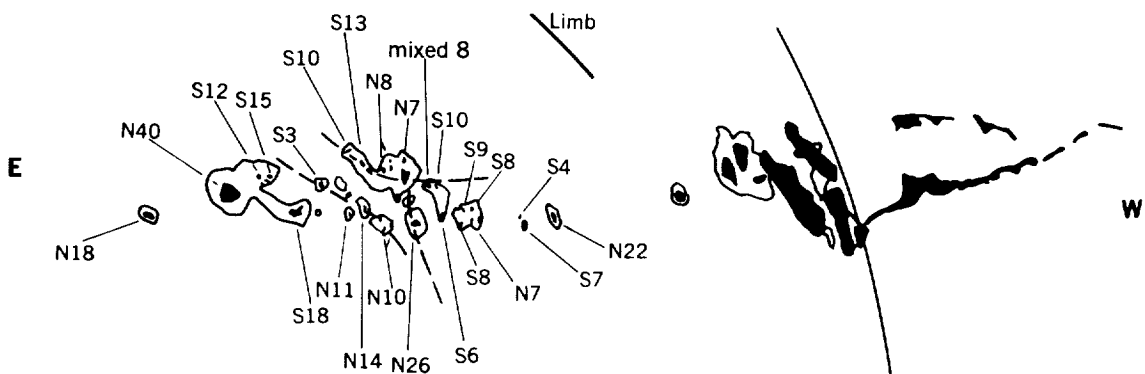

Figure A1—The February 23, 1956 Event in Region 56-AA. (Drawings by Ellison, Reference A4). N refers to north magnetic polarity and S to south. Field strengths are given in units of 100 gauss.

discrete frequencies. No doubt Type-IV emission would have been recorded if the means for spectral measurement of solar radio emission had existed.

This PCA event marks the first observed case of ionospheric disturbances in the dark hemisphere of the earth caused by solar protons. There was also a large cosmic ray increase at ground level. On February 25 at 0307 an SC magnetic storm began which lasted about one day. In all, there were four SC geomagnetic storms during this disk passage.

The third passage of the region again began with strong yellow line emission, bright surges, and east limb loop prominences. The plage was still very large and bright, but decreased in size during the passage. The spot group, still very large and complex at the beginning of this passage, became smaller and more stable before reaching the west limb. There were also some flares of moderate size associated with ionospheric effects and radio bursts. By the time of west limb passage, there was only moderate activity in the region. By the fourth passage, activity had decreased to a very low level.

August 9, August 29-September 2, September 26, 1957—Regions 57-JL and 57-JG

Two active regions were involved in the PCA events of August 29-September 2, 1957. Region 57-JL was located 30 degrees south of the solar equator and Region 57-JG, 20 degrees north; these regions were only about 20 degrees apart in longitude.

For Region 57-JG, the first disk passage occurred in late July and early August. On its east limb appearance there were bright surges. The plage was small and bright and the spot group complex though moderate in size, and flares were frequent. On August 9 a small PCA event occurred which may have been connected with flares in this region, although identification of the event with a particular flare is uncertain. The second east limb appearance revealed faint loop prominences. Both the spot group and plage had become extremely large. During this passage there were many important flares, the majority of which were associated in time with radio noise and ionospheric disturbances.

At the same time Region 57-JL was experiencing its first and only disk passage. Its spot group and plage were moderate in size, but a large number of important flares were produced, most of which were associated in time with radio bursts and fadeouts. Activity diminished somewhat after central meridian passage on August 30, and had ceased by the following rotation.

On August 28 two flares of importances 3+ and 2+ occurred in Region 57-JL with maxima at 0940 and 2020. The 3+ flare was associated with Type-IV radio emission, and was probably connected with the small PCA event that began on August 29 at 0030 and the geomagnetic storm at 1909 on the same day. Around 1300 on August 29 a large increase in absorption was preceded by a ground-level cosmic ray event. There were two flares of

importance 2 associated in time with this event: one in Region 57-JG with maximum at 0555, the other in 57-JL with maximum at 1037. On August 31 a magnetic storm occurred at 1812.

Another PCA event occurring August 31 at 1530, was preceded by three flares: a 2+ flare in the 57-JL region and a 2 flare in 57-JG with maxima at the same time, 0552. There was Type-IV emission at this time, as well as during the importance 3 flare in 57-JG at 1312. Another geomagnetic storm began at 0314 on September 2. Also on September 2 another PCA event began at about 1730. Type-IV emission was present during a 1+ flare in Region 57-JG with maximum at 1303 and a 2+ flare in 57-JL with maximum at almost the same time (1316). The fourth geomagnetic storm of this period began at 1300 on September 4.

The third disk passage of 57-JG began in late September with east limb surges. The plage was still very large, but the spot group had decreased in size and, initially, the level of activity was somewhat lower. As the region rotated toward the central meridian, the spots began to develop rapidly into a large complex group that lasted about a week. Many flares were produced, some of which were time-associated with radio fadeouts. An importance 3 flare with maximum at 1955 on September 26 was followed by a PCA at 2315 and a geomagnetic storm at 0016 on September 29. The west limb passage was marked by coronal loop prominences, and the fourth rotation in late October began with them, as well as with surges. Activity was considerably lower during this appearance. In November a slight increase in activity was shown by a large number of flares, and faint coronal yellow line emission at the west limb. The December passage revealed only traces of the region remaining.

March 23-25, 1958—Region 58-J

Region 58-J developed after central meridian passage during the first few days of March, 1958, and produced many small flares before its west limb passage, when loop prominences appeared. The loop prominences appeared at the east limb late in March, along with surges and strong yellow line emission. There were now two extremely large plages with large complex spot groups, which grew in area and complexity until they reached the western part of the disk. Many of the important flares on this passage occurred between the two spot groups; and a large percentage of these flares were associated with short wave radio fadeouts (SWF). On March 23 a 3+ flare with maximum at 1005 was followed by a moderate PCA event starting at 1830 and reaching a 5 db maximum.

About three hours before the SC of the associated geomagnetic storm the absorption began to increase toward a maximum of 12 db. This increase in absorption two days after the 3+ flare may have come about through some storage mechanism in interplanetary space between the sun and earth or it may have resulted from one or both of two importance 2

flares occurring at about 0600 on March 25. One of the March 25 flares occurred in the same region (58-J) that had produced the 3+ flare and the other, in a northern region about 25 degrees away in longitude.

The activity in Region 58-J had begun to decrease by the time of west limb passage, and in two weeks the region had disappeared completely.

July 7, 1958—Region 58-P

On the first rotation of this region early in June, there were large bright surges at the east limb around 40°N and 30°N. Two large plages and spot groups appeared at these latitudes — the one at 40°N was unusually active for such a high latitude, but its growth and decay were rapid. The two regions produced a large number of flares and SWF's. A 1+ flare at 1056 on June 6 may have contributed to the PCA at 1345, although Type-IV radio emission occurred in connection with an earlier flare in a different region.

By the next rotation in July, only the 30°N plage and spot group remained; these were moderate in area. There were many minor flares during the passage and an unexpected 3+ flare with maximum at 0115 on July 7 associated with a Type-IV outburst. A large PCA event began at about 0130 and there was an SC geomagnetic storm at 1728 on July 8 that produced a spectacular aurora down to the 40th parallel. The region, however, had disappeared by the next rotation.

August 21-26, September 22, 1958—Region 58-BF

There were surges and loop prominences on the east limb, and a bright plage and complex spot group on the disk during the first rotation of Region 58-BF. The plage and spot group grew during the next few days and many large flares occurred — most associated in time with SWF's and major radio noise bursts. There was a small PCA event at about 1500 on August 21, preceded by two flares in the region with maxima at 2254 on August 19 (importance 2) and at 0044 on August 20 (importance 2+). The former was associated in time with Type-IV emission.

An SC geomagnetic storm occurred on August 22 at 0227. On the same day, an importance 3 flare with maximum at 1448, associated with Type-IV emission, was followed by a fairly large PCA at 1530. Another magnetic storm started on August 24 at 0140. On August 26 another importance 3 flare, with maximum at 0027 and associated with Type-IV emission, produced a large PCA event at about 0100. The geomagnetic storm began on August 27 at 0243.

During the next disk passage, in September, the activity was reduced. There was yellow line emission at the east limb. The plage was still very bright, but its area and the

area and complexity of the spot group had declined. The small PCA event of September 22 at 1400 and the geomagnetic storm of September 25 at 0408 probably resulted from an importance 2 flare with maximum at 1017 on the 22nd.

The region had disappeared by the next rotation (in October).

May 10, 1959—Region 58-BT

The first truly long-lived region observed to occur well after solar maximum appeared first in December 1958, with moderate yellow line emission and small surges at the east limb. The plage remained large and bright during the passage; the spot group, initially small, developed over the two-week period. There were many minor flares; and small surges, faint yellow line emission, and loop prominences were observed on the west limb.

In January there were bright yellow line emission, surges, and sprays at the east limb. The spot group was large and complex and the plage was still bright. During this passage there were high speed dark surges and large flares – including one of importance 3, associated with an SWF and major radio noise burst.

In February, faint yellow line emission, surges, and a spray prominence at the east limb marked the beginning of the disk passage of a larger plage and a spot group that had retained its size and complexity. None of the several flares was more important than 1+. A loop and bright and dark surges were seen on the disk; and a spray prominence, loops, and surges at the west limb.

Activity in March was about the same as in February, although the size and brightness of the plage had decreased. Active prominences were observed at both limbs. The region had almost disappeared by the time of the April passage, but signs of activity began to show on the western part of the disk, and small surges at the west limb.

The May passage began with strong surges and moderate loops. The plage had become larger and brighter than at any previous time and the spot was also larger. There were 170 flares reported during the passage (almost a record), including two 3's and a 3+. The latter flare occurred at 2102 on May 10, with a severe SWF, and Type-IV radio emission lasting for about 2-1/2 hours. The optical flare lasted around 6 hours. There was a strong PCA event at about 2300 on May 10. The SC geomagnetic storm beginning at 2328 on May 11 produced intense auroral activity. On succeeding days several large flares produced many SWF's. The number of high speed dark surges during this passage was unusually high.

There was a slight decline in activity during the latter half of the May passage, with moderate yellow line emission and small surges observed at the west limb. Activity had declined greatly by the time of the June passage, and there were no signs of activity in July.

June 13, July 10, 14, 16, 1959—Region 59-Q

Region 59-Q developed on the disk around the middle of May and had grown considerably larger by the time it had reached the west limb. The second rotation began on June 9 with moderate yellow line coronal emission and large loop prominences and surges. A bright plage and complex spot group produced many large flares, particularly in the first half of the rotation. On June 13 at about 1330, there was a PCA which was probably associated with the 1+ flare at 0358. There were many SWF's during this time, including one at 0358 on June 13, but geomagnetic activity remained low until June 23, about 36^h after a flare of importance 2. As the region approached the west limb, the number of large flares decreased while the number of subflares increased. There were moderate surges at the limb. Therefore, it seemed that activity was dying out.

Two days before the whole large bright plage had rotated onto the disk for Passage Number 3, a flare occurred with associated radio bursts and an SWF. At the east limb on July 7, there were loop prominences and moderate surges. Initially the spot group was small, but it began to develop on July 9 and became very large and complex during the next few days while the plage grew larger and brighter. There were many flares of moderate size. A 3+ flare which appeared on July 10 before 0210, with maximum at 0240, produced a large PCA at about 0400 with a Type-IV radio outburst at 0223. An SC geomagnetic storm began on July 11 at 1625.

On July 14 when Region 59-Q was in the center of the disk, a 3+ flare at 0319 with maximum at 0349 caused a severe SWF. There was a Type-IV outburst at 0330 and a large PCA event commencing prior to 0700. The severe SC geomagnetic storm from this flare began on July 15 at 0803. On July 16, an importance 3 flare at 1555 was followed by a high speed dark surge and an SWF.

At 2114 on July 16, there was a 3+ flare at 16°N, 30°W with maximum at 2132. This flare, lasting about four hours, was covered by H-alpha cinematography at the McMath-Hulbert, Climax, and Lockheed Observatories, so its development can be studied very closely. It began in three emission regions near the sunspot group; then the central spot became extended, toward the east and northeast, into an S-shaped bright filament 280,000 km long (at the time of flare maximum) with one end quite far from the spot (see Figures A2a and A2b and References A7 and A8). The flare filaments covered all but one of the principal umbrae in the spot group. Fourteen magnetograms, obtained at the Mount Wilson Observatory during the course of the flare, showed no changes in the spot-region magnetic fields greater than the experimental uncertainties.

At the McMath-Hulbert Observatory, spectroheliograms were taken at the center of the H-alpha line and also at wavelengths displaced 1 Angström from the center toward both shorter and longer wavelengths. These pictures show dark material moving upward before maximum and at maximum, and show dark loop-type filaments with descending material in
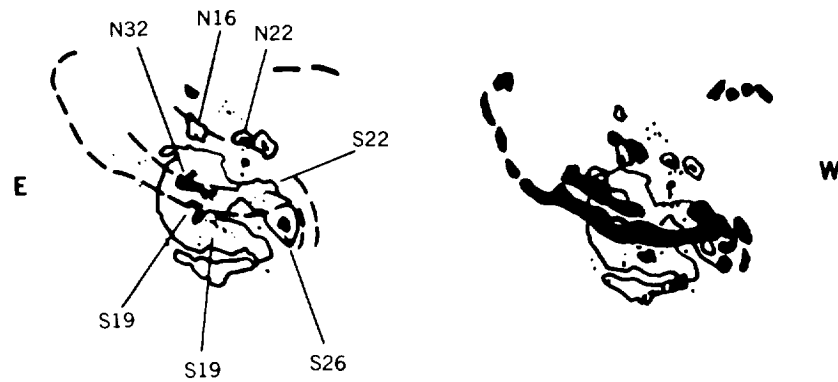
Figure A2—The July 16, 1959 Event in Region 59-Q. Same scale as
Figure A1. (Drawings by Ellison, Reference A4).

the post-maximum phase of the flare. The *nimbus** phenomenon (Reference A9) occurred
in association with this flare, and is, in fact, the earliest case found in the records.

Severe ionospheric disturbances occurred around 2115; Type-IV radio emission began
at 2118 and lasted about 4 hours. High-energy cosmic rays began to be detected at ground
level at about 2250, preceding the PCA. The SC geomagnetic storm began at 1638 on
July 17, while the July 15 storm was still in progress. About this time (three days after
central meridian passage) the number of major flares began to decrease and the number
of sub-flares to increase, just as during the same part of the previous rotation. The area of
the spot group began to decrease from a maximum of 2100 millionths of the solar hemi-
sphere. At the west limb, there were strong loop prominences and moderate surges.

In August the fourth passage began with the same types of prominences and surges,
and with yellow line emission. There were a few moderate flares with SWF's during the
first few days, but activity declined markedly after central meridian passage. There were
still traces of the region in September, but none in the following month.

March 31-April 5, April 28-May 6, 1960—Region 60-H

Region 60-H formed near the east limb around March 25. Although the small, bright
plage grew slowly, the area and complexity of the spot group increased rapidly. The most
rapid rate of growth occurred on March 28 and 29, when there were large, complex loop
prominences and high speed dark surges on the disk. On March 28 the region began to
produce large flares and continued to do so until the time of west limb passage, around

---

*In the nimbus phenomenon, a dark halo begins to surround the flare region a few minutes after maximum. It is about
300,000 km in diameter and remains one or two hours. This phenomenon seems to be associated with Type-IV radio emis-
sion. Ellison et al. (References A4 and A9) have suggested that the nimbus is the visible counterpart of the cloud of rela-
tivistic electrons postulated by Boischot and Denisse (Reference A10) who have attempted to associate Type-IV emission
with synchrotron processes in the flare region and with the production of cosmic rays.

April 6. Flares on March 30 at 1540, April 1 at 0845, and April 5 at 0215 produced PCA's on March 31 at 0300, April 1 at 0930, and April 5 before 0800, respectively. For two of these, there were Type-IV outbursts at 1519 on March 30 and 0207 on April 5.

On March 31 began the most severe geomagnetic storm since the one on July 15, 1959 producing bright auroral displays in the southern part of the United States. Two SC geomagnetic storms, beginning on April 2 at 2313 and on April 5 at 1300, were superimposed on the March 31 storm already in progress; another occurred on April 7. Ionospheric disturbances occurred throughout the period March 28-April 6, the most severe ones on March 29 and April 5. West limb passage occurred with weak loop prominences and surges.

The second rotation began around April 21 with a stable plage and a spot greatly reduced in size. After central meridian passage (April 27) the region began to grow. Region 60-H produced a series of flares on April 29 (at 11°N, 20°W), starting before 0220, which caused Type-IV emission starting at 0200, and a large PCA event before 0600.

A moderate PCA on April 28 has been attributed to an importance 3 flare in *Region 60-K*. During its first passage it had weak activity. When it reappeared on the east limb around April 24, it still seemed ordinary. The importance 3 flare at 0130 on April 28 with its geophysical effects was therefore quite unexpected. There was a severe SWF, and Type-IV emission occurred at 0145. Two SC geomagnetic storms occurred, at 0132 and 1213, on April 30; but the second may have come from the April 29 series of flares in Region 60-H. Activity in Region 60-K declined after the one large flare.

On May 4 when Region 60-H was on the west limb, a flare began at 1000 UT about 20,000 km above the limb as an increase in brightness in a previously existing, abnormally bright prominence. Ellison et al. (Reference A4) have studied the history of this flare in detail as recorded on motion picture film with a Lyot birefringent filter at the Cape of Good Hope. The flare expanded, reached maximum brightness around 1015, and lasted until about 1045 (see Figure A3). At maximum, the top was 31,000 km above the limb. The only visible connections between the chromosphere and the flare were bright filaments on either end. At 1035, a large system of loop prominences appeared, and reached a height of 57,000 km by 1213.
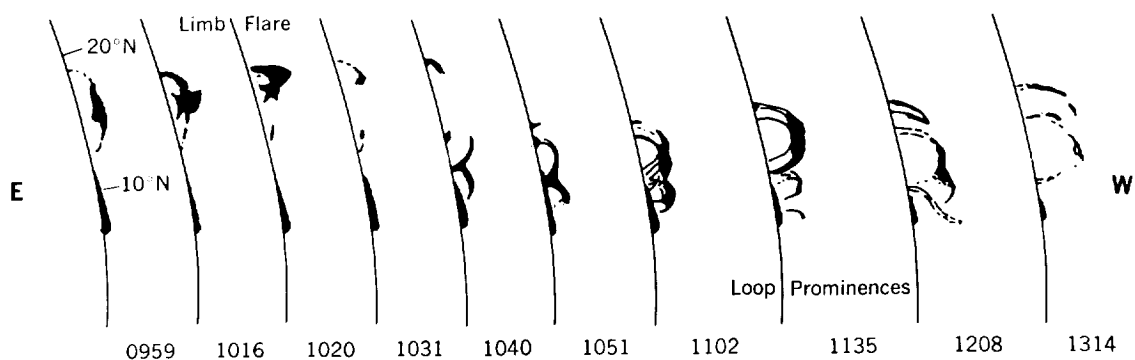

Figure A3—The May 4, 1960 Event in Region 60-H as seen at the Cape of Good Hope. Same scale as Figure A1. (Drawings by Ellison, Reference A4).

The time variation of H-alpha emission and the sudden ionospheric disturbances (SID) that occurred about 1013 show that the event was a real flare, not merely the very bright coronal loop prominence suggested by some observers. At 1030, cosmic rays were detected at ground level and the PCA began about 1044 at Thule, Greenland. There also was a minor geomagnetic storm on May 6 at 1650.

A considerable increase in polar cap absorption occurred before 1830 on May 6, and before the end of the May 4 PCA.

It is tempting to ascribe this increased absorption to the arrival of increased numbers of protons from the May 4 flare at the time of the geomagnetic storm, or possibly to a flare in the same active region just behind the west limb, although no evidence has been found to indicate that an *invisible* flare behind the limb can produce cosmic ray effects at the earth. It is probably safer, however, to attribute the additional PCA to a flare of importance 3 in Region 60-L at 1404 on May 6. On its first rotation in April, the region consisted of a small bright plage and a spot group of moderate size and flare activity. There were also surge-type prominences at the west limb. The second rotation showed faint yellow line emission at the east limb. The plage and spot were somewhat larger than before, but stable. As in the case of Region 60-K, the importance 3 flare was unexpected. There was a minor SWF, and Type-IV emission started at 1414 and lasted for two hours. An SC geomagnetic storm began at 0421 on May 8. After the single large flare, activity declined within the region.

September 3, 1960—Region 60-X

In July, surge prominences at both limb passages and a growing plage and spot group marked the first passage of Region 60-X. All major flares occurred after central meridian passage (July 17), as the spot group became more complex. In August, there were surges and small loop prominences. The plage was by then very bright and covered twice the July area, although the spot group remained about the same. There were at least 8 major flares, most accompanied by intense radio bursts and SWF's. Three geomagnetic storms occurred during the second passage. At west limb, there were surge, loop, and spray prominences.

By the third rotation (in September), the activity in Region 60-X had apparently decreased somewhat, although there was still prominence activity at both limbs. A flare near the east limb on September 3, with maximum at 0037 and an SWF, produced a small ground level cosmic ray event; the corresponding PCA began before 0800.

By the time of west limb passage, the region had declined considerably in activity, and only a trace remained in October.

November 12-21, 1960—Region 60-HH

During the first east limb passage of Region 60-HH in October, weak loops and surges were observed; but the plage was not seen until two or three days later, in association with a small stable spot. The spot vanished and the plage brightened. Spots reappeared before

west limb passage, however, and numerous sub-flares occurred. Weak surges and moderate yellow line emission appeared at the limb.

On the second rotation in November, strong surges at the east limb were followed by the appearance of a large, complex spot group and a very bright plage which increased in size for the next ten days. The spot group changed in detail but remained large and complex. At least one major flare and many smaller ones, with large radio bursts, occurred almost every day.

At 1315 on November 12, a 3+ flare occurred at 26°N, 04°W, and lasted for about 6 hours. It began near the eastern end of the spot group (Reference A9) and then extended rapidly westward during the flash phase (about 1323-1329), completely covering the two major umbrae by 1328 (see Figures A4a and A4b). The nimbus phenomenon was observed at 1332, about 5 minutes after the start of a Type-IV outburst, and was still present an hour later. The Type-IV emission lasted for about 4-1/2 hours. These phenomena were accompanied by severe ionospheric disturbances.

The ground level cosmic ray increase at about 1328 occurred at approximately the same time (1348) as the SC of a great geomagnetic storm probably caused by a major flare at about 0315 on November 11, which was not observed optically but produced ionospheric disturbances and radio bursts. This superposition of cosmic ray increase and geomagnetic activity apparently produced many interesting variations in the cosmic ray records. Analysis of these variations has led to new developments of theory regarding magnetic fields and particle propagation conditions in interplanetary space. The PCA began about 1445; and the geomagnetic storm from the November 12 flare arrived at 1023, November 13 and produced a bright aurora visible in the northern United States.

At 0207 on November 15, another 3+ flare occurred in the same region, which was now at 26°N, 33°W. The spot group had reached its maximum area by November 14, and the
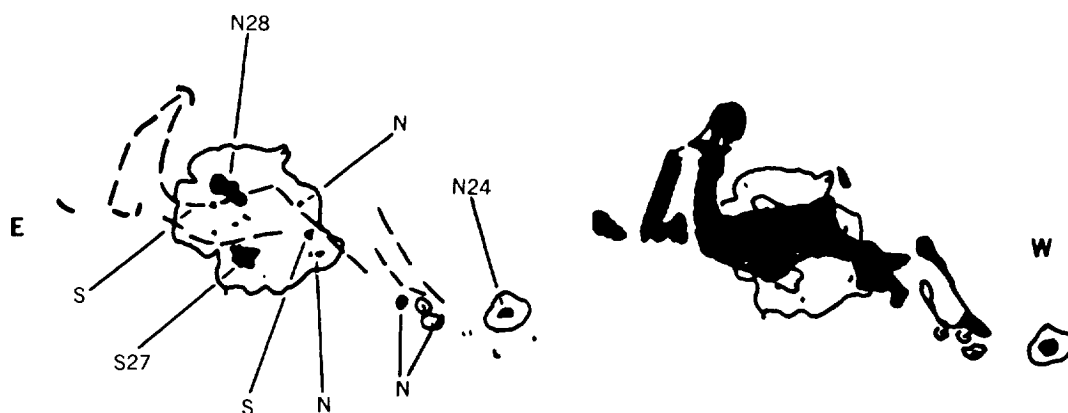
Figure A4—The November 12, 1960 Event in Region 60-HH. Same scale as Figure A1. (Drawings by Ellison, Reference A4).

penumbra was already beginning to break up at the time of this flare (see Figures A5a and A5b). The intensity curve for the H-alpha line shows a very sharp rise, indicating a flash phase only three minutes in length. A high velocity surge was observed and again severe SWF's and other ionospheric disturbances were reported. Type-IV emission began about 0221 and lasted about 4 hours. Magnetic activity had quieted by November 15 and the cosmic ray increase, which began about 0236, was much less complicated than the one on November 12. The PCA began about 0505 on November 15. An SC geomagnetic storm began at 1304 on the same day, but probably was caused by a 2+ flare on November 14.

By November 20, the active region had disappeared behind the west limb and was, in fact, about 113 degrees west of the sun's central meridian (23 degrees behind the limb). The flare occurring on November 20 with maximum at 2020 was so high above the limb that it could still be observed from the earth (Reference A11). Calculations based on a central meridian distance of 113 degrees show that the part observed must have been more than 63,000 km above the limb. The flare first appeared at 1955 as a small mound (Figure A6) that grew in area and brightness until 2022, when it began to break up and move outward at a speed of about 1000 km/sec. The flare had disappeared by 2032, and was followed by a series of loop prominences much like the ones on May 4, 1960. There was an SWF and a strong radio outburst on 2800 Mc (Reference A12). Ground level cosmic ray effects began about 2055, and a PCA about 0500 on November 21. A minor SC geomagnetic storm began at 0631 on November 21, but probably had no connection with the November 20 flare.

In December, the region had strong surges and loops at the east limb. The plage was still bright, but the spot group had become stable and much smaller. There were, however, several large flares, including one on December 5, with geomagnetic effects. At the west limb there was yellow line emission. In January 1961, the activity was only moderate with a new, fairly complex spot group and numerous subflares. There was no geomagnetic activity. In February (the fifth passage) only traces of the region remained.
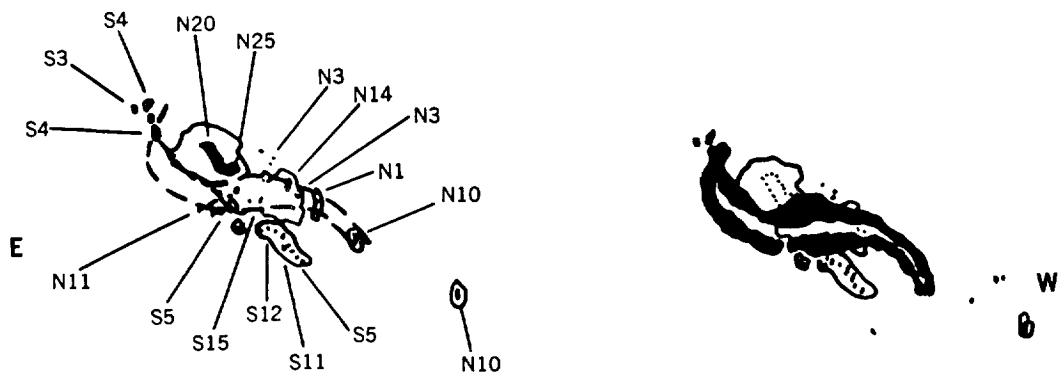

Figure A5—The November 15, 1960 Event in the Region 60-HH. Same scale as Figure A1. (Drawings by Ellison, Reference A4).
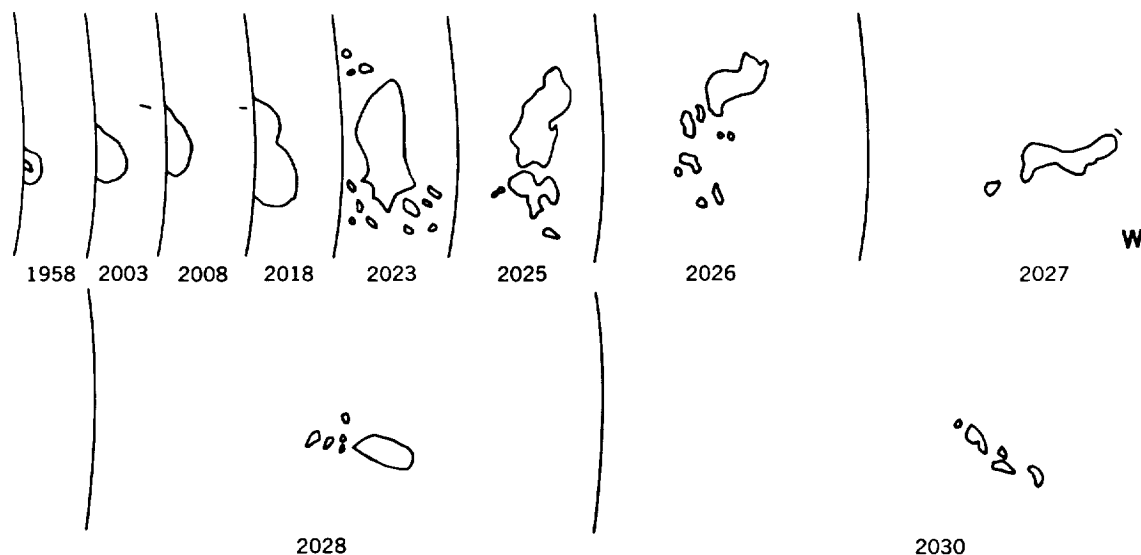
Figure A6—The November 20, 1960 Event in Region 60-HH as observed at the High Altitude Observatory, Climax. Same scale as Figure A1. (Drawings by Ellison, Reference A4).

July 12-21, 1961

This active region first appeared in June as a fairly large, stable spot group and a rather small, very bright plage. No limb activity was observed; a considerable number of subflares occurred during this first passage. There were surges as the region reappeared on the east limb on July 7. By this time the spot group was developing rapidly and by July 12, the group was twice as large as it had been in June. The plage continued to be large and bright. Production of flares of moderate size began on July 10 and the first large one (importance 3) occurred at 1615 on July 11 at 07°S, 31°E with maximum at 1700. Type-IV emission started at 1702 and a PCA at about 0000 on July 12. A severe SWF, lasting about 4 hours, was associated with this flare. An SC geomagnetic storm began at 1115 on July 13, producing a visible aurora on July 14 as far south as Boulder, Colorado.

On July 12 at about 1001, a 3+ flare began that was photographed (Figure A7) at one-minute intervals by the Lyot heliograph at the Cape of Good Hope (Reference A13). First, there was a line of bright points between the principal umbrae that slowly became brighter until the start of the flash phase at 1019. During the next six minutes, the points became elongated and finally merged into two parallel bright filaments. There was also a line of bright points, ·connected by thin filaments southeast of the main part of the flare, which lasted for only about 10 minutes. During this flare, the main umbrae were again covered by the two bright filaments, those of north polarity by one and those of south polarity by the other. The filaments, as in the case of most flares described herein, ran parallel to the magnetic axis (the line dividing regions of north and south polarity). The nimbus
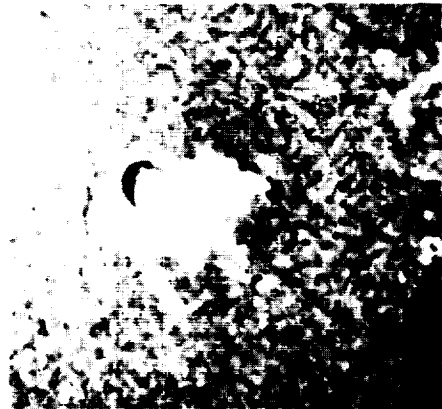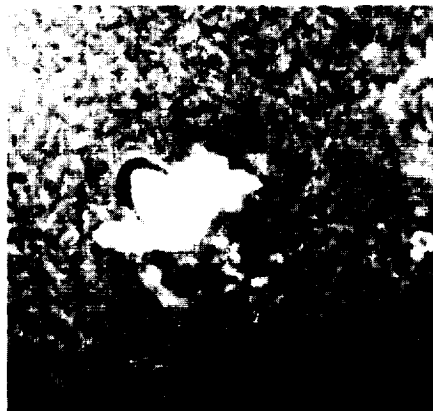
09959[23]   1026[19]
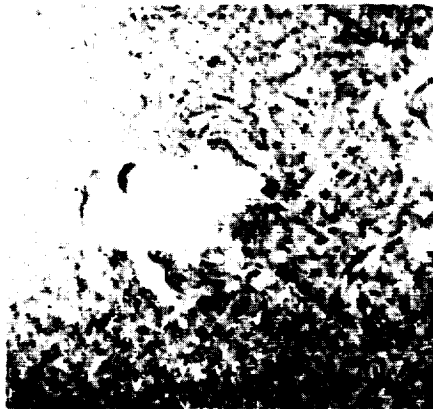
1043[19]   1053[19]

1100[19]   1336[23]

Figure A7—The July 12, 1961 Event as photographed at the Cape of Good Hope.

phenomenon occurred, intense Type-IV emission started at about 1020, and a PCA began before 0700 on July 13. There was also a severe SWF.

On July 15 at 1434 UT, there was a 3+ flare in a region in the sun's northern hemisphere, separated only about 33° in longitude from the main region. This flare produced Type-IV emission at 1435, a severe SWF, a PCA at 1545, and probably the SC geomagnetic storm at 1827 on July 17.

This region first appeared near the central meridian of the sun on June 19, a rebirth of a region that had appeared in May as a tiny spot and small, fairly bright plage and had lasted only one rotation. In June the plage was small and very bright, and produced quite a few subflares. On June 21-24, several of these subflares constituted the only reported activity that could be associated in time with Type-IV radio bursts. The spot had become large by June 21. No activity was observed as the region crossed the west limb.

There were surges on the east limb on July 8 at the beginning of the second rotation. The plage was large and bright, although less so than the main plage in the southern hemisphere; but the spot area was much smaller than before. Flare activity was low until the unexpected importance 3 flare on July 15, and also afterward. No activity was observed during west limb transit. The region persisted through August and September, and then disappeared. There was also an importance 2 flare in the main region with maximum at 1512, followed by Type-IV emission at 1522. A PCA occurred at 1545, possibly resulting from a combination of proton beams from both flares.

The importance 3+ flare of July 18 began at 0920 with a few bright points (see Figure A8a and also Figure A9). At about 0940, a long bright filament appeared and began to elongate toward the north. The large prominence cloud (indicated by D on Figure A8a) started blowing off at about the same time and disappeared in about 5 minutes, leaving in its place a string of bright patches that joined later to form a large bright filament. By 1015 there were two bright parallel filaments covering the principal umbrae. The nimbus phenomenon again occurred and is indicated by the dashed circle in Figure A8a. Surprisingly, the dark marking labeled E survived with very little change. Figure A8b presents the magnetic field data for this region (Reference A14). The large penumbra of July 12 had broken up into four separate spots of north polarity by July 15, and only one isolated spot of south polarity remained. Type-IV emission began about 0940, but was much less intense than that from the July 12 flare. However, the July 18 flare produced a ground level event at 0950 as well as a PCA at 1135.

On July 20, a 3+ flare on the west limb at 07°S with two maxima at 1620 and 1830 again caused a ground level event (at 1620) although a much smaller one than the event of July 18. There was Type-IV emission at 1607 and the PCA came at about 0030 on July 21.

This active region reappeared in August with a plage split into two parts, greatly reduced in size, with no spots. Its last appearance occurred in September as a smaller, fainter plage without spots.

0930¹⁵   0944¹⁵   0950¹³   0955¹⁵

D

E

1001¹⁵   1015¹⁵   1028⁴⁴   1044¹⁵

W
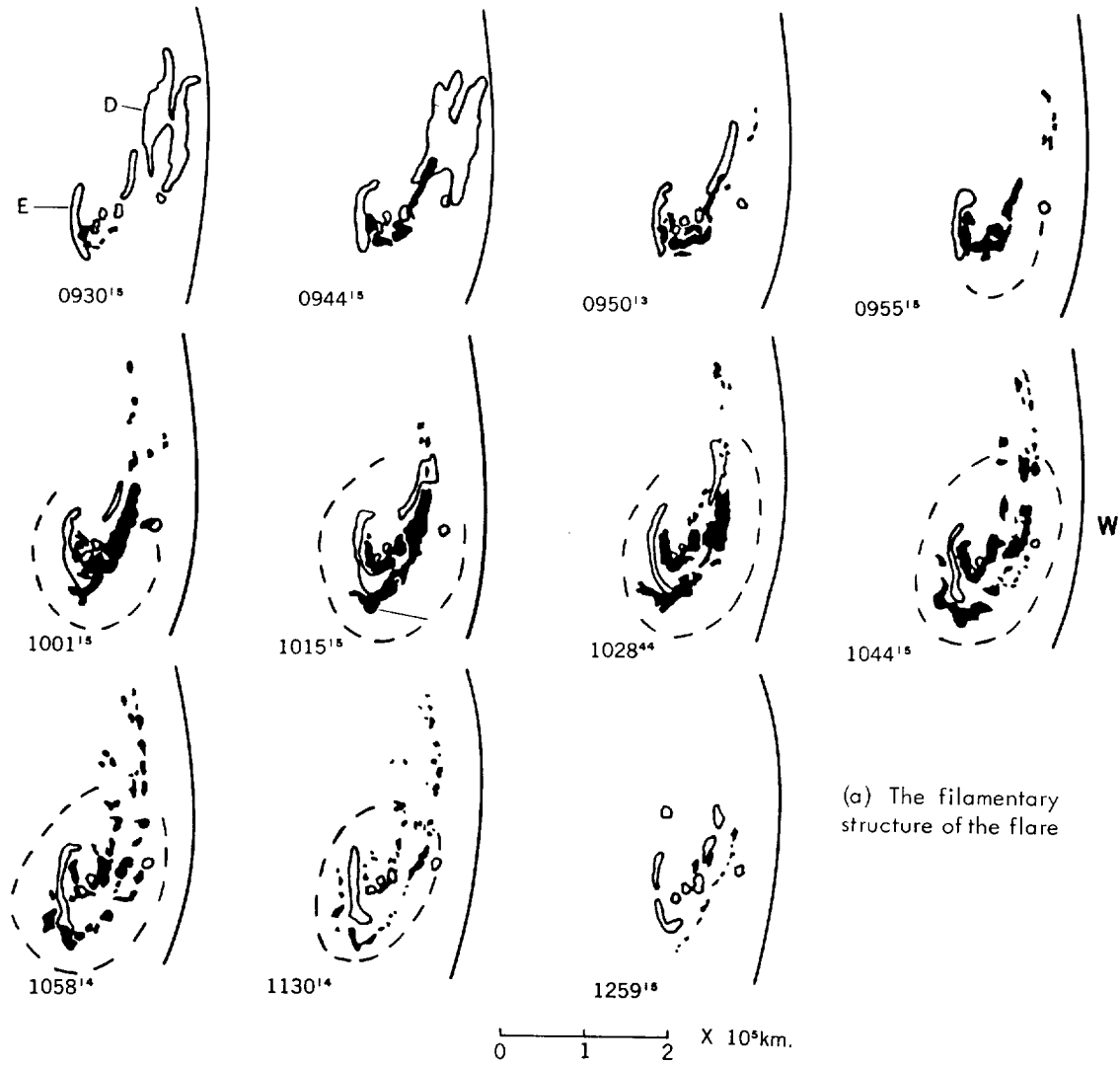
(a) The filamentary
structure of the flare

1058¹⁴   1130¹⁴   1259¹⁵

0   1   2   X 10⁵km.

(b) Magnetic map
for the event

N21
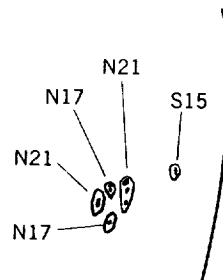N17   S15
N21
N17

Figure A8—The July 18, 1961 Event as observed at the Cape of Good Hope. (Drawings by Ellison, Reference A13).

0934¹⁵   1013⁴⁵

1043⁴³   1052⁴³

1057⁴³   1157⁴³

Figure A9—The July 18, 1961 Event as photographed at the Cape of Good Hope.

September 10 and 28, 1961

In early August, this region was born on the disk as a small spot and a small bright plage. It had moderate subflare activity. On the second rotation, in late August, no east limb activity was observed, but a large, rather faint plage and large, complex spot group were revealed. Numerous flares occurred and at least one-third of them were accompanied by SWF's. Several high speed dark and bright features were observed in connection with some of the flares, and Type-IV emission was recorded a few times. A flare at 1950 UT on September 10, when the region (12°N) had reached the west limb, produced Type-IV emission at 2025 and a PCA at about 2300.

The third rotation began in late September with a surge at the east limb. As the region rotated into view, it was found that the original plage had become smaller and brighter, with a small spot. This plage died on the disk during the passage. A new plage had formed on the hidden side of the sun, about 15° east of the old plage and at the same latitude, since the second rotation in August-September. This plage had about the same brightness and size as the old one and contained a fairly complex spot group of moderate size. The old plage produced a few subflares, while the new one tended to produce somewhat larger flares: 1 and 1+. This also was the site of the importance-3 flare on September 28 at 2202 which produced Type-IV emission at 2212, a PCA at 2335, and an SC geomagnetic storm at 2111 on September 30. After the flare of September 28, observed activity in the region consisted mostly of subflares, although there were surges at the west limb on October 8 and 9.

The next rotation in October-November showed a smaller, fainter plage and no spot. In November-December, the plage had split into two parts, one with a tiny spot. In late December, both plages seemed to die on the disk, but the larger one regenerated by the time of central meridian passage and produced a few subflares and small flares. Moderate activity was still present in January 1962; slight activity was observed in February.

REFERENCES

A1. Losh, H. M., "Distribution of Sun-Spots in Longitude," Publ. Observ., Univ. of Michigan 7(5):127-145, September 1938.

A2. "Preliminary Report of Solar Activity," issued weekly by the High Altitude Observatory, U. of Colorado, Boulder. These reports are combined and issued in final form in the Solar Activity Summaries by the High Altitude Observatory.

A3. Notuki, M., Hatanaka, T., and Unno, W., "A Very Unusual Flare on February 23, 1956," Publ. Astronom. Soc. Japan 8; 52-54, 1956.

A4. Ellison, M. A., McKenna, S. M. P., and Reid, J. H., "Cosmic Ray Flares," Dunsink Observ. Publ. 1(3):53-88, 1961.

A5. Ellison, M. A., "The Observation of Solar Flares 1954-57," in: Conseil International des Unions Scientifiques, "9ᵉ Rapport de la Commission pour l'Étude des Relations entre les Phénomènes Solaires et Terrestres," Paris: J. & R. Sennac, 1957, pp. 15-25.

A6. Summaries of Mount Wilson Magnetic Observations of Sunspots, published in *Publ. Astronom. Soc. Pacific,* May 1920-April 1959.

A7. Dodson, H. D., and Hedeman, E. R., "Intense Solar Flares of July 16, 1959," *Sky and Telescope* 19(6):339-341, April 1960.

A8. Howard, R., and Babcock, H. W., "Magnetic Fields Associated with the Solar Flare of July 16, 1959," *Astrophys. J.* 132(1):218-220, July 1960.

A9. Ellison, M. A., McKenna, S. M. P., and Reid, J. H., "Flares Associated with the 1960 November Event and the Flare Nimbus Phenomenon," *Mon. Not. Roy. Astronom. Soc.* 122(6):491-501, 1961.

A10. Boischot, A., and Denisse, J.-F., "Les Émissions de Type IV et l'Origine des Rayons Cosmiques Associés aux Éruptions Chromosphériques," *Comptes Rendus, Academie des Sciences* (Paris) 245(25):2194-2197, December 16, 1957.

A11. Hansen, R. T., "Cosmic-Ray Flare of November 20, 1960," *Phys. Rev. Letters* 6(6):260-262, March 15, 1961.

A12. Covington, A. E., and Harvey, G. A., "10.7-cm Solar Noise Burst of November 20, 1960," *Phys. Rev. Letters* 6(2):51-52, January 15, 1961.

A13. Ellison, M. A., McKenna, S. M. P., and Reid, J. H., "Cosmic Ray Flares Associated with the 1961 July Event" (preprint), 1962.

A14. "Solnechnye Dannye" ("Solar Data") Nos. 1-12, 1960, published by the Academy of Sciences, U.S.S.R.

Table of Solar Proton Events

by

Harriet H. Malitson

Finite Solar Proton Manual   *Dec. 1963*

p 109–117   *refs*   (*See N64-17889*   *10-28*)   *OTS: $2.75*

A 5)

The list of solar proton events from 1949 to the present given in Table B1 requires considerable explanation and a few words of warning. As a starting point, part of the table contained in a paper by Warwick and Haurwitz (Reference B1) was used. Events and data from many other sources were added in an effort to extend the list in time and completeness. No doubt there are other lists in existence that contain weak events not included in Table B1. New events are continually being discovered as old records are re-examined and information is published, e.g., the events of October 6, 1959 and September 26, 1960.

In the first part of the list, especially for the events before 1956, it should be noted that identification depends on the interpretation of ionospheric data obtained before the use of the riometer. Most of the identifications were taken from a synoptic study of vertical-incidence ionosonde data from high latitude stations by Collins, Jelly, and Matthews (Reference B2). It is uncertain whether all these events were truly PCA's; many of them seem to have occurred during geomagnetic storms, and some of the blackouts recorded may have been due to auroral rather than true polar cap phenomena.

Even if we assume that all the PCA events listed prior to 1956 were real, we must not infer that the list presented here is complete; it is not a list of all events which *occurred*, but only those *detected*. Methods of detecting solar proton beams are constantly being improved; and we are probably detecting a larger percentage of all events each year as we pick up the weaker ones. We cannot draw many conclusions about the variation in the frequency of proton events over the eleven year cycle of solar activity, since we have nothing resembling a homogeneous body of data until sometime in 1957, when the riometer came into use and balloon and satellite data began to be obtained. All we can say is that the frequency was fairly high at solar maximum (1958), with a lower limit of one event per month, and is falling off toward minimum (expected around 1965); at least 8 events occurred in 1961.

The following is an explanation of the data in Table B1.

Columns 1 and 2: The date of occurrence of the solar proton event, and the earliest reported beginning time as determined by riometer readings or other ionospheric effects.

The symbol b signifies that the true starting time was probably earlier than the time of the first observation.

Column 3: The duration of the event in days. These values are probably inaccurate for the earlier events owing to the effects of geomagnetic storms. For events following each other within a few days, the duration is usually just the interval from one event to the next.

Column 4: For most events from 1956 on, the maximum absorption (in decibels) recorded on a riometer at high latitude is given for each event. This reading will differ somewhat in any given event, depending on the location of the riometer. However, the values give some idea of the relative sizes of the events in the lower energy range (10-100 Mev).

Column 5: These numbers indicate the sources of information for each proton event. This is not intended to be an exhaustive list.

Column 6: The GLE (ground level event) indicates that there were particles in the higher energy range (above 1 Bev) and that their arrival was detected at ground level. The earliest reported time of arrival is given, when known.

Columns 7-12: The flare data are taken from References B3-B7. In some cases more than one flare is listed for a single event because of the difficulty in determining which flare, of several occurring close together in time, was the significant one. For each flare, the approximate time of maximum brightness is given. The symbol a means that the true time of maximum was probably later than the time given. In the next column, the position of the flare on the solar disk is given. This is the heliographic position, measured N or S with respect to the solar equator and E or W with respect to the central meridian of the sun as seen from the earth at that particular time. The McMath-Hulbert Observatory serial number for the place in which the flare occurred, and the estimated importance of the flare are also given. The notation "probably no patrol" indicates that there was no known flare patrol operating during the period when an associated flare might have occurred.

Columns 13 and 14: For events starting with August 31, 1956, the beginning times are given for Type IV radio outbursts occurring around the time of the PCA-associated flares. Through March 30, 1960, the Type IV outbursts are taken from the lists of Pick-Gutmann (Reference B8). For later events, data were obtained from References B3, B9, and B10. Spectral observations of solar radio emission have been made only during the last few years, so no information prior to 1956 is available.

Columns 15-17: Beginning times are given for geomagnetic storms occurring after the flares listed, and thought to be associated with them. In some cases, particularly for the earlier events, storms in progress at the time of the PCA event are shown. These,

of course, would be associated with an earlier flare or with none at all. A_p is the daily equivalent amplitude of the geomagnetic disturbance, ranging from 0 to 400. A_p is the daily average of the eight 3-hour indexes a_p which represent one-half the average gamma range of the most disturbed of the three force components of the earth's magnetic field at certain standard geomagnetic observatories around the earth. The geomagnetic-storm information was obtained from References B3 and B11.

REFERENCES

B1. Warwick, C. S., and Haurwitz, M. W., "A Study of Solar Activity Associated with Polar-Cap Absorption," *J. Geophys. Res.* 67(4):1317-1332, April 1962.

B2. Collins, C., Jelly, D. H., and Matthews, A. G., "High-Frequency Radio-Wave Black-Outs at Medium and High Latitudes During a Solar Cycle," *Can. J. Phys.* 39(1):35-52, January 1961.

B3. "CRPL-F, Part B, Solar-Geophysical Data," issued monthly by National Bureau of Standards, Central Radio Propagation Lab., Boulder, Colorado.

B4. "International Astronomical Union, Quarterly Bulletin on Solar Activity," published by the Eidgenössische Sternwarte, Zürich, Switzerland.

B5. Dodson, H. W., and Hedeman, E. R., "McMath-Hulbert Observatory Working List of IGY Flares," Univ. Colorado, High Altitude Observ., Internat. Geophys. Year World Data Center A: Solar Activity, IGY Solar Activity Rept. Ser. No. 12, June 25, 1960.

B6. Dodson, H. W., and Hedeman, E. R., "McMath-Hulbert Observatory Working List of Flares and Daily Flare Index for IGC-1959," Univ. Colorado, High Altitude Observ., Internat. Geophys. Year World Data Center A: Solar Activity, IGY Solar Activity Rept. Ser. No. 15, June 26, 1951.

B7. Hedeman, E. R., private communication.

B8. Pick-Gutmann, M., "Évolution des Émissions Radioélectriques Solaires de Type IV et leur Relation avec d'autres Phénomènes Solaires et Géophysiques," *Annales d'Astrophysique* 24(3):183-210, May-June 1961.

B9. "Spectral Classification of Solar Activity (25-210 Mc/s)," issued monthly by Commonwealth Scientific and Industrial Research Organization, Radiophysics Laboratory, Sydney, Australia.

B10. "Preliminary Report of Solar Activity," issued weekly by the High Altitude Observatory, U. of Colorado, Boulder. These reports are combined and issued in final form in the Solar Activity Summaries by the High Altitude Observatory.

B11. Tabulations of Geomagnetic and Solar Data contained in the *J. Geophys. Res.*

B12. Dorman, L. I., "Cosmic Ray Variations," Moscow: State Publishing House for Technical and Theoretical Literature, 1957; Translation prepared by Technical Documents Liaison Office, Wright-Patterson Air Force Base, 1958.

112

B13. Bailey, D. K., and Harrington, J. M., "A Survey of Polar Cap Absorption Events (Solar Proton Events) in the Period 1952 through 1960,: in: *Proc. Internat. Conf. on Cosmic Rays and the Earth Storm, Kyoto, September 1961. II. Joint Sessions,* Tokyo: Physical Society of Japan, 1962, pp. 334-336.

B14. Little, C. G., and Leinbach, H., "Some Measurements of High-Latitude Ionospheric Absorption Using Extraterrestrial Radio Wave," *Proc. IRE,* 46(1):334-348, January 1958.

B15. Bailey, D. K., "Abnormal Ionization in the Lower Ionosphere Associated with Cosmic-Ray Flux Enhancements," *Proc. IRE,* 47(2):255-266, February 1959.

B16. "Convegno Internazionale sui Raggi Cosmici, Verenna, June 1957, Rendiconti," *Supplemento al Nuovo Cimento* 8(2), 1958.

B17. McCracken, K. G., "The Production of Cosmic Radiation by a Solar Flare on August 31, 1956," *Nuovo Cimento* 13(6):1074-1080, September 16, 1959.

B18. Collins, C., and Jelly, D. H., "Ionospheric Disturbance at the Time of Cosmic Ray Increases," *Nature* 189(4759):128-129, January 14, 1961.

B19. Reid, G. C., and Leinbach, H., "Low-Energy Cosmic-Ray Events Associated with Solar Flares," *J. Geophys. Res.* 64(11):1801-1805, November 1959.

B20. Hakura, Y., and Goh, T., "Pre-SC Polar Cap Ionospheric Blackout and Type IV Solar Radio Outburst," *J. Radio Res. Lab.* (Japan) 6(28):635-650, October 1959.

B21. Leinbach, H., private communication.

B22. Ortner, J., List of 60 Polar Cap Absorption Events 1958-60, Based on Riometer Data, Kiruna Geophys. Observ., Sweden, 1961 (unpublished).

B23. Hultqvist, B., Aarons, J., and Ortner, J., "Effects of the Solar Flares of 7 July 1958," *Tellus* 11(3):319-331, August 1959.

B24. Rymko, N. P., Tulinov, V. F., and Charakhch'yan, A. N., "A Case of a Sharp Increase in Cosmic-Ray Intensity in the Stratosphere," *Zhurnal Eksperimental'noi i Teoreticheskoi Fiziki* 36(6):1687-1689, June 1959 (in Russian); Translation in *Soviet Physics — JETP* 9(6):1202-1203, December 1959.

B25. Leinbach, H., and Reid, G. C., "Ionization of the Upper Atmosphere by Low-Energy Charged Particles from a Solar Flare," *Phys. Rev. Letters* 2(2):61-63, January 15, 1959.

B26. Rothwell, P., and McIlwain, C., "Satellite Observations of Solar Cosmic Rays (August 1958)," *Nature* 184(4681):138-140, July 1959.

B27. Anderson, K. A., Arnoldy, R., et al., "Observations of Low-Energy Solar Cosmic Rays from the Flare of 22 August 1958," *J. Geophys. Res.* 64(9):1133-1147, September 1959.

B28. Hultqvist, B., "On Lower Ionosphere Electron Detachment and Recombination Coefficients Obtained from Measurements of Nondeviative Ionospheric Absorption," *Arkiv für Geofysik* 3(2-3):97-110, 1961.

B29. Hultqvist, B., "On the Interpretation of Ionization in the Lower Ionosphere Occurring on Both Day and Night Side of the Earth within a Few Hours after Some Solar Flares," *Tellus* 11(3):332-343, August 1959.

B30. Eriksen, K. W., Holt, O., and Landmark, B., "A Note on the Polar Absorption Event of 11-18 May 1959," *J. Atmos. Terrest. Phys.* 18(1):78-81, April 1960.

B31. Ney, E. P., Winckler, J. R., and Freier, P. S., "Protons from the Sun on May 12, 1959," *Phys. Rev. Letters* 3(4):183-185, August 15, 1959.

B32. Charakhch'yan, A. N., Tulinov, V. F., and Charakhch'yan, T. N., "Large Cosmic-Ray Intensity Fluctuations in the Stratosphere," *Zhurnal Eksperimental'noi i Teoreticheskoi Fiziki* 38(4):1031-1036, April 1960 (in Russian); Translation in *Soviet Physics — JETP* 11(4):742-746, October 1960.

B33. Winckler, J. R., and Bhavsar, P. D., "Low-Energy Solar Cosmic Rays and the Geomagnetic Storm of May 12, 1959," *J. Geophys. Res.* 65(9):2637-2655, September 1960.

B34. Brown, R. R., and D'Arcy, R. G., "Observations of Solar Flare Radiation at High Latitude During the Period July 10-17, 1959," *Phys. Rev. Letters* 3(8):390-392, October 15, 1959.

B35. Anderson, K. A., and Enemark, D. C., "Observations of Solar Cosmic Rays Near the North Magnetic Pole," *J. Geophys. Res.* 65(9):2657-2671, September 1960.

B36. Křivský, L., Hladký, J., et al., "Solar Flare Connected with an Increase of Intensity of Cosmic Rays," *Nuovo Cimento* 15(4):695-696, February 16, 1960.

B37. Leinbach, H., "The Polar Cap Absorption Events of March 31 through May 13, 1960," Univ. of Alaska Geophys. Inst., June 21, 1960.

B38. Arnoldy, R. L., Hoffman, R. A., and Winckler, J. R., "Solar Cosmic Rays and Soft Radiation Observed at 5,000,000 Kilometers from Earth," *J. Geophys. Res.* 65(9): 3004-3007, September 1960.

B39. Fan, C. Y., Meyer, P., and Simpson, J. A., "Preliminary Results from the Space Probe Pioneer V," *J. Geophys. Res.* 65(6):1862-1863, June 1960.

B40. Van Allen, J. A., and Lin, W. C., "Outer Radiation Belt and Solar Proton Observations with Explorer VII during March-April 1960," *J. Geophys. Res.* 65(9):2998-3003, September 1960.

B41. Winckler, J. R., Bhavsar, P. D., et al., "Delayed Propagation of Solar Cosmic Rays on September 3, 1960," *Phys. Rev. Letters* 6(9):488-491, May 1, 1961.

B42. Fichtel, C. E., private communication.

Table 81

	Polar Cap Absorption Events						Solar Flare Data						Type IV Radio Outbursts		Geomagnetic Storms		
Date	Time of Start (UT)	Duration (days)	Maximum Absorption (db)	Reference	GLE	Date	Time of Maximum (UT)	Lat. (degrees)	Long. (degrees)	McMath Plage No.	Importance	Date	Time of Start (UT)	Date	Time of Start (UT)	Maximum
Jan 23	1200	4		B2			a 0103	N25	0	1795	3			24	1827	155
Apr 11	1400	4		B2			a 0040 / a 0727	N25 / S04	E70 / E04	1844	1 / 1			(11 / 12)	0725 / 1721	29 / 25
May 10	2000	4		B2			0345 / 2011	S18 / S20	E19 / E12	1859 / 1859	2 / 3			(11 / 12)	0204 / 0540	15 / 170
1949 Jun 04	1800	4		B2			1627	N04	W51	1875	2			(03 / 04)	2153 / 2114	59 / 27
Aug 03	1200	6		B2		03	a 0051	S20	W20	1924	1			(03)	0205	18
							8 other flares in same region				1			04	0043	64
						05	0807	S22	W55	1924	3			06	1112	9
Nov 19	1200	3	Large	B2.B12	1045		1033	S02	W72	1997	3			(19)	1756	42
Feb 02	0200	2		B2		01	a 2215	N20	W79	2043	3			(02 / 03)	0635 / 2322	27 / 1
1950 Feb 22	1200	3		B2		21	2344	N11	W26	2055	3			23	1043	49
						22	0302	N13	W29	2055	2			(26 / 29)	2330 / 0721	39 / 14
Mar 27	1000	3		B2			Probably no patrol							(27)	1205	
May 27	0800	5		B2			Probably no patrol							(06)	0750	36
Mar 07	1.00	9		B2			Probably no patrol							(04)	2650	
Apr 02	1.00	8		B2			Probably no patrol									
1951 Jun 11				B2		11	a 0630	S08	W48	2341	2			14	1751	27
						12	a 0425	N07	W15	2343	2			(17 / 18)	1702 / 2314	34 / 37
						13	a 0341 / a 0341	S13 / N10	E57 / W18	2347 / 2343	3 / 3					
Oct 27	0800	3	Weak Indef.	B2			Probably no patrol							28	1154	
1953 Mar 02	1800	3		B2			Probably no patrol							(02)	0422	
May 19	1.30	2	Small	B13			Probably no patrol							(18)	2205	21
1955 Jan 17		2	Poss. weak	B2		16	b 2130	N33	W41	3055	3			(17 / 18)	a 0300 / a 1500	43 / 59
Feb 23	0430	3	8.4	B12.B14-16	0344		0342	N23	W80	3400	3			(2?)	0307	100
1956 Mar 11	1600	4		B2			Probably no patrol							(10)	a 0000	241
Apr 27		2	Poss. weak	B2			2100	N15	W34	3474	1			(26 / 28)	2111 / 1727	172 / 64
Aug 31	1500	2.5		B13.B17 Small			1241	N16	E16	3643	3	1231		Sep 02	0230	82

Date	Time			Region	Time	Lat	Long	No.	I	Day	Time	Day	Time	No.
1956 Nov 13	2100	2		B13	1501	N16	W10	3753	2		1431	(13	2136	86)
Jan 20	1500	2.5		B13,B18 Small	1120	S27	W18	3820	2.			21	1255	82
Apr 03	1500	2.5	Small	B13	0835	S15	W60	3907	3		0826	05	0707	37
May 19	0200	0.5	1	B19	0813	S11	W15	3979	1-	18		21	0910	13
Jun 22	0530	3		B19	a0236	N23	E12	4024	2		0231	25	0046	84
Jul 03	0845	2	6	B19,B20	0740 / 0838	N14	W40	4039	3.		0632	04	2342	56
Jul 24	2015	0.5	2	B19	1827	S24	W27	4070	3		1801	27	1939	8
Aug 09	2245	1	2.5	B21	0628	S09	E75	4099	2			(09	1347	16)
				(Also flares in 4083, 4098, 4099)	1355	S33	W77	4082	1					
Aug 29	0030	0.5		B20	0940	S30	E35	4125	3-	28	0920	29	1909	38
					2020	S28	E30	4125	2-	28				
1957 Aug 29	1300	2	9	B19,B20 GLE	0555	N24	E35	4124	2			31	1812	33
					1037	S25	E20	4125	2		0548			
Aug 31	1530	2	5	B21	0552	S31	W02	4125	2-			Sep.02	0314	135
					0552	N13	E03	4124	2		1302			
					1312	N25	W02	4124	3					
Sep 02	1730	1.5	9	B19	1303	N10	W26	4124	1-		1257	04	1300	145
					1316	S34	W36	4125	2-					
Sep 12	b1200	1.5	0.5	B19,B20	1513	N11	W18	4134	2		1500	13 / (21	0045 / 1005	130 / 74)
Sep 21	1630	2	5	B19,B20	1338	N10	W03	4152	3		1331	22	1345	174
Sep 26	2315	1	2	B19	1836 / 1955	S26 / N22	E28 / E15	4161 / 4159	1 / 3	20	1836	29	0016	6
Oct 21	0630	1	5	B19,B20	1642	S26	W45	4189	3-	20	1636	21	2241	23
Feb 10	b0700	1	12	B19,B20	2141	S12	W14	4404	2.	09	2105	11	0125	199
Mar 23	1830	1.5	5	B13	1005	S14	E78	4476	3-		1003	25	1540	33
Mar 25	1300	4.5	12	B19,B20	0530 / 0603	N17 / S15	E25 / E50	4474 / 4476	2 / 2					
Apr 10	1000	2	4.5	B19	1440 / 1450	N11 / N24	W41 / W58	4490 / 4485	1 / 1	09				
1958 Jun 06	1345			B20	0100 / 0914	N25 / N18	W63 / W78	4485 / 4485	1 / 1	10		07	0040	77
Jul 07	0130	4	17	B19,B20 B22-B24	0439 / a1050	N10 / N43	W78 / E42	4578 / 4597	2 / 1		0437	08	1728	200
Jul 26	0405	1	1.5	B19,B25	0115 / 0033	N25 / N25	W08 / E07	4634 / 4634	3 / 1		002.	31	152.	15
Aug 16	0600	2.5	15	B19,B20 B22,B26	0056 / 0303	S17 / S14	W42 / W44	4655 / 4655	2 / 3			17	0322	32
Aug 21	1500	0.5	3	B19	0440	S14	W50	4686	3		0448	22	0227	34
					2254 / 0044	N13 / N16	E26 / E18	4708 / 4708	2 / 2	19 / 20	2140	19		

Table B1 (Cont'd)

	Polar Cap Absorption Events					Solar Flare Data						Type IV Radio Outbursts		Geomagnetic Storms		
Date	Time of Start (UT)	Duration (days)	Maximum Absorption (db)	Reference	GLE	Date	Time of Maximum (UT)	Heliog. Position Lat. (degrees)	Long. (degrees)	McMath Plage No.	Importance	Date	Time of Start (UT)	Date	Time of Start (UT)	Maximum A_p
Aug 22	1530	3.5	>10	B19,B20 B22,B26 B27			1448	N18	W10	4708	3		1430	24	0140	85
1958																
Aug 26	0100	3	>13	B19,B20 B22,B26			0027	N20	W54	4708	3		0023	27	0243	64
Sep 22	1400	3.5	4	B19,B20			0750 1017	S19 N17	W42 W65	4765 4756	2 2			25	0408	62
May 10	2300	7	>15	B19,B22 B28-B33			2140 a2315	N18	E48	5148	3		2100 2202 2336	11	2328	108
Jun 13	1330	>2	1.5	B21			0400	N17	E57	5204	1+			11	1625	44
Jul 10	0400	4	>15	B19,B22 B34			0240	N20	E66	5270	3		0223			
Jul 14	b0700	3	~20	B19,B22 B34			0349	N16	E06	5269	3		0330	15	0803	235
1959																
Jul 17	a0200	7	~18	B19,B22,2250 B34,B35(16th)	16		2132	N15	W30	5269	3	16	2118	17	1638	1.9
Sep 02	0400	2	Small	B13	01 01		1702 1948	S12 N12	W52 E60	5340 5355	2 2-		1914	03	2159	103
Oct 06			Small	B36		Small 1530	1425	N30	E65	5408	1-					
1960																
Mar 31	0300	1	7	B22,B37	30		1540	N12	E12	5615	2	30	1519	31	0800	241
Apr 01	0930	2	3	B22, B37-B40			0858	N12	W10	5615	3			02 05	2313 1300	68 34
Apr 05	b0800	2	3	B22,B37			0245	N12	W61	5615	2		0207	06 07	a1500 1511	22
Apr 28	0200	1	3	B22,B37			0137	S05	E34	5645	3		0145	(27	2020	84)
Apr 29	b0600	5	14	B22,B37			0220 0420	N12 N10	W20 W22	5642 5642	2 3		0200 0350			
May 04	1044	2	5	B22,B37,1030			0554	N14	W20	5642	2		0606	30	0132 1213	174
May 06	b1830	4	>15	B22,B37			1015	N14	W90	5642	2		1414	06	1650	60
May 13	0620	3	4.5	B22,B37			1450 0521	S10 S10	E08 E85	5653 5663	3 1		0530	08	0421	128
Sep 03	b0800	3	2.5	B21,B41,Small			0550 0037	N29 N18	W07 E88	5654 5838	3 2+			1o 02 04	1351 1158 0230 a0900	42 35) 118
Sep 26	1328	2	Small	B42			0538	S21	W64	5858	2		a0554			

Nov 12	1445	3	>15	B21	1328		1330	N26	W04	5925	3.		1327	(12 13)	1348) 1023	280
1960 Nov 15	0505	3.5	>20	B21	0236	20	0221	N26	W33	5925	3-		0221	15	1304 0631	94
Nov 21	0500	1	5	B21	Small 2055 (20th)		2020	N23	W113	5925	≥2			21		45
Jul 12	0000	1	1.5	B21		11	1700	S07	E31	6171	3	11	1702	13	1115	102
Jul 13	b0700	2.5	20	B21		12	1025	S07	E24	6171	3.	12	b1400	14	0730	98
Jul 15	1545	3	3	B21			1440 1600	N14	E13	6172	3		1435			
1961 Jul 18	1135	2.5	9	B21			1512	S07	V'20	6171	2		1522	17	1827	93
Jul 21	0300	1	5	B21	0950	20	1000	S06	W58	6171	3+		0940	20	0249	35
					Small 1620 (20th)		1620 1830	S06	W90	6171	3-	20	1607	23	a0600	17
Sep 10	2300		8	B21			2020	N12	W90	6212	≥1		1935			
Sep 28	2335		1.8	B21			2223	N14	E30	6235	3		2212	30	2111	114
Nov 10			1	B21			1444	N08	W90	6264	2+		1440			